INSTITUTE
FOR
AEROSPACE STUDIES

UNIVERSITY OF TORONTO

STUDY OF THE BARRINGER REFRACTOR PLATE CORRELATION SPECTROMETER AS A REMOTE SENSING INSTRUMENT

by

Millan M. Millan, Stanley J. Townsend, John Davies

August, 1970.

UTIAS Report No.146

STUDY OF THE BARRINGER REFRACTOR PLATE CORRELATION SPECTROMETER AS A REMOTE SENSING INSTRUMENT

by

Millan M. Millan*, Stanley J. Townsend II, John Davies**

* Research Assistant, Institute for Aerospace Studies, also Applied Mathematics Department, Research & Development Division, Barringer Research Limited.

II Associate Professor, Institute for Aerospace Studies.

** Manager, Research & Development Division, Barringer Research Ltd.

UTIAS Report No. 146

Manuscript submitted October, 1969

Revision received February, 1970

ACKNOWLEDGEMENTS

We wish to thank Dr. G. N. Patterson, Director, Institute for Aerospace Studies and Dr. A. R. Barringer, President, Barringer Research Limited, for the opportunity to link the University and the industrial communities in a cooperative research program. The University has contributed its academic supervision, and Industry has contributed its financial support in the form of the contracts mentioned below.

The main financial support for this work came from the National Research Council, Ottawa, under Project Optics 912.

Further assistance was obtained from the US Department of Health, Education and Welfare for work on the Stack Monitor, under contract PH22-68-44.

National Aeronautics and Space Administration assistance under contract NAS9-9492 is also acknowledged as being contributive to some of the work contained herein.

The analysis reported herein is based on the thesis submitted by one of us, Millan M. Millan, in conformity with the requirements for the degree of Master of Applied Science, University of Toronto.

TABLE OF CONTENTS

		Page
	SUMMARY	
	TABLE OF SYMBOLS	
1.	INTRODUCTION	1
2.	OPERATION OF THE CORRELATION SPECTROMETER	3
3.	SIGNAL ORIGIN	6
4.	ANALYSIS OF THE SINGLE-SLIT SIGNAL	20
5.	ANALYSIS OF THE MULTIPLE-SLIT SIGNAL	32
6.	SENSITIVITY AND DISCRIMINATION	41
7.	THE DOUBLE-SIDED MEASUREMENT	50
8.	REMOTE SENSING OF PLUMES	78
9.	REMOTE SENSING FROM A BALLOON-SUPPORTED PLATFORM	89
10.	CONCLUSION	89

SUMMARY

A theoretical study of the Barringer Refractor Plate Correlation Spectrometer is made, and several applications of the sensor are considered for the remote sensing of pollutant gases in the atmosphere.

The instrument is intended to detect and measure the amount of a specified gas present between a suitable light source and the sensor. The technique used is that of correlation spectroscopy which is based upon the measurement of the degree of similarity between the molecular absorption spectrum of a chosen gas and the actual total absorption spectra of all the gases seen by the instrument.

The mechanical and electrical characteristics of the instrument are described, and an analysis is performed of the optical characteristics of the instrument. The interactions between the characteristics of the light source irradiating the gas, the transmission spectrum of the instrument, the transmission spectrum of the correlation mask and the electronic circuitry are discussed.

The application of the instrument to the remote sensing of pollutants in smoke-stack plumes and to the remote sensing of ground-covering atmospheric pollutants from a balloon-supported platform is discussed.

LIST OF SYMBOLS

A	Aperture of the spectral system (cm^2)
$a(\lambda)$	Absorption crossection per molecule of the chosen gas (cm^{-2})
a_j	Average value of $a(\lambda)$ over waveband j (cm^{-2})
$b_i(\lambda)$	Absorption crossection per molecule of interfering gases (cm^{-2})
c	Concentration of absorbants (cm^{-3})
cL	Concentration times pathlength of the chosen gas (ppm-m)
c_iL_i	Concentration times pathlength of interfering gases (ppm-m)
H	Irradiance of a parallel beam of light ($W\ cm^{-2}\ nm^{-1}$)
J	Photodetector reference current (Amperes)
J'	Photodetector signal current (Amperes)
L	Pathlength (cm), (m)
L.P.	Low Pass (Filter)
m	Slope of spectral distribution
N_λ	Spectral radiance ($W\ cm^{-2}\ sr^{-1}\ nm^{-1}$)
N_a	Value of spectral radiance at the beginning of the chosen waveband
N.B.	Narrow Band (Filter)
n	Number of slits of the mask
P_λ	Spectral Radiant Power ($W\ nm^{-1}$)
P_j	Integrated spectral radiant power or radiant power incident onto the photodetector in position -j- of the absorption spectrum with respect to the mask (Watts)
R	Instrument's response (Volts)
Q.I.	Quartz Iodine (Lamp)
r	Range between plume and instrument (meters)
V	Voltage across the dynode chain of the photodetector (Volts)
$F(\lambda)$	Function representing the exit slits of the mask
$G(\lambda)$	Function representing the power spectrum incident on the mask

α	Instrument's impedance (Ohms)
α	Correlation variable (section 2)
$\beta(\lambda)$	Filter optics transmission function
$\Delta_{\lambda i}$	Width of slit i (nm) (Å)
Δ	Width of slits, when all have same width (nm) (Å)
λ	Wavelength (nm) (Å)
λ_{ji}	Beginning wavelength of slit -i- in position -j- with respect to the spectrum (nm) (Å)
λ'_{ji}	End wavelength of slit -i- in position -j- with respect to the spectrum (nm) (Å)
λ_i	Equal to λ_{1i} (nm) (Å)
$\sigma_{FG}(\alpha)$	Correlation function between $F(\lambda)$ and $G(\lambda)$ at the relative separation of α (Watts)
$\sigma(r)$	Extinction coefficient (section 8)
$\phi(\xi)$	Functional relationship between integrated radiant powers incident in position -2- and -1- of the spectrum with respect to a single slit, and no chosen gas present (i.e. $cL = 0$).
$\psi(\xi)$	Functional relationship between integrated Radiant powers incident in position -2- and -1- of the spectrum with respect to a mask and no chosen gas present.
Ω	Acceptance solid angle of the instrument's optics (sr)

1. INTRODUCTION

In determining the quality of our atmospheric environment, the detection, both qualitative and quantitative, of pollutant gases is of prime importance. Remote sensing by optical techniques allows the surveillance of extensive areas rapidly and repetitively in time. If to this advantage can be added the ability to sample quantitatively, either at a point or within a cone defined by the angular field of view of the instrument and the optical depth for various absorption processes, a very powerful technique can be developed for atmospheric monitoring.

This study is an analysis of the Barringer Refractor Plate Remote Sensor. The instrument is intended to detect and to measure the amount of a chosen gas present between a suitable light source and the instrument. The technique used is that of correlation spectroscopy which is based upon the measurement of the degree of similarity between the molecular absorption spectrum of a chosen gas and the actual total absorption spectra of all the gases seen by the instrument. A dispersion grating is used to cast the total spectrum onto the exit plane of the instrument. Situated in the exit plane is a mask that transmits energy only at wavelengths characteristic of the absorption spectrum of the particular gas being studied. The instrument then measures the correlation of the incident total energy spectrum with the transmission spectrum on the mask for each of two relative positions of the spectra; the difference of the two energy correlations is given as an electrical output which can be related to the amount of the chosen gas in the instrument's field of view.

In evaluating the performance of the instrument, we will first discuss the mechanical, electrical and then the optical behaviour of the spectrometer. The mechanical and electrical behaviour are relatively straightforward. The geometrical layout of the spectrometer and the relative motion of the total spectrum with respect to the particular gas spectrum are discussed. The analysis then follows of what form the output signal takes when the pollutant-gas spectrum is sampled with a transmission mask which consists of a single slit passing all the radiant power

incident on it. This is followed by a similar but extended analysis when the transmission mask consists of multiple slits of certain widths and spacings relative to each other as is characteristic of the absorption spectrum of the chosen gas.

There is a method of treating the information contained in the electrical signal in order to make the error in the signal less sensitive to changes in gas concentration and to variations with wavelength both of the intensity of the light source irradiating the gas and of the spectrometer transmission function. This method is treated in the section on the double-sided measurement. Basically, it refers to the possibility of using electrical signals from each of the two correlations of the spectra alternately as the reference signal. Thus, although each referenced signal is subject to an error the difference between the differently referenced signals is significantly less subject to error.

In the analysis, particular emphasis is placed on: (1) error-generating phenomena, (2) the extent to which the reading on the instrument represents qualitatively and/or quantitatively the presence of the gas under study and (3) the calculation of the appropriate system parameters needed to optimize both the response sensitivity and the discrimination to the chosen gas.

Finally, two applications of the instrument are discussed. The first is the remote sensing of smokestack plumes and the second is remote sensing from above the earth's atmosphere on a balloon platform.

2. OPERATION OF THE CORRELATION SPECTROMETER

A correlation spectrometer system typically consists of a light source, field-defining fore-optics, an entrance slit, collimating elements, dispersive element, exit mask and photodetector. Radiant power from the light source is focussed onto the entrance slit, dispersed by a prism or grating and refocussed onto the plane of the exit mask. The incoming spectrum is then made to cross-correlate against the mask by moving one relative to the other in some cyclical fashion and collecting the output on a photodetector.

The sensor optical system is shown schematically in Figure 2-1. The field-defining fore-optics are comprised of the mirrors M_1 and M_2, a cylindrical lens and the spectrometer entrance slit. The spectrometer is an f/3.6 Ebert-Fastie configuration of 1/4 meter focal length. The dispersed (power) spectrum of the incoming radiation is focussed at the exit mask. By proper dimensionalizing of the units, taking into account the dispersion of the system, we can express the power spectrum in Watts per nanometer (Wnm^{-1}) per unit height in the exit plane. The angular position of the grating determines which portion of the spectrum is incident on the exit aperture, the latter being that geometrical area on the exit plane with the property that all the radiant power incident on it can be properly focussed onto the photodetector.

This exit aperture defines the possible limits of the exit mask. The exit mask is made up of a certain number of slits through which the incident spectral radiant power can pass from the exit plane to the photodetector.

In order to obtain a time-varying signal from the photodetector, the incoming spectral radiant power has to be spatially and/or time modulated; in this system both methods can be used.

The spatial modulation is achieved by means of two fork-driven refractor plates, situated immediately after the entrance slit. Although these plates have continuous motion at a frequency of 100 Hz there are effectively only two positions

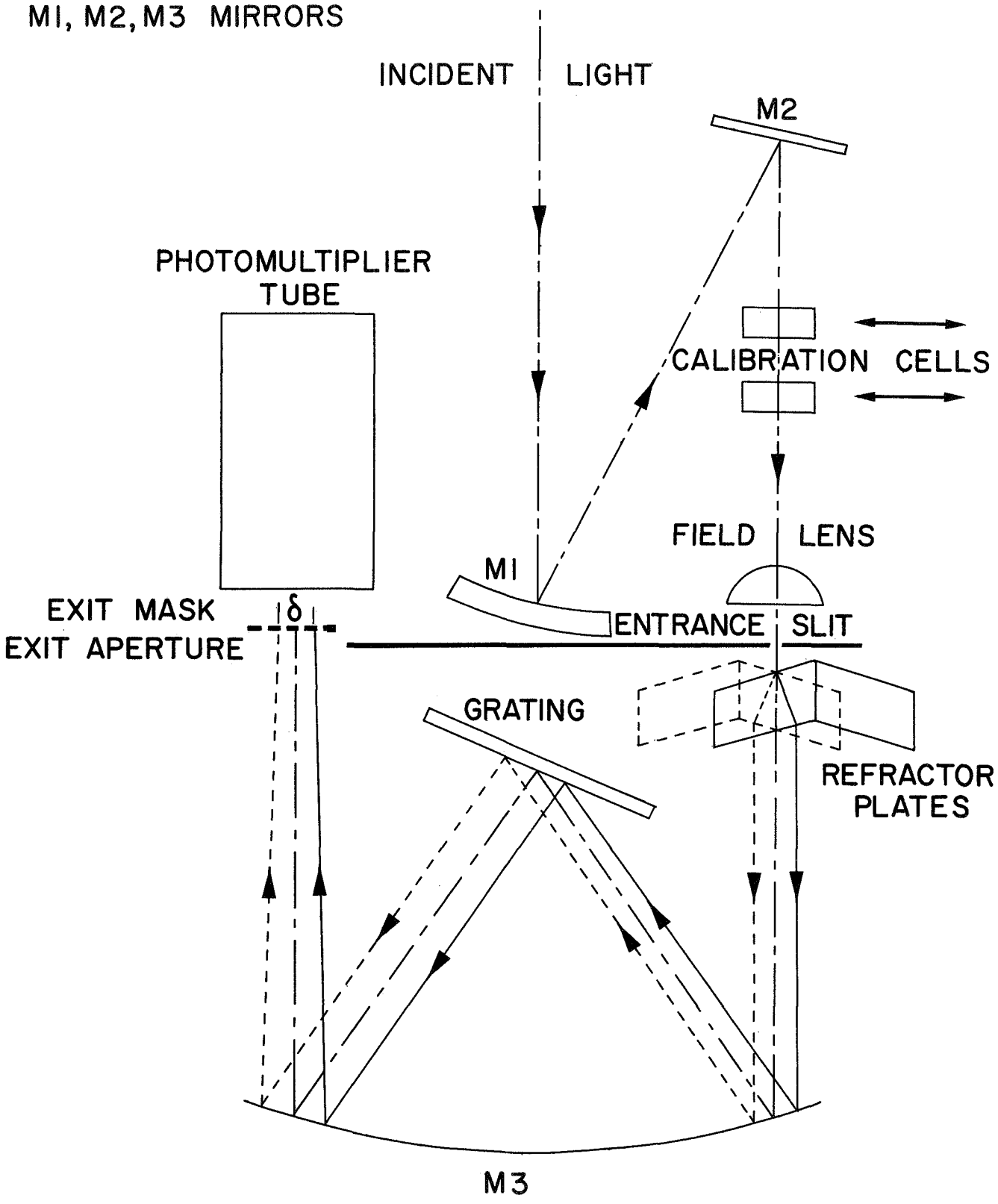

FIGURE 2-1
OPTICAL LAYOUT OF THE CORRELATION SPECTROMETER

of the plates seen by the incoming light beam. For half of the time each refractor plate sits at a fixed angle to the beam; thus, the beam "jumps" discontinuously between two different paths, producing a pre-determined, two-position, cyclical displacement of the spectrum with respect to the exit mask. In this system, then, the mask in the exit plane remains stationary and the spectrum "jumps" back and forth an amount δ . The refractor plates always introduce spatial modulation or "jump". Time modulation of the light source is sometimes introduced.

Also used, with or without time modulation of the light source, is another system employing spatial modulation. Superimposed on the sudden jumping of the spectrum across the exit mask is a smoothly drifting motion of the spectrum introduced by smooth rotation of the grating. This latter method is called spectral scanning.

Particular characteristics of the refractor plate type of modulation are:

(a) The trajectory of the refractor plates is quasi-lineal.

(b) The amplitude of the beam displacement is wavelength dependent.

(c) The apparent position of the entrance slit as viewed from the Ebert mirror not only moves sideways but also changes in depth; this change is wavelength dependent and hence different wavelengths focus at different distances normal to the exit aperture.

(d) The apparent position of the slit as viewed from the Ebert mirror does not change when the refractor plate through which it is viewed moves without rotation, until the second plate (at an angle to the first) comes into the beam. The slit stays in one position and almost suddenly appears on the other position.

(e) In all cases the waveband used for any chosen gas is sufficiently narrow so that the parameters referred to in (b) (c) can be taken as those corresponding to the wavelength of the nominal center of the waveband.

3. SIGNAL ORIGIN

3.1 Light Input to the Spectrometer

The characteristics of the light source irradiating the gas and the absorption characteristics of the gas determine the spectral distribution of the radiant power entering the entrance slit. We shall consider the spectral radiance of the instrument's light source (illuminated plate, sky, ground, etc.) to be uniform throughout the field of view of the instrument, unless otherwise specified.

We next treat the absorption characteristics of the intervening gas. The gas will alter the incoming spectrum according to the microscopic absorption cross section at each wavelength and the concentration of absorbing molecules. The determination of the product of the concentration of the chosen gas times the pathlength of the gas is based originally on the Lambert Law of absorption; that is, the irradiance of a parallel, monochromatic beam of radiation passing through a medium that absorbs but does not scatter is attenuated according to

$$H = H_o e^{-a\ cL} \qquad (3\text{-}1)$$

where

H_o is the irradiance of the beam at a fixed wavelength (Watts/cm^2)

a is the absorption coefficient of the gas for the same wavelength (cm^2/molecule)

c is the concentration of the medium (gas) ($\frac{\text{molecules}}{cm^3}$)

L is the path travelled by the beam through the medium (cm)

If cL is constant throughout the beam, and the gas absorption characteristics are known at least at two wavelengths and the absorption crossections are different at those two wavelengths and H_o is the same for both wavelengths, then, the product cL could be determined simply from:

$$H_1 = H_o e^{-a_1 cL}$$

$$H_2 = H_o e^{-a_2 cL} \qquad \frac{H_1}{H_2} = e^{-(a_1 - a_2) cL} \qquad cL = \frac{\ln(H_1/H_2)}{a_2 - a_1} \qquad (3\text{-}2)$$

where a_1 and a_2 would be the absorption coefficients at wavelengths 1 and 2 respectively.

The situation with the spectrometer and an irradiating light source is more complicated. Light that has travelled through the sample of the gas will be dispersed on a plane and, by means of exit slits, will have to be studied at different wavelengths. Moreover, the slits have finite width and H_o is not constant but varies with wavelength, as do a_1 and a_2. Therefore, Expressions (3-2) become:

$$P_1 = \int_{\lambda_1}^{\lambda_1 + \Delta\lambda_1} N_\lambda \, e^{-a(\lambda) cL} \, d\lambda$$

$$P_2 = \int_{\lambda_2}^{\lambda_2 + \Delta\lambda_2} N_\lambda \, e^{-a(\lambda) cL} \, d\lambda$$

$$\frac{P_1}{P_2} = e^{-(a_1 - a_2) cL} \frac{\int_{\lambda_1}^{\lambda_1 + \Delta\lambda_1} N_\lambda \, d\lambda}{\int_{\lambda_2}^{\lambda_2 + \Delta\lambda_2} N_\lambda \, d\lambda} \qquad (3\text{-}3)$$

where, this time, a_1 and a_2 are the average absorption crossections per molecule in the bands $(\lambda_1, \lambda_1 + \Delta\lambda_1)$ and $(\lambda_2, \lambda_2 + \Delta\lambda_2)$. P_1 and P_2 have the dimensions of Watts, that is, power passing through the slits per unit height of slit. In general, not only the quotient of P_1 and P_2 can be used to determine cL, but also any other suitable relationship between them. The determination of cL is now obviously not as straightforward as before, and unless something is known about N_λ, in general, it will not be possible.

The working units chosen for cL are not $(\frac{\text{molecules}}{\text{cm}^2})$ but parts per million by volume of the atmosphere along a meter path length (ppm-m). To pass from ppm-m to $\frac{\text{molecules}}{\text{cm}^2}$ at S.T.P. the following relation is used:

$$\text{cL in } \frac{\text{molecules}}{\text{cm}^2} = \text{cL in (ppm-m)}, \frac{6.024 \times 10^{16}}{22.4}$$

In the presence of other absorbing gases that we can assume would modify N_λ, the determination of cL would become impossible unless enough is known about the absorption patterns of these other gases as well as the characteristics of the light source. It is in this situation that devices which are more (or if possible, exclusively) responsive to the chosen gas, become necessary.

The simple case analyzed above of one slit sampling the power in each of two positions in the spectrum can be extended to analyzing an array of slits in a mask, again sampling the passing power at two positions. One would expect that if the slits are properly chosen as to width and separation, the effect of the spectral distribution of the light source and influence due to other absorbing gases, could be minimized.

3.2 Correlation Functions

It is worthwhile to study in detail the correlation between the power passing through the mask for the spectrum in two positions. The mathematical definition of correlation function is the integral of the product of two functions after one of them has been displaced by a distance along the independent variable axis (in our case the λ axis).

Thus

$$\sigma_{FG}(\alpha) = \int_{-\infty}^{\infty} F(\lambda) \cdot G(\lambda + \alpha)\, d\lambda \qquad (3\text{-}4)$$

In general, the spectrum on the exit plane of the spectrometer is:

$$A\Omega\ N_\lambda\ \beta(\lambda)\ e^{-a(\lambda)cL}\ .\ e^{-I(\lambda)} \equiv G(\lambda) \tag{3-5}$$

The spectrum may have been produced by the absorption of a single chosen gas $[a(\lambda)cL]$ and/or amounts of other gases $[I(\lambda)]$.

$$F(\lambda) \begin{cases} = 1 \text{ in all points of the open intervals } (\lambda_{1i}, \lambda'_{1i}) \\ = 0 \text{ at any other point} \end{cases}$$

(see Figure 3-1)

The value of the correlation function when $\alpha=0$ is

$$\sigma_{FG}(o) = \int_{-\infty}^{\infty} A\Omega\ N_\lambda\ \beta(\lambda)\ e^{-a(\lambda)cL}\ .\ e^{-I(\lambda)}\ .\ F(\lambda)\ d\lambda$$

$$= \sum_{i=1}^{n} \int_{\lambda_{1i}}^{\lambda'_{1i}} A\Omega\ N_\lambda\ \beta(\lambda)\ e^{-a(\lambda)cL}\ .e^{-I(\lambda)}\ d\lambda \tag{3-6}$$

and the value for $\alpha = -\delta$ is

$$\sigma_{FG}(-\delta) = \int_{-\infty}^{\infty} A\Omega\ \ N_{\lambda-\delta}\ .\ \beta(\lambda-\delta)\ e^{-a(\lambda-\delta)cL}\ .\ e^{-I(\lambda-\delta)}\ .\ F(\lambda)d\lambda \tag{3-7}$$

But

$$\int_{-\infty}^{\infty} F(\lambda)\ G\ (\lambda-\delta)d\lambda = \int_{-\infty}^{\infty} F(\lambda+\delta)\ G(\lambda)d\lambda \tag{3-8}$$

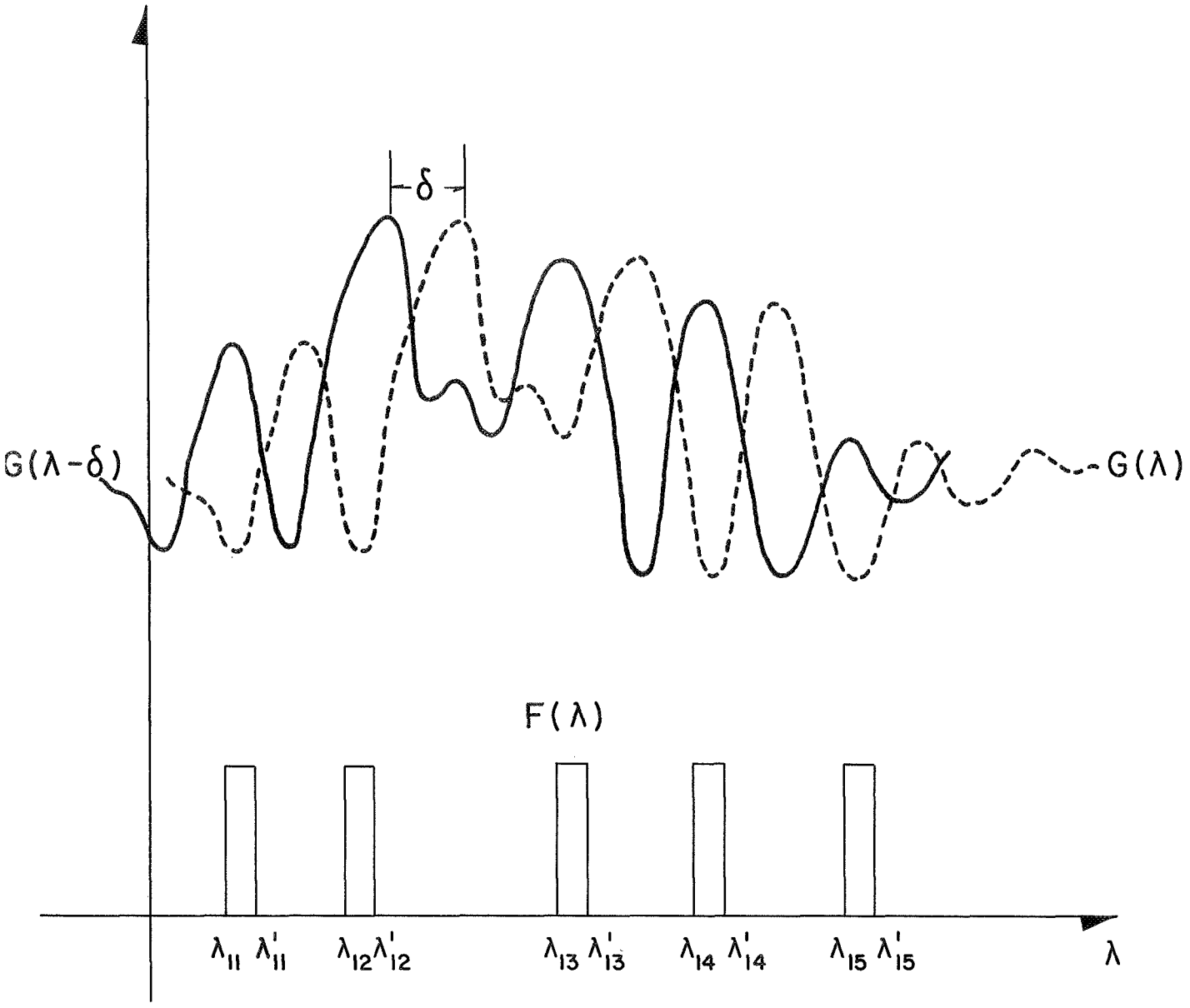

FIGURE 3-1
POWER SPECTRUM G (λ), AT TWO POSITIONSλ, AND λ-δ, AND SLITS OF THE MASK FUNCTION F(λ)

where $F(\lambda+\delta)$ is defined as

$$F(\lambda+\delta)\begin{cases} = 1 \text{ in all points of the open intervals } (\lambda_{1i} + \delta,\ \lambda'_{1i} + \delta) \\ = 0 \text{ at all other points} \end{cases}$$

and $\lambda_{2i} = \lambda_{1i} + \delta$

$\lambda'_{2i} = \lambda'_{1i} + \delta$

Therefore,

$$\sigma_{FG}(-\delta) = \sigma_{GF}(\delta) = \sum_{i=1}^{n} \int_{\lambda_{2i}}^{\lambda'_{2i}} A\Omega\, N_\lambda\, \beta(\lambda)\, e^{-a(\lambda)cL} \cdot e^{-I(\lambda)}\, d\lambda \qquad (3\text{-}9)$$

If N_λ is expressed ($W\ cm^{-2}\ sr^{-1}\ nm^{-1}$)

A is expressed in cm^2

Ω is expressed in sr

λ is expressed in nm

$\sigma_{FG}(o)$ is the radiant power passing through the mask when in position $\alpha=0$ (position (1) with respect to the spectrum) and is denoted P_1

$\sigma_{FG}(-\delta)$ is the radiant power passing through the mask when in position $\alpha=-\delta$ (position (2) with respect to the spectrum) and is denoted P_2

The observable chosen is then:

> the difference of the two correlation functions between a power spectrum and an array of slits (mask) for two positions of one with respect to the other.

The reason for the name correlation spectroscopy, then, is based on the relation between the mask pattern $[F(\lambda)]$ and the true absorption pattern of the chosen gas.

Because it is obviously simpler and physically more significant to speak of radiant power passing through the slits of the mask rather than the correlation function between the spectrum and the mask-defining function, the term power will subsequently be used.

3.3 Response of the Instrument

Now with reference to the instrument described in Section 2, the physical observable chosen for the determination of cL is the difference in two values of phototube current generated by a light spectrum falling onto two different positions on the mask situated in front of the phototube. The response of the phototube in Amperes per Watt of incident radiation is a function of the voltage across the dynode chain. An automatic gain control circuit (AGC) and synchronous detector are used in the following manner:

(a) One of the positions of the spectrum, position (1), is selected. We will call P_1 the power in Watts falling on the phototube with the spectrum in this position.

(b) A phototube current, J, in Amperes is selected and held fixed.

(c) The voltage V across the dynode chain is variable and is automatically adjusted by the AGC and synchronous detector in such a way that the response to the P_1 Watts is always J Amperes, and the voltage is locked on and held at that moment with the spectrum in position (1).

(d) For the next position (2) of the spectrum, the incident power will be P_2 and the response, J', as indicated in Figure 3-2.

(e) This cycle is repeated for each oscillation of the fork with the synchronous detector locked onto state (1) as a reference and the AGC controlling the phototube voltage.

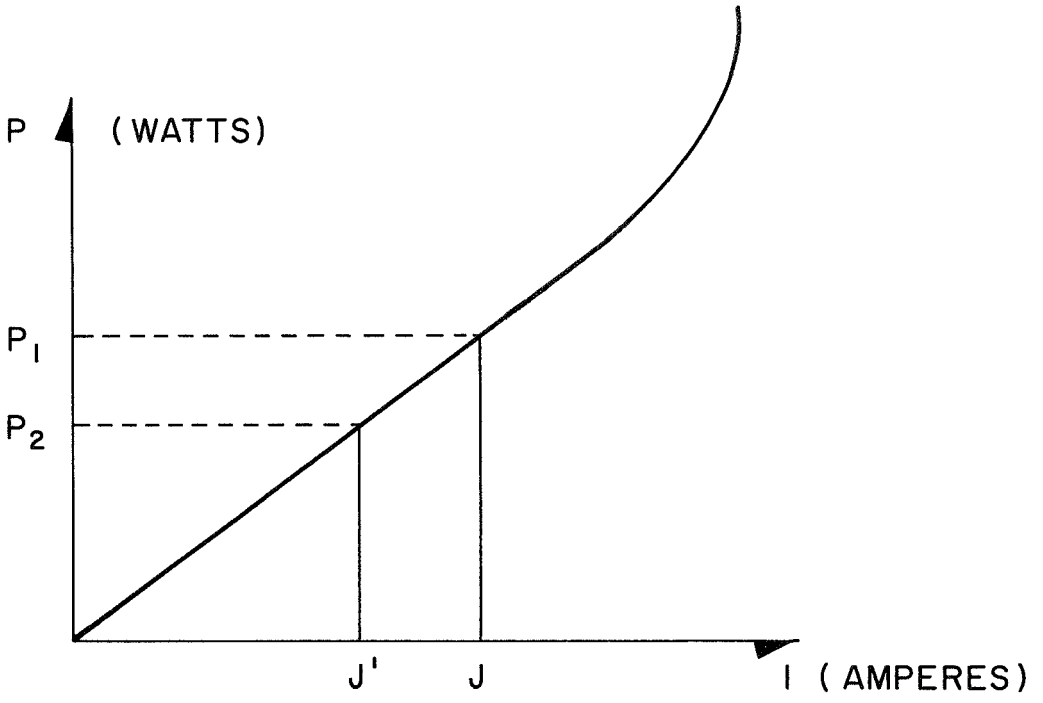

FIGURE 3-2

PHOTOTUBE RESPONSE CHARACTERISTICS

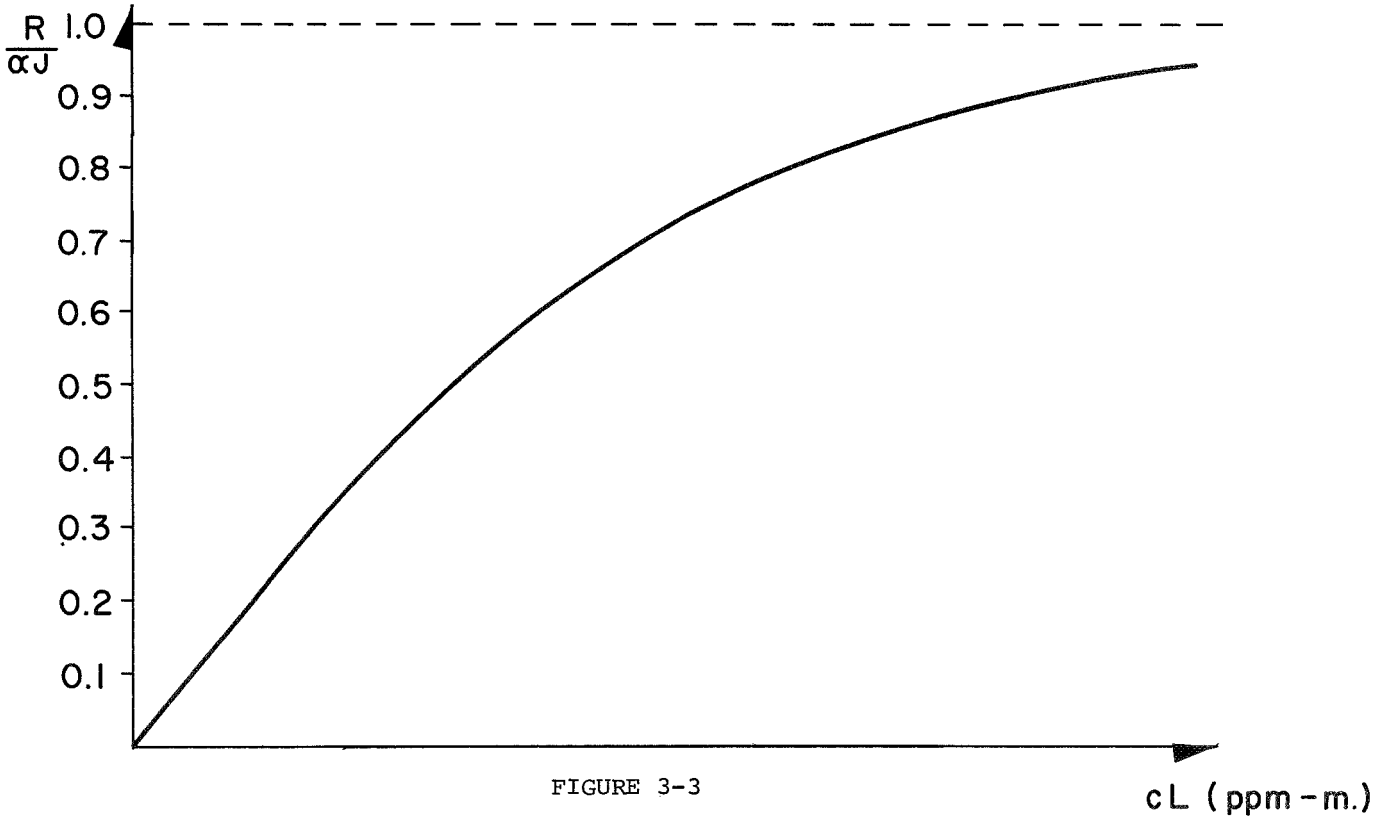

FIGURE 3-3

RESPONSE CURVE OF THE INSTRUMENT

Thus, in the correlation spectrometer under study, position (1) is chosen as a reference to control the Automatic Gain Control loop. The current, J', corresponding to position (2) will, in general, be different from J and for this specific case the difference $(J - J')$ is the physical observable chosen.

The difference D may be written as:

$$D = J - J' = J\left(1 - \frac{J'}{J}\right) \tag{3-10}$$

When both positions (1) and (2) are within the lineal response of the phototube

$$\frac{J'}{J} = \frac{P_2}{P_1}$$

which allows us to write

$$D = J\left(1 - \frac{P_2}{P_1}\right) \tag{3-11}$$

where

P_1 is the spectral power received by the phototube corresponding to position (1) of the spectrum with respect to the mask.

P_2 is the power corresponding to position (2) of the spectrum with respect to the mask.

D is expressed in Amperes. When this current is converted into voltage by feeding it into a high impedance load, the response of the instrument can be expressed as

$$R = \alpha J\left(1 - \frac{P_2}{P_1}\right) \text{ in Volts} \tag{3-12}$$

where

α is the impedance of the load (Ohms)

J is the selected response of the phototube. (Amperes)

In this technique the spectrum jumps in an infinitesimal amount of the time, from position (1) to position (2) with respect to the mask, remaining in each position an amount of time, large compared with that of the jump. This small time is therefore neglected, and in the following analysis it is assumed that the spectrum is in position (1) or (2) without passing through any intermediate position.

So far, nothing definite has been said about the nature of $a(\lambda)$ except that it is the absorption coefficient per molecule of the gas chosen. The only point of concern for this study is that we choose a spectral region where $a(\lambda)$ has a well defined structure, thus producing a marked absorption spectra on the light passing through the gas. When this spectral region is incident on the exit aperture where the mask is located, and the spectrum is jumped alternately from position 1 to position 2, the response is produced.

If the instrument is pointed at a target of spectral radiance N_λ (W cm^{-2} sr^{-1} nm^{-1}) and the greatest representative dimension of the patch of target as seen from the instrument is small in relation to the distance between the instrument and the target, and the concentration of the absorbing gas varies only with $\underline{\ell}$ ($\underline{\ell}$ being the pathlength between the target and the instrument), the response (3-12) can be expressed as:

$$R = \alpha J \left\{ 1 - \frac{\sum_{i=1}^{n} \int_{\lambda_{2i}}^{\lambda'_{2i}} \beta(\lambda) N_\lambda e^{-a(\lambda)} \cdot \int_0^{\ell} c(\ell) d\ell \, d\lambda}{\sum_{i=1}^{n} \int_{\lambda_{1i}}^{\lambda'_{1i}} \beta(\lambda) N_\lambda e^{-a(\lambda)} \cdot \int_0^{\ell} c(\lambda) d\ell \, d\lambda} \right\} \qquad (3\text{-}13)$$

For $\underline{c}$ a function of ℓ only, $\int_0^{\ell} c(\ell)\, d\ell = \langle c \rangle \cdot \ell = cL$, where cL is the integrated concentration times pathlength. We will assume for now that the product cL is constant over the acceptance solid angle of the instrument. The reading becomes:

$$R = \alpha J \left\{ 1 - \frac{\sum_{i=1}^{n} \int_{\lambda_{2i}}^{\lambda'_{2i}} \beta(\lambda)\, N_\lambda\, e^{-a(\lambda)cL}\, d\lambda}{\sum_{i=1}^{n} \int_{\lambda_{1i}}^{\lambda'_{1i}} \beta(\lambda)\, N_\lambda\, e^{-a(\lambda)cL}\, d\lambda} \right\} \qquad (3\text{-}14)$$

Notice that

$$\sum_{i=1}^{n} \int_{\lambda_{1i}}^{\lambda'_{1i}} \beta(\lambda)\, N_\lambda\, e^{-a(\lambda)cL}\, d\lambda = \sum_{i=1}^{n} \int_{\lambda_{1i}}^{\lambda_{1i} + \Delta\lambda_i} \beta(\lambda)\, N_\lambda\, e^{-a(\lambda)cL}\, d\lambda$$

and

$$\sum_{i=1}^{n} \int_{\lambda_{2i}}^{\lambda'_{2i}} \beta(\lambda)\, N_\lambda\, e^{-a(\lambda)cL}\, d\lambda = \sum_{i=1}^{n} \int_{\lambda_{1i} + \delta}^{\lambda_{1i} + \delta + \Delta\lambda_i} \beta(\lambda)\, N_\lambda\, e^{-a(\lambda)cL}\, d\lambda$$

$a(\lambda)$ being the absorption crossection per molecule, a function of wavelength at a given temperature and pressure.

λ_{1i}, λ'_{1i} the beginning and end wavelength of the mask corresponding to slit (i) for position (1) of the spectrum with respect to the mask (nm)

λ_{2i}, λ'_{2i} is the same for position 2.

$\Delta\lambda_i = \lambda'_{2i} - \lambda_{2i} = \lambda'_{1i} - \lambda_{1i}$ width of slit i (nm)

$\lambda_i = \lambda_{1i}$ beginning wavelengths of slit i in position (1)

$\beta(\lambda)$ the filter optics transmission function.

$\delta = (\lambda_{2i} - \lambda_{1i})$, i = 1, n amplitude of the "jump", common for all slits (nm)

n the number of slits in the mask

A the instrument's aperture (cm^2)

Ω the instrument's acceptance solid angle (sr)

For a particular instrument with a given mask-jump and filter combination, working in the spectral region where the gas has the absorption spectrum, α, J, n, λ_i, $\Delta\lambda_i$, and δ are fixed. The emphasis is on the relationship between these fixed instrument parameters and the power-affecting parameters $\beta(\lambda)$, $a(\lambda)$, N_λ and cL.

As we can see, the response of the instrument is a complicated function of the variables and functions

$$\alpha,\ J,\ n,\ \beta(\lambda),\ N_\lambda,\ \lambda_i,\ \Delta\lambda_i,\ \delta,\ cL,\ a(\lambda)$$

The sensitivity of the instrument at the point where the concentration is cL is defined as the absolute value of the response curve slope [R (in Volts) versus cL in ppm-m] at that point. The incremental sensitivity is defined as the change

in response which corresponds to a small change in cL.

Thus the sensitivity is $\left| \left(\frac{\partial R}{\partial cL}\right)_{cL} \right|$

and the incremental sensitivity

$$\Delta R \simeq \left(\frac{\partial R}{\partial cL}\right)_{cL} \Delta cL \qquad (3\text{-}15)$$

The sensitivity

$$\left| \left(\frac{\partial R}{\partial cL}\right)_{cL} \right| = f[\alpha, J, n, \beta(\lambda), N_\lambda, \lambda_i, \Delta\lambda_i, \delta, cL, a(\lambda)] \qquad (3\text{-}16)$$

is also a function of the same variable affecting the reading, including the concentration itself, as can be seen directly by observation of Figure 3-3. The result is obvious since R is not a lineal function of cL. The determination of when R is quasi linear with cL is part of this study.

The simplest form for the response of a multislit instrument occurs when:

(a) The width, $\Delta\lambda$, of every slit is the same.
(b) N_λ is constant over the waveband of interest and equal to N_o.
(c) $a(\lambda)$ is a periodic function of λ over the same waveband interval.
(d) c is constant along the path L which is also constant
(e) The optics response of the instrument is lineal-constant over the waveband of interest; therefore $\beta(\lambda) = \beta_o$
(f) Only the gas under study is absorbing.

With the above conditions fulfilled, it will be possible to find two values a_1 and a_2, such that 3-14 becomes

$$R = \alpha J \left\{ 1 - \frac{n \beta_o \Delta\lambda N_o e^{-a_2 cL} A \Omega}{n \beta_o \Delta\lambda N_o e^{-a_1 cL} A \Omega} \right\} \qquad (3\text{-}17)$$

In this case, the response of the instrument to changes of cL is given by the simple relationship

$$R = \alpha J \left\{ 1 - e^{-(a_2 - a_1)cL} \right\} \qquad (3\text{-}18)$$

We refer to a_1 and a_2 as the "average" absorption crossections per molecule in positions (1) and (2) respectively and to expression 3-18 as the calibrated reading for a constant light source. The laboratory calibration with controlled (cL), light source and equal width slits is considered to follow the expression 3-18 reasonably well.

Equation 3-18 is true only under optimum laboratory conditions. For normal use, when most of the above assumptions do not hold, Equation 3-14 will be used.

The idealized reading, when taken with no absorbing gas present, will be considered the instrument's absolute zero readout.

Referring to equation 3-14 and considering that there is no absorbing gas in the field of view, the output (zero offset) obtained is

$$R_o = \alpha J \left\{ 1 - \frac{\sum_{i=1}^{n} \int_{\lambda_{2i}}^{\lambda'_{2i}} \beta(\lambda)\, N_\lambda \, d\lambda}{\sum_{i=1}^{n} \int_{\lambda_{1i}}^{\lambda'_{1i}} \beta(\lambda)\, N_\lambda \, d\lambda} \right\} \qquad (3\text{-}19)$$

R_o is not zero because the sum of the integrals for the number of slits $\underline{n}$ in the position λ_{1i} will in general be different from that of the sum of the integrals for the slits in position λ_{2i}. The reading (zero offset) will depend on N_λ, $\beta(\lambda)$, number of slits, their widths and the amplitude of the jump.

As we shall see in the following sections, the zero offset gives a direct indication of the degree of interference in the measurement by other gases and/or structure in the light source, and is directly related to the sensitivity and specificity to the chosen gas. In general, the smaller the zero offset is, the more specific to the gas the measurement becomes.

4. ANALYSIS OF THE SINGLE-SLIT SIGNAL

In order to study in a progressive sequence the response of the instrument and its sensitivity, we will begin with the simple system of a single slit, examining the influence of the system parameters on the response of the system.

Let us consider a single narrow slit on the exit plane when the gas under study is absorbing.

The power incident on the phototube when the spectrum is in position (1) is:

$$A\Omega \int_{\lambda_1}^{\lambda_1'} N_\lambda \, \beta(\lambda) \, e^{-a(\lambda)cL} \, d\lambda = A\Omega \, e^{-a_1 cL} \int_{\lambda_1}^{\lambda_1'} N_\lambda \, \beta(\lambda) \, d\lambda \qquad (4\text{-}1)$$

When in position (2) it becomes

$$A\Omega \, e^{-a_2 cL} \int_{\lambda_2}^{\lambda_2'} N_\lambda \, \beta(\lambda) \, d\lambda$$

$\lambda_1' - \lambda_2 = \lambda_1' - \lambda_1 = \Delta\lambda$ is the width of the slit

The response of the instrument would be

$$R = \alpha J \left\{ 1 - \frac{e^{-a_2 cL} \int_{\lambda_2}^{\lambda_2'} N_\lambda \, \beta(\lambda) \, d\lambda}{e^{-a_1 cL} \int_{\lambda_1}^{\lambda_1'} N_\lambda \, \beta(\lambda) \, d\lambda} \right\} \qquad (4\text{-}2)$$

where a_1 and a_2 are the average absorption crossections per molecule of the gas over the narrow bands defined by the two positions of the slit. Relatively speaking, we can think of the spectrum as fixed and the slit as doing the jumping.

We can always find a function $\phi(\lambda)$ such that each point of $N_\lambda\ \beta(\lambda)$ in spectral region (1) or $N_{\lambda 1}\ \beta(\lambda)$ with respect to the slit in position (λ_1, λ_1'), is transformed into each point of $N_\lambda\ \beta(\lambda)$ of spectral region (2) or $N_{\lambda 2}\ \beta(\lambda)_2$ with respect to the slit in position (λ_2, λ_2'), in a point to point correspondence.

Relative to the slit

$$N_{\lambda 2}\ \beta(\lambda)_2 = N_{\lambda 1}\beta(\lambda)_1 \cdot \phi(\lambda) \tag{4-3}$$

thus

$$\int_{\lambda_2}^{\lambda_2'} N_{\lambda 2}\ \beta(\lambda)_2 d\lambda = \int_{\lambda_1}^{\lambda_1'} N_{\lambda 1}\ \beta(\lambda)_1\ \phi(\lambda) d\lambda = \phi(\xi) \int_{\lambda_1}^{\lambda_1'} N_1 \beta(\lambda)_1 d\lambda \tag{4-4}$$

where by the mean value theorem $0 \leq \phi(\xi) \leq \infty$ and $\lambda_1 \leq \xi \leq \lambda_1'$

Note that physically,

$$\phi(\xi) = \frac{A\Omega \int_{\lambda_2}^{\lambda_2'} N_{\lambda 2}\ \beta(\lambda)_2 d\lambda}{A\Omega \int_{\lambda_1}^{\lambda_1'} N_{\lambda 1}\ \beta(\lambda)_1 d\lambda} \tag{4-5}$$

is just the ratio of the radiant power onto the phototube in position (2) to the radiant power in position (1) when no gas is present. Substituting the power ratio at no gas concentrations, Equation 4-5, into Equation 4-2 gives the response of the instrument as

$$R = \alpha J \left[1 - e^{-(a_2 - a_1)cL} \cdot \phi(\xi)\right] \tag{4-6}$$

In this way, we divide the factors affecting the response of the instrument into two main categories, one depending on anything other than the gas under study, $\phi(\xi)$, and the other only on the gas chosen, cL. The function, $\phi(\xi)$, depends only on the spectral radiance of the source (N_λ) and the transmission $\beta(\lambda)$ of the instrument. Absorption due to any other gases and/or structure in the spectral distribution of the source can be grouped under the function N_λ.

We can see immediately that if $N_{\lambda 1}\beta(\lambda)_1 \equiv N_{\lambda 2}\beta(\lambda)_2$; i.e. $\phi(\xi) = 1$, then for α and J fixed, the response of the instrument will depend exclusively on cL and the particular values of a_2 and a_1.

In the general case that no gas is present (cL = 0), the reading is

$$R = \alpha J \quad [1 - \phi(\xi)] \tag{4-7}$$

and not zero, as we have shown before in a more general case. In both cases, this reading is the zero offset, present whenever $\phi(\xi) \neq 1$. It is worth noticing that this offset depends only on the ratio of the integrated spectral radiant powers incident on the phototube and is independent of the spectral distribution across their respective slit-defined wavebands. This, of course, does not apply to multiple slits, except in particular cases, as we shall see later.

The sensitivity is

$$\left| \left(\frac{\partial R}{\partial cL}\right)_{cL} \right| = \left| \alpha J \, (a_2 - a_1) \, e^{-(a_2 - a_1)cL} \, . \phi(\xi) \right| \tag{4-8}$$

For the variations of both R and $\frac{\partial R}{\partial cL}$ with cL, we consider

$(a_2 - a_1)$ $\begin{cases} < 0; & \text{average absorption coefficient in region (1) is greater than in region (2)} \\ = 0, & \text{average absorption coefficient in region (1) is equal to that in (2)} \\ > 0, & \text{average absorption coefficient in region (1) is smaller than in (2)} \end{cases}$

$$\phi(\xi) \begin{cases} < 1, & \text{background radiant power corresponding to region (1) is greater than in (2)} \\ = 1, & \text{background radiant power corresponding to region (1) is equal to (2)} \\ > 1, & \text{background radiant power corresponding to region (1) is smaller than in (2)} \end{cases}$$

Initially, let us assume that $(a_2 - a_1) > 0$ and $(a_2 - a_1) < 0$ have the same absolute value; therefore, they will be denoted as $(a_2 - a_1)$ (+) or $(a_2 - a_1)$ (-).

The case $(a_2 - a_1) = 0$ is equivalent to either

(a) no gas is present

(b) the gas is present but does not absorb

(c) the gas is present and absorbs equally in (1) and (2).

In either case, the gas chosen could not be detected using the two-position single-slit technique.

Case $\phi(\xi) < 1$

For $(a_2 - a_1)$ (+)

The zero offset is positive and equal to $\alpha J\,[1 - \phi(\xi)]$. With increasing cL, the reading increases according to

$$R = \alpha J \left\{ 1 - e^{-(a_2 - a_1)cL}_{\cdot(<1)} \right\}$$

The sensitivity $\frac{\partial R}{\partial cL} = \alpha J\,(a_2 - a_1)\, e^{-(a_2 - a_1)cL}_{\cdot(<1)}$ has a maximum when cL = 0 and decreases to zero.

For $(a_2 - a_1)$ (-)

The zero offset is positive and equal to $\alpha J\ [1 - (<1)]$. The reading first decreases to zero and then increases negatively without limit* according to

$$R = \alpha J \quad 1 - e^{|a_2 - a_1|.\ cL}.(<1)$$

The sensitivity $\alpha J\ |(a_2 - a_1)|e^{|a_2 - a_1|cL}.(<1)$ has a minimum for cL=0 and increases without limit.* See Figure 4-1.

Case $\phi(\xi) = 1$

For $(a_2 - a_1)$ (+) the zero offset is zero. By increasing cL, R increases until it reaches the asymptote at a value of αJ according to

$$R = \alpha J\left\{1 - e^{-(a_2 - a_1)cL}\right\}$$

The sensitivity has a maximum for cL = 0, and decreases according to

$$\alpha J\ (a_2 - a_1)\ e^{-(a_2 - a_1)cL}$$

For $(a_2 - a_1)$ (-) the zero offset is zero and the reading increases negatively with increasing cL according to

$$R = \alpha J\left\{1 - e^{|a_2 - a_1|cL}\right\} \qquad \text{(see Figure 4-2)}$$

The sensitivity has a minimum at cL = 0 and increases with cL according to

$$\alpha J\ \ |a_2 - a_1|\ e^{-|\ a_2 - a_1|cL}$$

*Physically, in the instrument either nonlinearity of the phototube response would be reached and/or electronic limiting of the output. Which concentration causes this phenomenon depends on the value of $|a_2 - a_1|$.

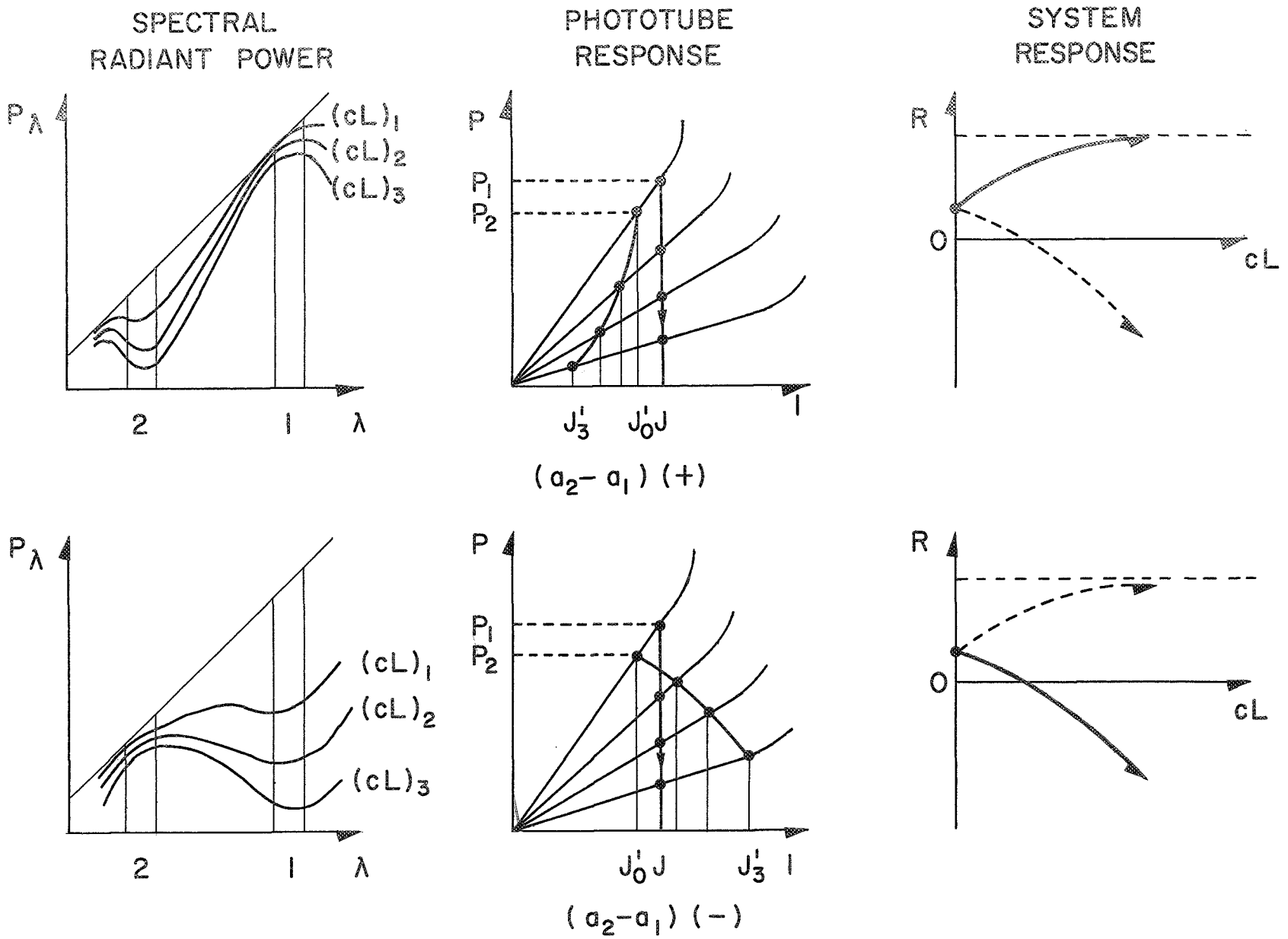

FIGURE 4-1

RESPONSE CURVES FOR $\phi(\xi) < 1$

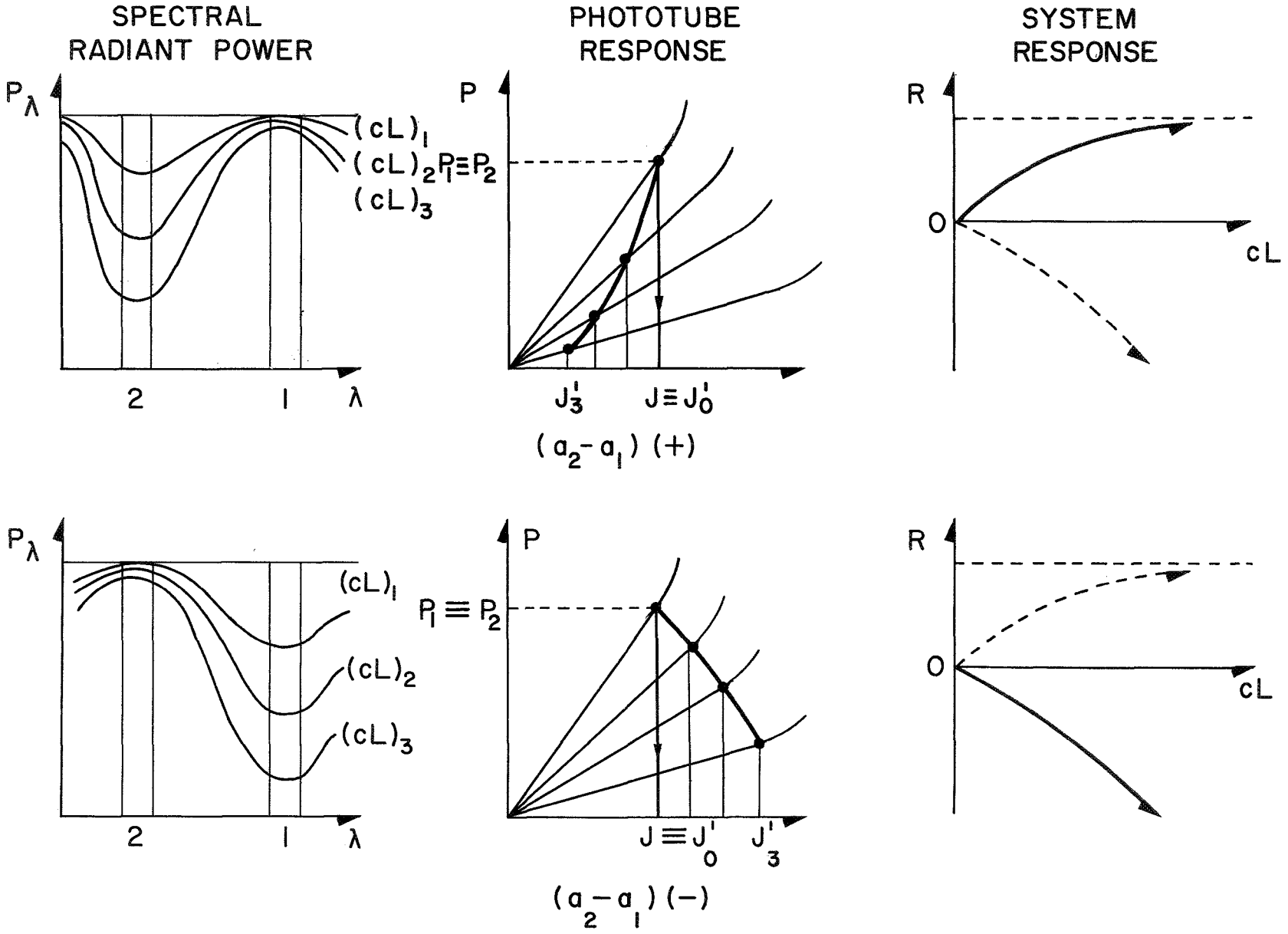

FIGURE 4-2

RESPONSE CURVES FOR $\phi(\xi) = 1$

Case $\phi(\xi) > 1$

For $(a_2 - a_1)$ (+)

The zero offset is negative and equal to $\alpha J[1 - (>1)]$. By increasing cL, it becomes zero and then increases according to

$$R = \alpha J \left\{ 1 - e^{-(a_2 - a_1)cL}_{.(>1)} \right\}$$ as shown in Figure 4-3

The sensitivity has a maximum for cL = 0, and decreases according to

$$\alpha J \ (a_2 - a_1) \ e^{-(a_2 - a_1)cL}_{.(>1)}$$

For $(a_2 - a_1)$ (-)

The zero offset is negative and the reading increases negatively with increasing cL according to

$$R = \alpha J \left\{ 1 - e^{|a_2 - a_1|cL}_{.(>1)} \right\}$$

The sensitivity has a minimum at cL = 0 and increases with cL according to

$$\alpha J \ \ |a_2 - a_1| \ e^{\ |a_2 - a_1|cL}_{(>1)}$$

In general, there exists an entire family of curves similar to the ones shown, for each value of $\phi(\xi)$ and $(a_2 - a_1)$.

With respect to $(a_2 - a_1) < 0$, as soon as cL exceeds a certain value, [dependent of the value of $(a_2 - a_1)$] the instrument becomes non-linear. We shall consider only the case $(a_2 - a_1) > 0$ now. Any reading taken in this case, will be denoted a "single-sided" measurement. The $(a_2 - a_1)$ (-) case will be studied later, in Section 7 on double-sided measurements.

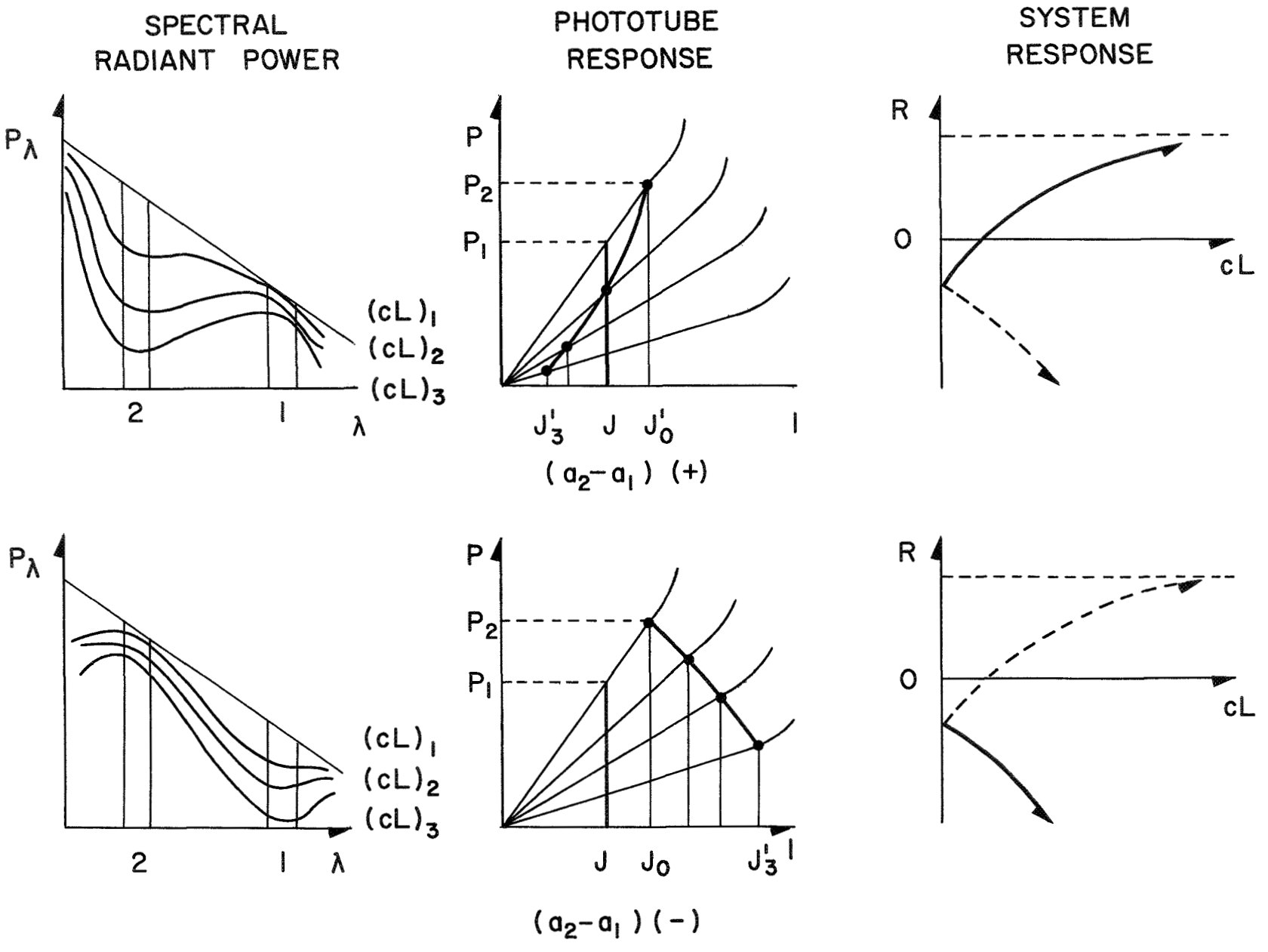

FIGURE 4-3

RESPONSE CURVES FOR $\phi(\xi) > 1$

From the analysis of Figures 4-1 , 4-2 and 4-3 , we find that the most sensitive combination for measuring with a single slit is $\phi(\xi)>1$ and $(a_2 - a_1) > 0$ (in the single-sided measurement). Within this whole family of responses, the maximal occurs when both $\phi(\xi)$ and $(a_2 - a_1)$ have maximum values. When the slit samples in the highest absorption and the highest transmission wavelength of the absorption spectrum of the gas under study, and $\phi(\xi)$ has the proper value, the maximum sensitivity to the chosen gas achievable with this type of instrument is obtained. The discrimination, however, is not very good since any small change in $\phi(\xi)$ will seriously affect the reading.

It would appear that once N_λ, $\beta(\lambda)$ and $a(\lambda)$ are known, we could use the remaining parameters $\Delta\lambda$ and δ [which determine $\phi(\xi)$ and $(a_2 - a_1)$] in order to produce any response curve that might be desired. This is possible but only within the limits imposed by the mutual dependence of $a(\lambda)$, N_λ, and $\beta(\lambda)$ on wavelength λ. The study of the sensitivity and discrimination leading to the optimization of the instrument is based on that fact.

In summary, the zero offset from a single slit depends on the presence of other absorbing gases and/or structure in the spectral distribution of the light source. These determine the value of $\phi(\xi)$. If any amount of the chosen gas is present and $\phi(\xi)$ is not known, the cL of this gas is not calculable and its effect has to be included as part of the zero offset. Nevertheless, by proper calibration, any value of cL above the one that could already be present in the zero offset can be determined, but only if $\phi(\xi)$ does not change (at least during the time of calibration and measurement).

The single-slit study is very illustrative, since it readily yields the analytical expression of the response curves, in contrast to the more involved process of the multiple slit mask.

Electronic Output of the Spectrometer

At this time, a brief description of the behaviour of the electronic output is appropriate.

The gain control can affect either α or J as desired. In the instrument, α, the load impedance, is the readily controllable parameter although J can also be changed.

The peak-to-peak instrument output is (+Ve) to (-Ve), the limiting value Ve being fixed by the electronic circuit design.

Let us first assume that the instrument is zeroed with its absolute zero readout, that there are no absorbing gases and that there is a flat background filter-optics spectral distribution (i.e., $N_\lambda \cdot \beta(\lambda)$, is a constant over the waveband interval).

Figure 4-4 represents the instrument in this state; the solid line represents a possible response curve, with a zero-concentration offset. Two sets of axes are superimposed, the (+Ve, -Ve, cL) set and the (R, cL) set. As previously mentioned, the total distance from +Ve to -Ve remains fixed, the change of gain (through either α or J) modifies the vertical scaling of the (R, cL) curve, as shown in Figure 4-5. Thus, the gain controls change the relative amplitude of R versus cL.

The offset control moves the axis set (+Ve, -Ve, cL) up or down, in such a fashion that the response curve can be brought to an all positive or all negative output, the same effect as produced by moving the zero to point 0' of Figure 4-6. Sometimes the value of αJ may be such that for a certain value of cL, the response exceeds the possible voltage output of the instrument, as shown at point L of Figure 4-6. In this situation the instrument is limiting and either a change of gain or an offset is necessary in order to bring the response back within the output range (+Ve, -Ve).

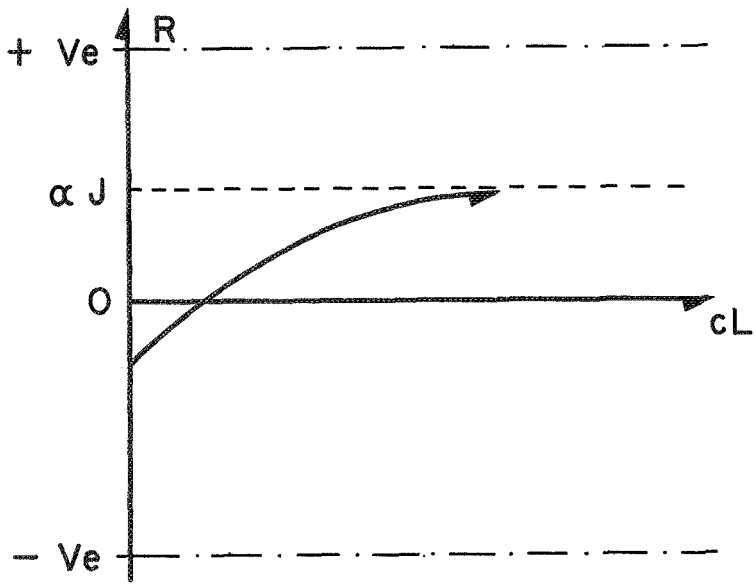

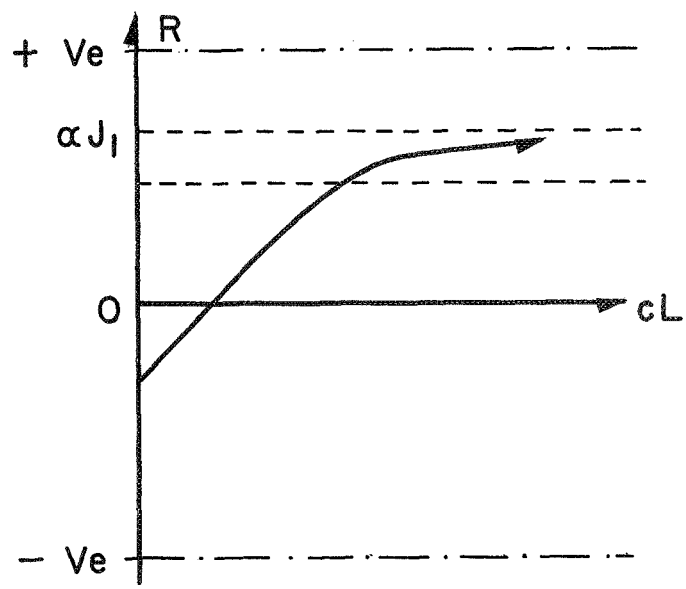

FIGURES 4-4, 4-5, & 4-6
VARIATION OF RESPONSE WITH GAIN
AND ZERO OFFSET CONTROLS

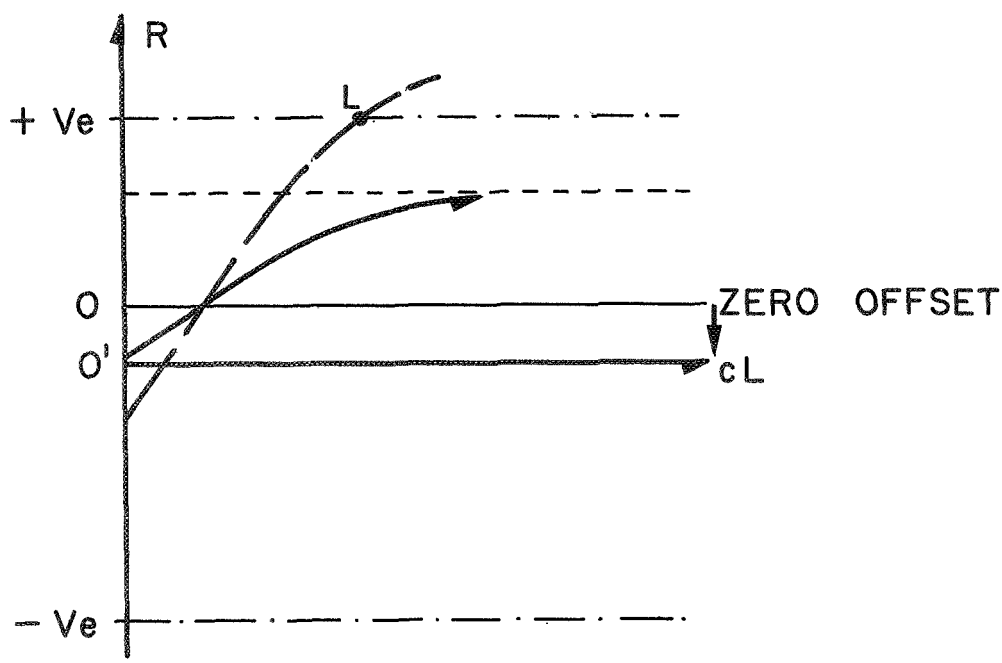

5. ANALYSIS OF THE MULTIPLE-SLIT SIGNAL

As we have seen, the single-slit response can be very sensitive to the chosen gas. Nevertheless, under the presence of unknown amounts of other absorbing gases and/or structure in the spectral distribution of the light source, it is highly unspecific. This is so, because the effects of other absorbing gases and/or structure, when they are time-varying, will cause fluctuations in the value of $\phi(\xi)$. These fluctuations, of course, could easily be mistaken as genuine signals caused by the variation of the gas concentration.

In the multi-slit or mask, each of the slits has its own $\phi(\xi)$ and $(a_2 - a_1)$. Therefore, by proper handling of the instrument parameters, one can expect to optimize the instrument response for the desired gas under a wide range of conditions.

The response of the multi-slit system

$$R = \alpha J \left\{ 1 - \frac{\sum_{i=1}^{n} \int_{\lambda_{2i}}^{\lambda'_{2i}} N_\lambda \, \beta(\lambda) \, e^{-a(\lambda)cL} \, d\lambda}{\sum_{i=1}^{n} \int_{\lambda_{1i}}^{\lambda'_{1i}} N_\lambda \, \beta(\lambda) \, e^{-a(\lambda)cL} \, d\lambda} \right\} \qquad (5\text{-}1)$$

can be analyzed for several simple cases.

The first and simplest case was studied in Section 3, Equations 3-17 and 3-18. The second case is when $N_\lambda \, \beta(\lambda)$ remains a constant $(\overline{N_o B_o})$ over the total waveband defined by the mask and jump, while the absorption coefficient varies with wavelength.

In this case expression 5-1 becomes:

$$R = \alpha J \left\{ 1 - \frac{\sum_{i=1}^{n} e^{-a_{2i} cL} \Delta\lambda_i N_o \beta_o}{\sum_{i=1}^{n} e^{-a_{1i} cL} \Delta\lambda_i N_o \beta_o} \right\} = \alpha J \left\{ 1 - \frac{\sum_{i=1}^{n} e^{-a_{2i} cL} \Delta\lambda_i}{\sum_{i=1}^{n} e^{-a_{1i} cL} \Delta\lambda_i} \right\}$$

And, if we further assume that the width of each slit is the same

$$R = \alpha J \left\{ 1 - \frac{e^{-a_{21} cL} + e^{-a_{22} cL} + \cdots e^{-a_{2n} cL}}{e^{-a_{11} cL} + e^{-a_{12} cL} + \cdots e^{-a_{1n} cL}} \right\} \qquad (5\text{-}2a)$$

$$= \alpha J \frac{\sum_{i=1}^{n} (e^{-a_{1i} cL} - e^{-a_{2i} cL})}{\sum_{i=1}^{n} e^{-a_{1i} cL}} \qquad (5\text{-}2b)$$

Thus, the response, R, depends exclusively upon the average value of $a(\lambda)$, for each slit corresponding to the positions (1) and (2) of the mask. In this situation which particular slit has the largest effect on the signal will depend upon which value of cL exists. The a's with high value will dominate the low concentration signal since the difference of the terms in the numerator when both a and cL are low will effectively be one minus one or zero. When cL exceeds a certain value, some of the absorption bands with high a's might be completely washed out. The difference term, then, for these exponentials would go to zero, leaving the signal dominated by the bands with low values of a. In this case, the response function might not be monotonic but could be double valued, since the same value of R might be reached at two very different values of cL. In the case of SO_2, this effect occurs (see Figure 5-1), and it has been called saturation. The same process is nevertheless, inherent to any gas whose absorption bands behave similarly to those of SO_2. As shown in Figure 5-2 when cL exceeds a few

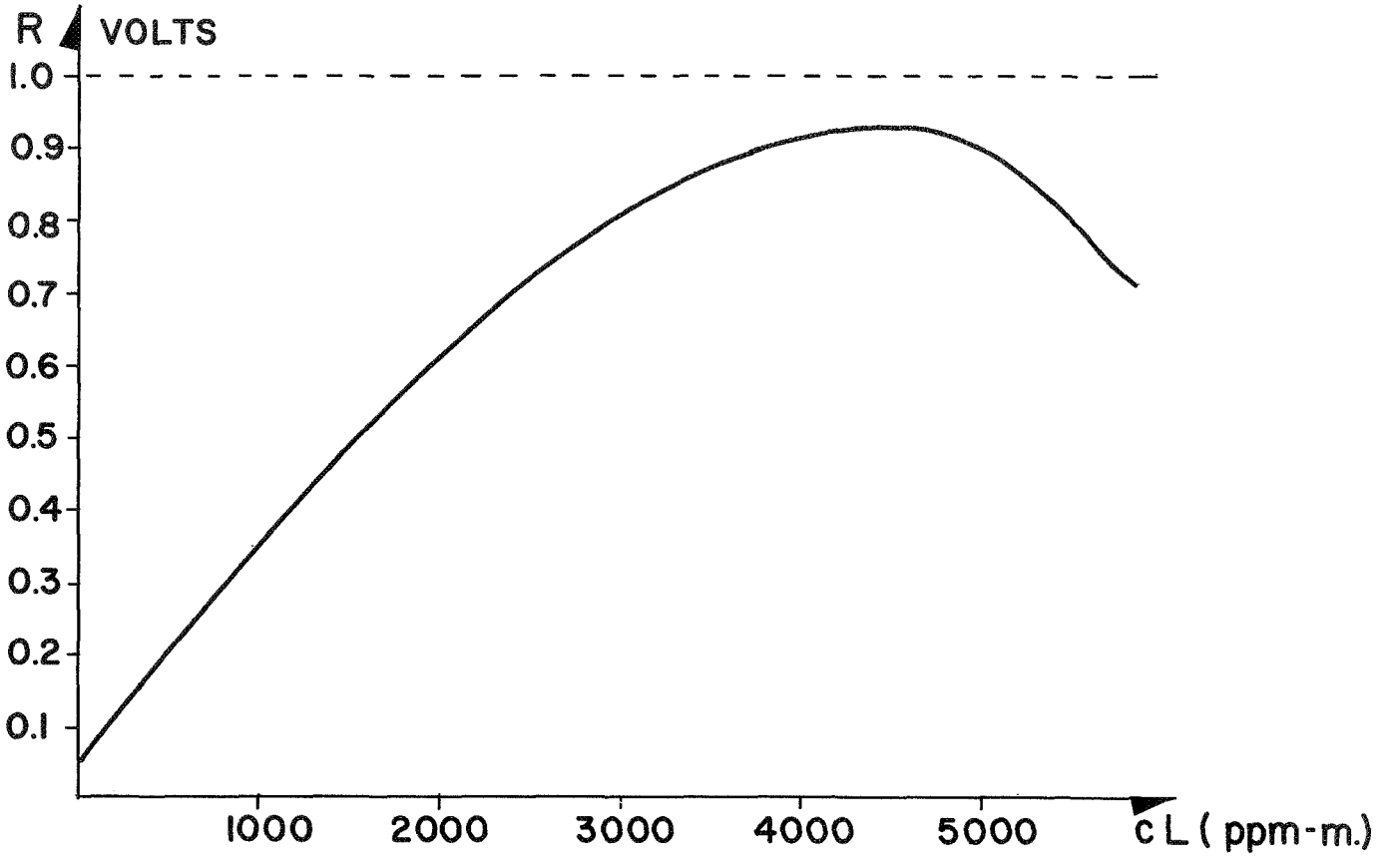

FIGURE (5-1)
RESPONSE CURVE SHOWING EFFECT OF
"SATURATION"

FIGURE 5-2
TRANSMISSION CURVES FOR TWO DIFFERENT
CONCENTRATIONS OF SO_2

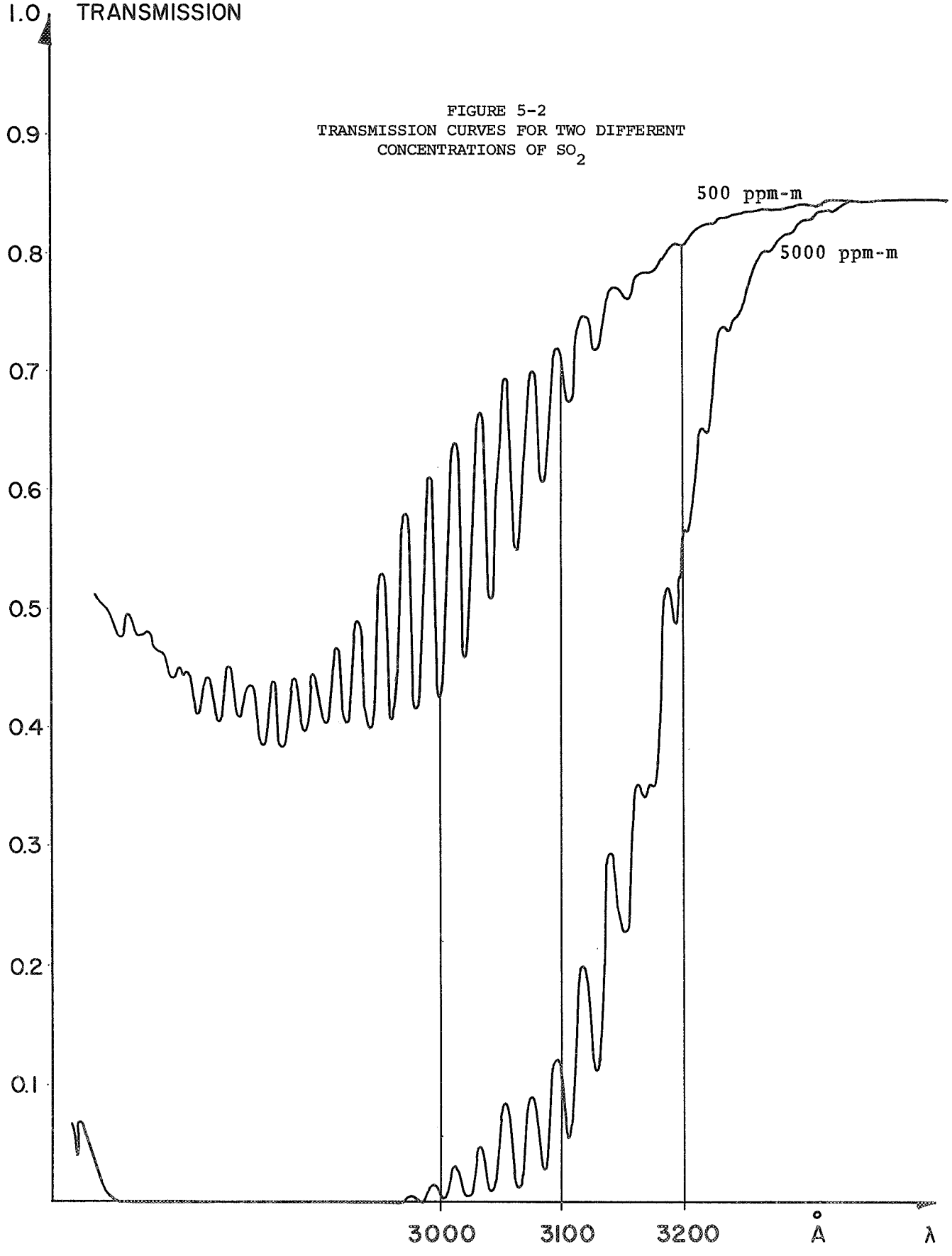

thousand (ppm-m), the lower wavelength bands are completely washed out and the signal is dominated by the bands above 3100 Å.

Saturation is avoided by using the different mask filter combinations to measure different ranges of concentrations (see Figure 5-3).

A third case is chosen in order to illustrate the influence of the background spectral distribution. We consider a linear variation of N_λ.

In this case we will assume:

(a) N_λ is linear, i.e. $N_\lambda = N_a + m\lambda$ (Figure 5-4)

(b) The average absorption coefficient is the same for each slit of the mask: a_1 for position (1) and a_2 for position (2).

(c) The response of the filter-optics transmission function $\beta(\lambda)$ is constant and equal to β_o.

(d) All the slit widths are the same and equal to Δ.

(e) The amplitude of the jump is equal to -2Δ.

If positions (1) and (2) are the ones shown in Figure 5-4

$$R = \alpha J \left\{ 1 - e^{-(a_2 - a_1)cL} \quad \frac{\sum_{i=1}^{n} \int_{\lambda_{2i}}^{\lambda'_{2i}} N_\lambda \, d\lambda}{\sum_{i=1}^{n} \int_{\lambda_{1i}}^{\lambda'_{1i}} N_\lambda \, d\lambda} \right\}$$

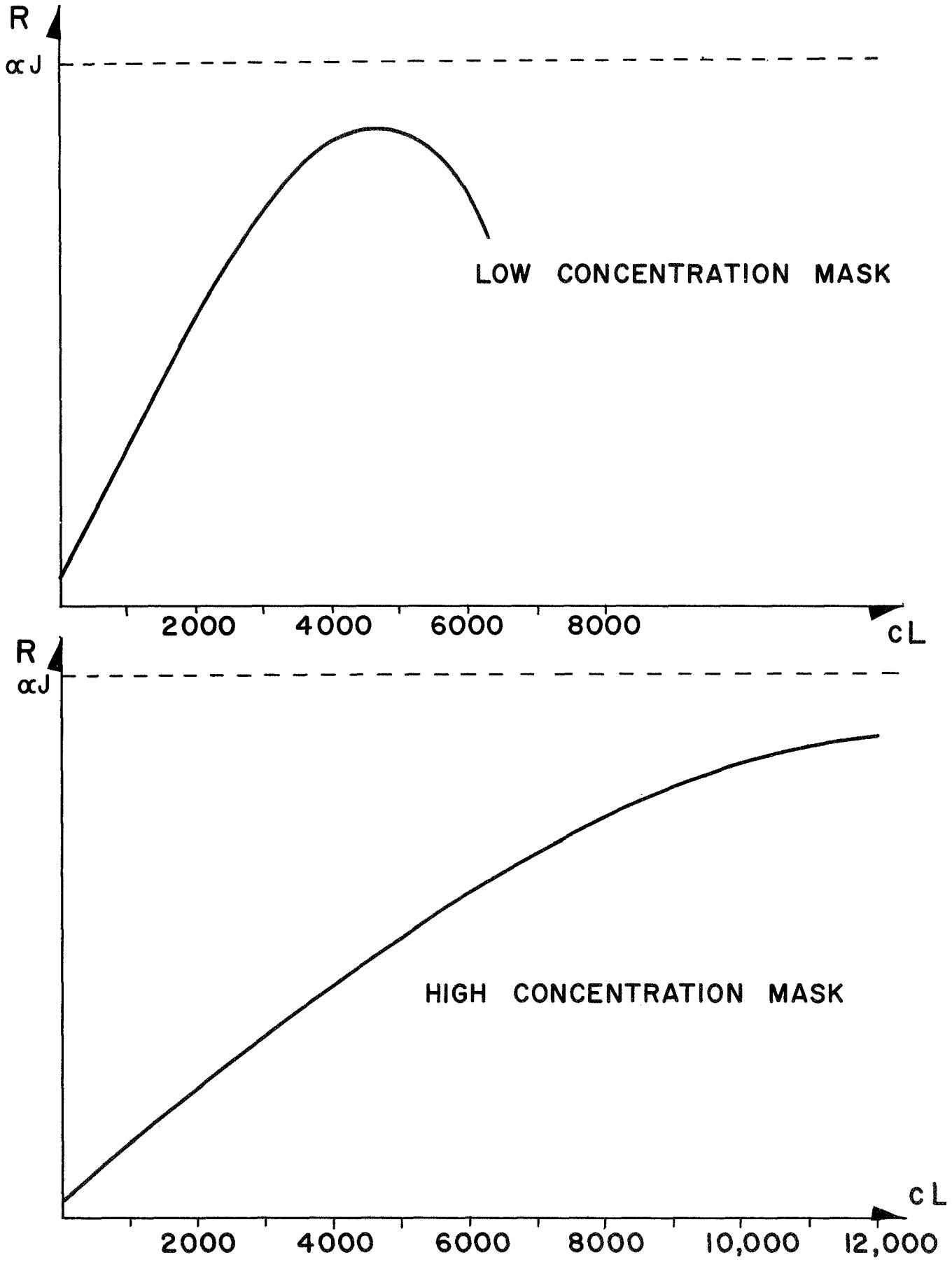

FIGURE 5-3
TYPES OF RESPONSES THAT CAN BE OBTAINED
WITH DIFFERENT MASKS

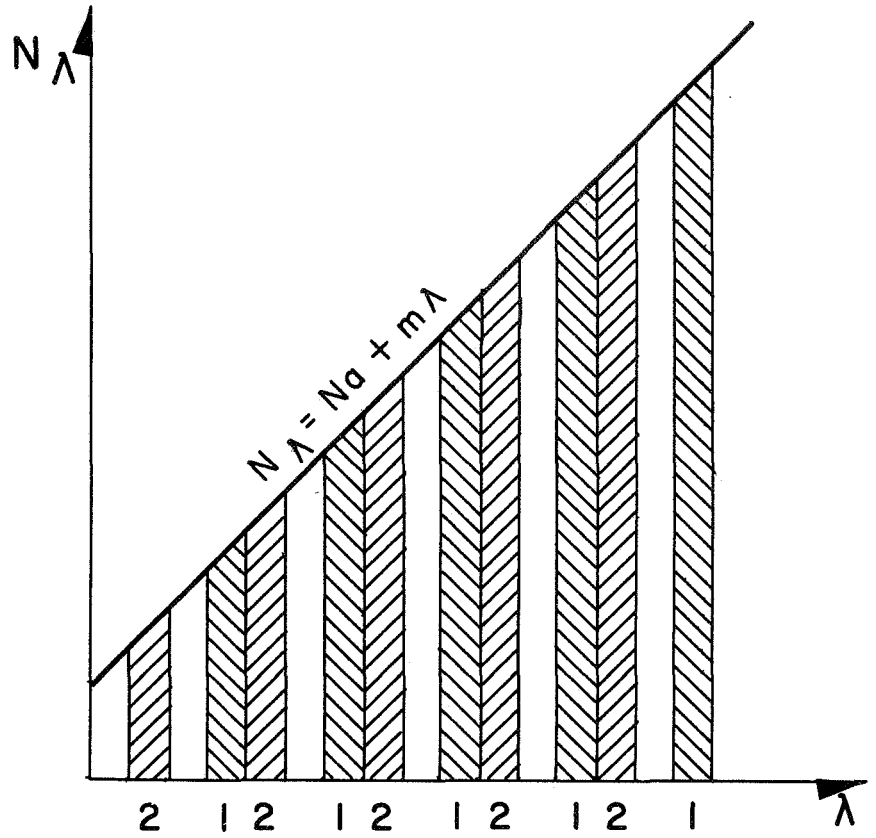

FIGURE 5-4
LINEAL SPECTRAL DISTRIBUTION,
ALL SLITS BEING USED

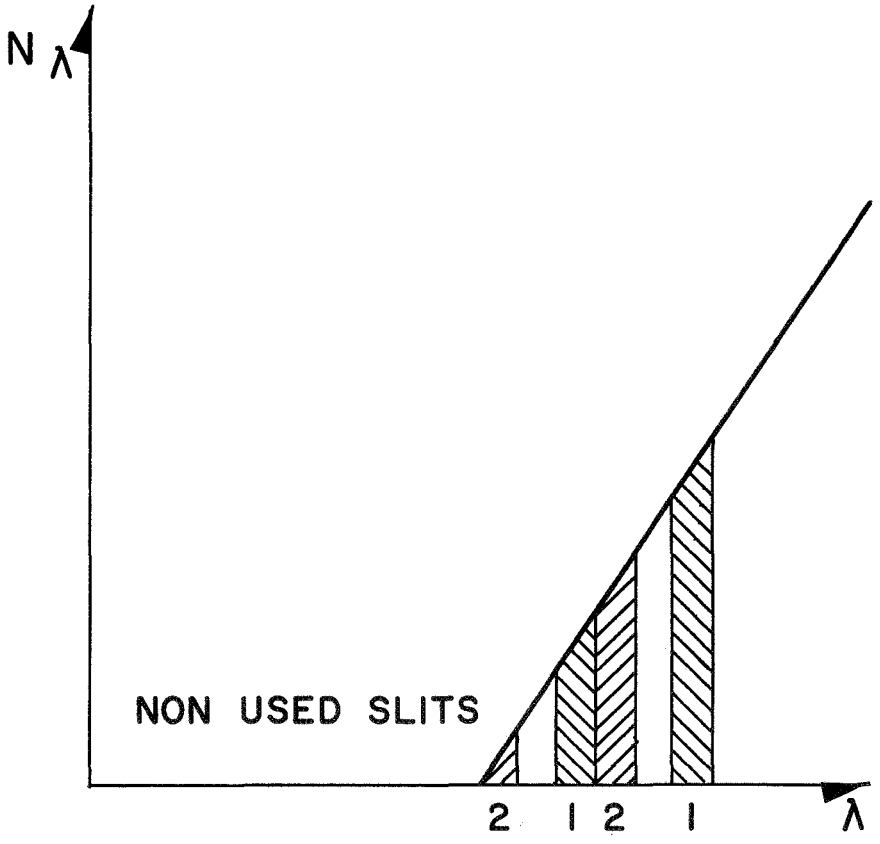

FIGURE 5-5
LINEAL SPECTRAL DISTRIBUTION
WITH NON-USED SLITS

but $$\sum_{i=1}^{n} \int_{\lambda_{2i}}^{\lambda'_{2i}} N_\lambda \, d\lambda = \int_0^{\Delta} (N_a + m\lambda)d\lambda + \int_{3\Delta}^{4\Delta} (N_a + m\lambda)d\lambda + \cdots \int_{3(n-1)\Delta}^{[3(n-1)+1]\Delta} (N_a + m\lambda)d\lambda$$

$$= n\Delta N_a + \frac{m}{2}\Delta^2\left\{1 + 7 + \cdots [6(n-1)+1]\right\} = n\Delta N_a + m\Delta^2 n[3n-2]$$

and $$\sum_{i=1}^{n} \int_{\lambda_{1i}}^{\lambda'_{1i}} N_\lambda \, d\lambda = \int_{2\Delta}^{3\Delta} (N_a + m\lambda)d\lambda + \int_{5\Delta}^{6\Delta} (N_a + m\lambda)d\lambda + \cdots \int_{(3n-1)\Delta}^{3n\Delta} (N_a + m\lambda)d\lambda$$

$$= n\Delta N_a + \frac{m}{2}\Delta^2[5 + 11 + (6n-1)] = n\Delta N_a + m\Delta^2 n[3n+2]$$

The response is

$$R = \alpha J\left\{1 - e^{-(a_2 - a_1)cL} \cdot \frac{N_a + m\Delta(3n-2)}{N_a + m\Delta(3n+2)}\right\}$$

If the positions (1) and (2) are reversed

$$R = \alpha J\left\{1 - e^{+(a_2 - a_1)cL} \cdot \frac{N_a + m\Delta(3n+2)}{N_a + m\Delta(3n-2)}\right\}$$

Thus, for $cL = 0$, $$\Psi(\xi) = \frac{N_a + m\Delta(3n\pm2)}{N_a + m\Delta(3n\mp2)}$$

When the spectral distribution is very steep ($m \to \infty$),

$\Psi(\xi)$ oscillates between $\left\{\begin{matrix} \frac{3n-2}{3n+2} \\ \frac{3n+2}{3n-2} \end{matrix}\right.$, and if we consider

6 slits, $\Psi(\xi)$ oscillates between $\left\{\begin{matrix} 0.8 \\ 1.25 \end{matrix}\right.$ and the zero offset, between $\left\{\begin{matrix} 0.2\ \alpha J \\ -0.25\ \alpha J \end{matrix}\right.$

Notice that $\psi(\xi)$ in this case represents the overall effect of the individual values $\phi(\xi)$ of each slit. It has sense only with respect to zero concentration, (zero-offset reading), because, as we have seen in the single slit case, the separation of the response factors into two parts, one affected by the gas characteristics and the other by the remaining system parameters, is generally not possible due to the mutual dependence of a (λ), $\beta(\lambda)$ and $N(\lambda)$ on wavelength (λ). Nevertheless, for properly calculated masks ~~under~~ certain circumstances, such as short ranges of concentrations, and when all a_1's and a_2's are well behaved, it will be possible to express the reading in the form:

$$R = \alpha J \left\{ 1 - e^{-\bar{a}cL} \psi(\xi) \right\} \qquad (5\text{-}3)$$

where, when $cL = 0$, $\psi(\xi)$ is defined by $\psi(\xi) = 1 - \frac{R}{\alpha J}$

and $\bar{a}$ is the value describing the total effect of all $(a_2 - a_1)$'s.

The variation of $\psi(\xi)$ with the background spectral distribution can be studied for the case just treated. If N_a is large, variations of m or steepness of the spectral distribution do not seriously affect the reading. When N_a becomes increasingly small, but not zero, the zero offset still remains well-behaved; it starts to seriously affect the readings only when N_a is zero and part of the mask becomes non-used as shown in Figure 5-5. The most severe case occurs when only a single slit remains; under these circumstances, the $\psi(\xi)$ of our example could oscillate between 0.2 and 5, with a corresponding uncertainty in the reading.

The reason for choosing $\delta = 2\Delta$ and $n = 6$ is that one of the most frequently used masks for the detection of SO_2 in the ultraviolet has 6 slits of equal width (6 Å) with a jump of 12 Å. The spacings are not the same, but are close enough to the regular spacing of the example just treated that the analysis becomes meaningful, in this case, when using the sky as a light source in the 3000 Å to 3150 Å waveband. We may find that under some circumstances (morning or afternoon at different times of the year) there is no available short ultraviolet; thus, the partial mask problem occurs.

In Figure 5-6 we show three calibration readings of SO_2. In the last two, very steep spectral distributions and low N_a occur. Notice that the distance between asymptotes in the first two curves is approximately 0.2, which agrees with the figure of $\psi(\xi) = 0.8$ previously found. (The zero offset equal to 0.2 αJ has been zeroed for the calibration.) The last curve, run later on in the afternoon, would indicate the partial mask problem with probably only 4 slits in use. The advantage of the mask is obvious in this example, since the zero offset (and thus the response) remains well behaved even for extreme and rapidly varying conditions.

In the most general case, the response of the multi-slit instrument will be a combination of all cases. The typical response curves will have the same general pattern of Figures 4-1, 2, 3 but because the $\phi(\xi)$'s will have different values, and the $(a_2 - a_1)$'s different values and/or signs for different slits, the response curve will be less exaggerated. For each particular case the response curve could be calculated by numerical computation or obtained by experimental means.

The calculations of cL of the gas chosen (above that which could be present in the zero offset) can be performed. When a calibration curve is run "at a given time" under prevailing conditions and based on the well-behaved zero offset, the value of any unkown cL can be found by interpolation. If the light source is the sky, the calibration curve will vary with time, therefore requiring a new calibration for each measurement.

6. SENSITIVITY AND DISCRIMINATION

The response curve of the multi-slit or mask system is not as readily available analytically as was that of the single slit system. Thus, the sensitivity and incremental sensitivity are better studied by inspection of the response curves. These can be obtained numerically, experimentally or by a combination of both means.

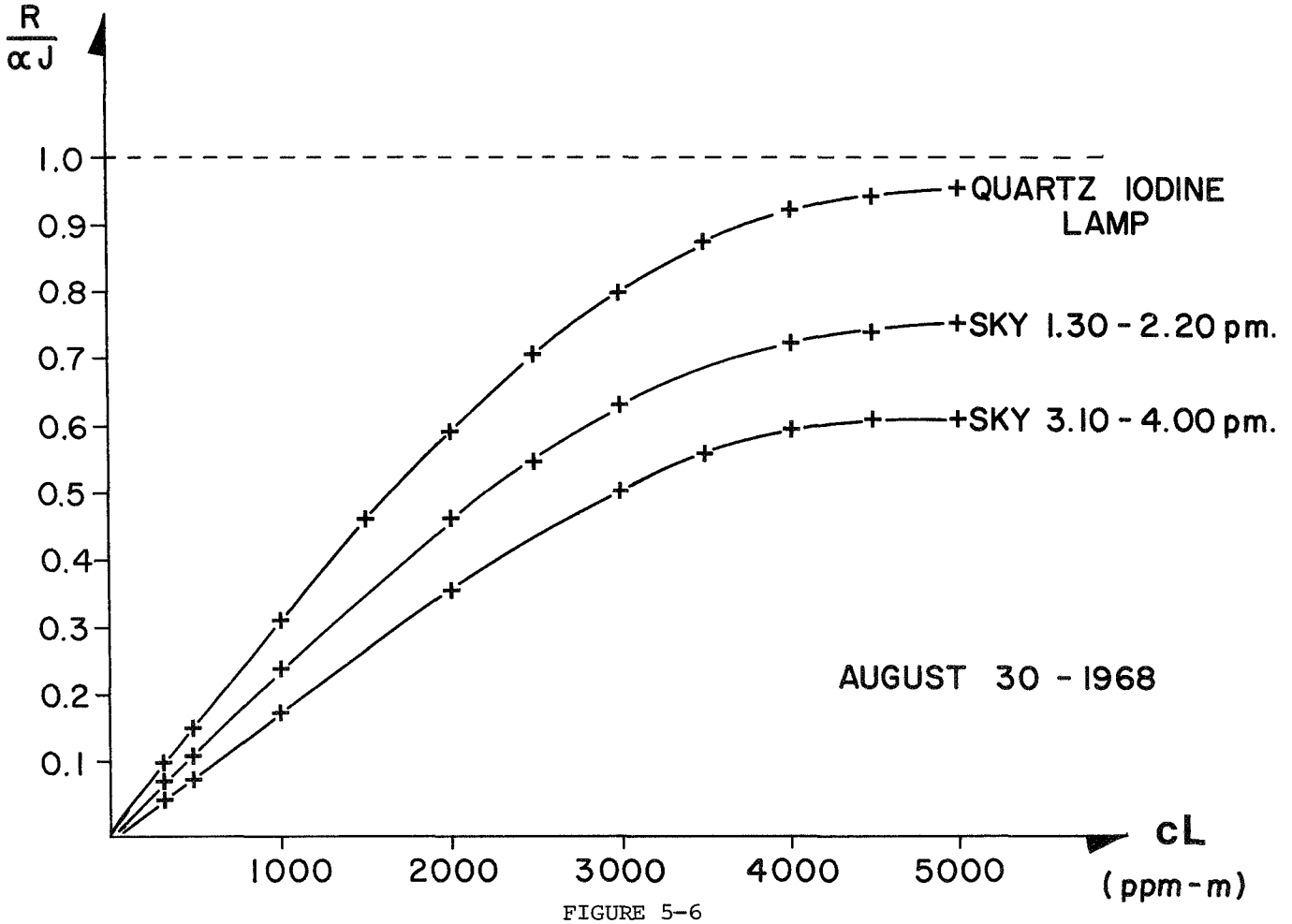

FIGURE 5-6
VARIATION OF THE RESPONSE CURVE WITH
CHANGES IN BACKGROUND SPECTRAL RADIANCE

As we have seen, the response of the instrument with the following conditions:

(a) The light proceeds from a source of spectral radiance N_λ (W cm^{-2} sr^{-1} nm^{-1}) uniform over the field of view of the instrument.

(b) The medium through which the light travels is uniform in constitution (cL's constant).

(c) The medium absorbs but does not scatter

is:

$$R = \alpha J \left\{ 1 - \frac{\sum_{i=1}^{n} \int_{\lambda_{2i}}^{\lambda'_{2i}} N_\lambda \, \beta(\lambda) \, e^{-I(\lambda)} \, e^{-a(\lambda) cL} \, d\lambda}{\sum_{i=1}^{n} \int_{\lambda_{1i}}^{\lambda'_{1i}} N_\lambda \, \beta(\lambda) \, e^{-I(\lambda)} \, e^{-a(\lambda) cL} \, d\lambda} \right\} \qquad (6\text{-}1)$$

where

$$e^{-I(\lambda)} = e^{-b_1 c_1 L_1} \cdot e^{-b_2 c_2 L_2} \text{ etc.}$$

describes the effect of any other absorbing gases present in the medium, possessing absorption bands or spectral structure in the waveband selected for the chosen gas. (In the previous sections, these were assumed to be integrated with N_λ.)

$b_i(\lambda)$ absorption coefficient of the gas species i.
$c_i L_i$ concentration x pathlength of gas species i.

Given these parameters, together with N_λ, the cL of the gas chosen can be calculated between the light source and the instrument. Unfortunately, in a real-life situation the presence of other gases is not necessarily known, and although some gases are known to be present, their cL's are not known.

In facing the problem of measuring the cL of the gas under these circumstances, we shall first recount the system parameters that we know or can control. These are:

$a(\lambda)$ Absorption coefficient of the chosen gas at a given temperature and pressure.

$\beta(\lambda)$ The transmission function, fixed for a given instrument, optics and filter. In general the transmission of the optics is fairly constant with wavelength within the waveband of interest; therefore, $\beta(\lambda)$ will represent the particular optical filter function in use. The choice of $\beta(\lambda)$ is somewhat limited because of the difficulty in the manufacturing of interference filters to exact specification. Although not quite controllable during manufacturing for each filter, $\beta(\lambda)$ can be known subsequently very accurately in digital form. This together with $a(\lambda)$, constitutes the main determinants of that region of the spectrum that is best for a particular gas.

n Number of slits.

$\Delta\lambda_i$ Width of slit i.

δ "Jump" or displacement of the spectrum with respect to the slits.

N_λ The spectral radiance; it can be known as accurately as $\beta(\lambda)$ or a (λ)if the light source is controlled. If controlled, N_λ determines an active system. When the instrument is intended to be used with sun or skylight, N_λ will in general not be known accurately and it would determine a passive system. Because of the obvious differences between them, we will study these separately.

6.1 COMPUTED RESPONSE OF AN ACTIVE SYSTEM USING A CONTROLLED LIGHT SOURCE

Equation 6-1 has been transformed into a computer program with the following inputs:

(a) Absorption coefficient of the main gas $a(\lambda)$.
(b) Transmission function of the filter $\beta(\lambda)$.
(c) Transmission coefficient of the optical system.
(d) Spectral radiance of the light source N_λ.
(e) Absorption coefficient of up to five possibly interfering gases $b_i(\lambda)$.
(f) Number of slits, n.
(g) Integers defining the slits.
(h) Amplitude of the jump.

The absorption coefficients of the gases $a(\lambda)$, $b_i(\lambda)$, and also $\beta(\lambda)$ are obtained with a CARY RECORDING SPECTRO PHOTOMETER MODEL 14 with higher resolution than the spectrometer of the remote sensor. The absorbances of the gases are obtained from known amounts of gas sealed in reference cells (Figure 6-1, 6-2). The selected positions of the traces of the CARY 14 are expanded and digitized every 2 Å. N_λ is known from the manufacturer of the light source. It is important to notice that unless the photon noise of the phototube is to be determined, relative values of N_λ are sufficient, since the theoretical response Equation 6-1 corrects for multiplicative factors. To determine the response of the instrument, the following steps are taken:

(a) By means of an independent search, the gases most likely to interfere in their worst concentrations, and the range of cL of the chosen gas are found.

(b) The absorption coefficients, filter functions and N_λ between the chosen wavelengths are digitized, indexed and entered into the program.

(c) By visual inspection of the absorbance trace of the gas under study and its filter function, one selects several sets of possibly useful absorption bands.

(d) The index numbers corresponding to the $a(\lambda)$ of these bands are chosen to make the possibly useful slits, and to determine the slit widths.

(e) The average distance from the absorption peaks to the maximum transmission peaks in a number of index integers is measured.

(f) The worst expected concentrations of the interfering gases are entered.

(g) The computer program is run with all the possible combinations of the previously found values:

The computer output yields the cL of the chosen gas versus

$R/\alpha J$, P_1 and P_2

where
$$P_1 = \sum_{i=1}^{n} \int_{\lambda_{li}}^{\lambda'_{li}} N_\lambda \, \beta(\lambda) \, e^{-I(\lambda)} \, e^{-a(\lambda)cL} \, d\lambda$$

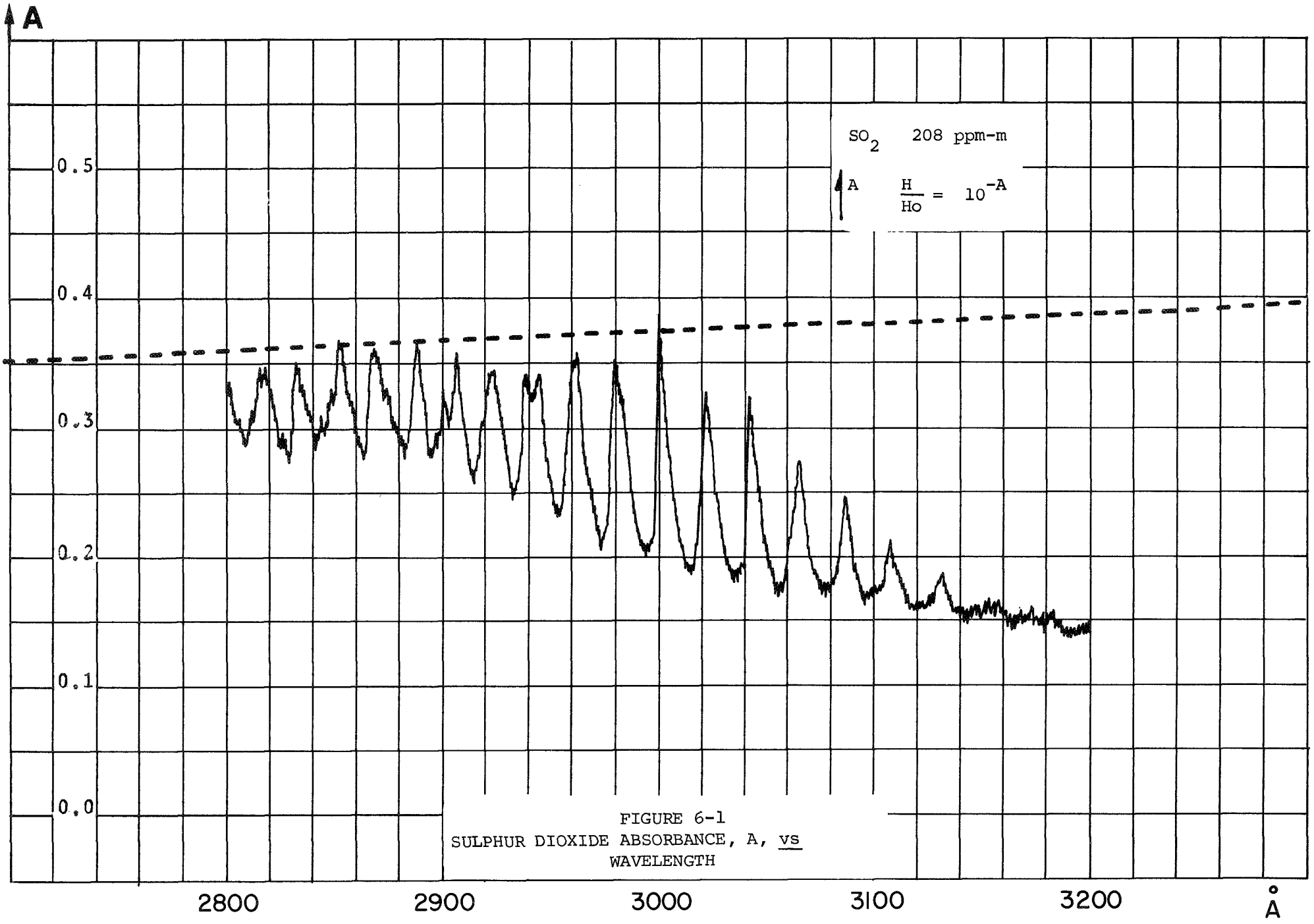

FIGURE 6-1
SULPHUR DIOXIDE ABSORBANCE, A, vs
WAVELENGTH

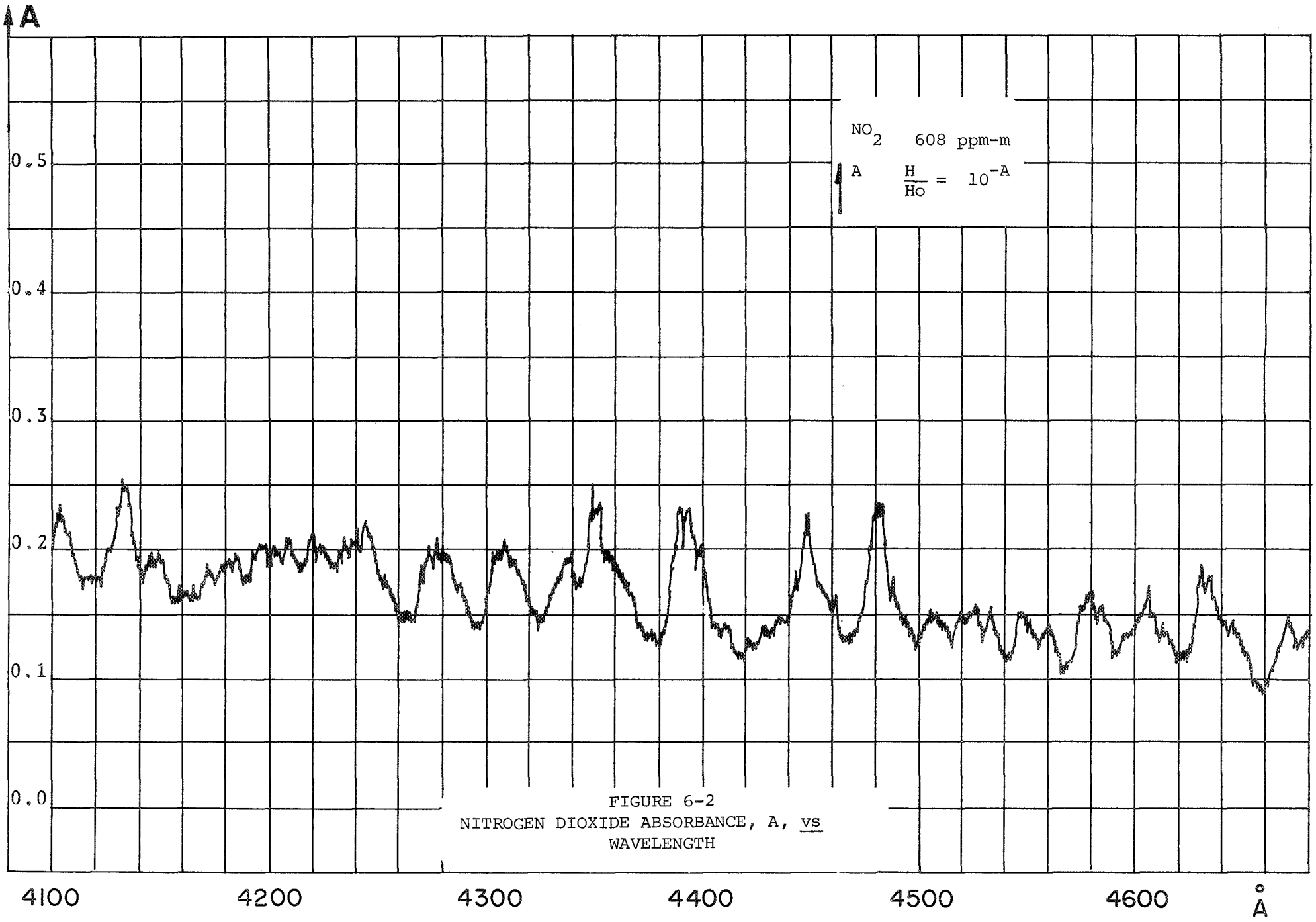

FIGURE 6-2
NITROGEN DIOXIDE ABSORBANCE, A, vs
WAVELENGTH

and

$$P_2 = \sum_{i=1}^{n} \int_{\lambda_{2i}}^{\lambda'_{2i}} N_\lambda \, \beta(\lambda) \, e^{-I(\lambda)} \, e^{-a(\lambda)cL} \, d\lambda$$

If the absolute values of N_λ are entered in [W cm^{-2} sr^{-1}(2 $\mathring{A}^{-1}$)], the multiplication P_1 and P_2 by $A\Omega$ will give the number of Watts incident on the phototube in both positions (1) and (2). These values are used to calculate the photon noise of the phototube.

The different response curves are plotted and studied. By this process the proper combination of numbers of slits, their widths, positions and amount of the jump can be determined for the waveband of interest. The effect on $R/\alpha J$ of the interfering gases and/or structure of the light source, may determine the elimination of slits, the change of widths, the inclusion of new slits, changes in the jump magnitude, and/or, in the ultimate case, the change of filter or of spectral region. Once the whole process is finished and the system parameters determined, a "worst expected condition" response curve for the predetermined range of concentrations of the chosen gas is obtained, Figure 6-3.

Another curve is obtained for $c_i L_i = 0$, in order to find the response of the instrument to the optics-filter-light source combination, Figure 6-3.

By comparing both, we find the two zero offsets, one with no interference and the other with the interference. Their difference represents the expected limit of uncertainty in the response to the gas and thus determines the sensitivity and expected error in the measurement. When dealing with a controlled light source this error can be made very small.

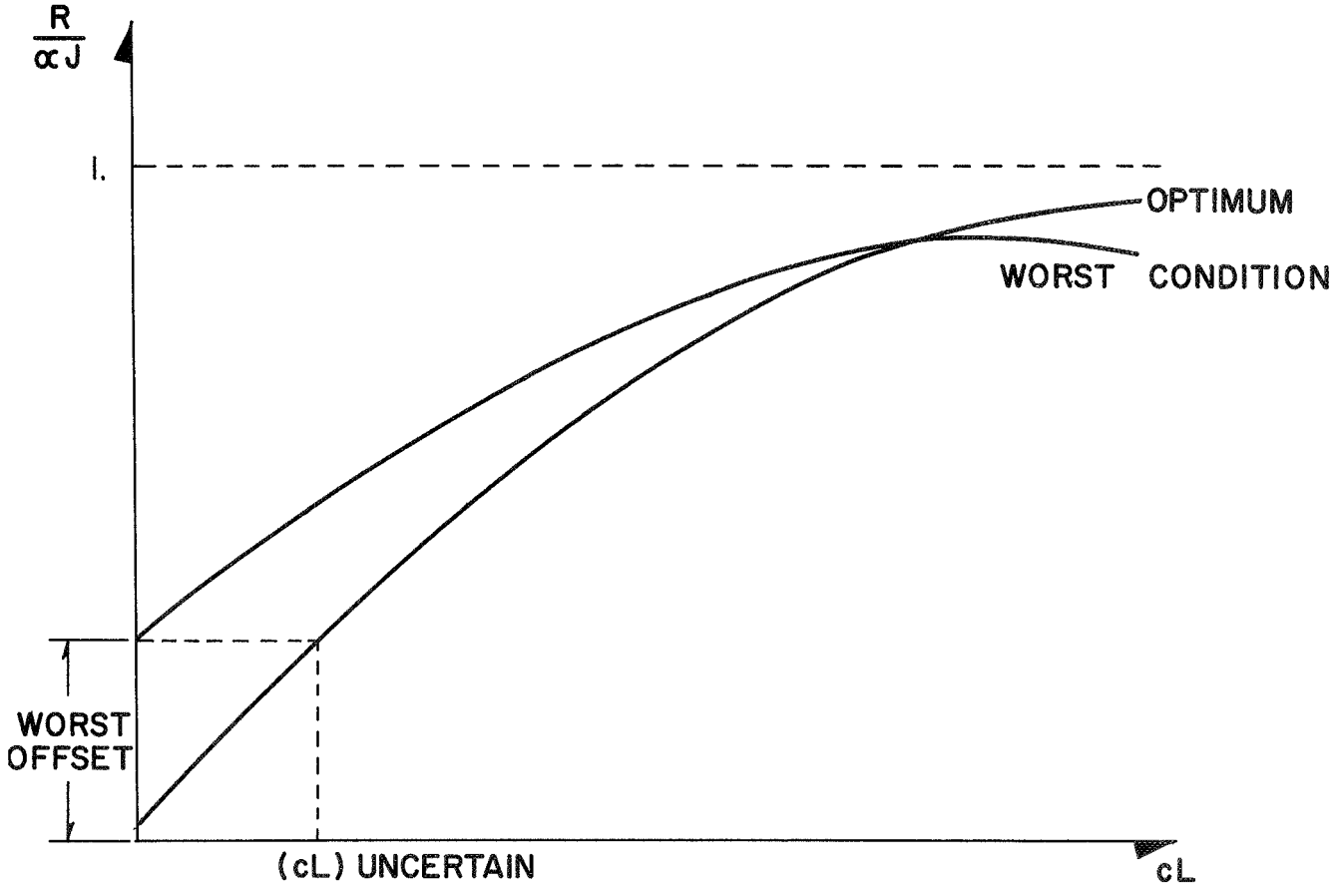

FIGURE 6-3
RESPONSE CURVES UNDER OPTIMUM
LABORATORY CONDITIONS AND UNDER
WORST SPECTRAL BACKGROUND
INTERFERENCE

6.2 COMPUTED RESPONSE OF A PASSIVE SYSTEM USING DAYLIGHT

When using daylight as the source, N_λ is not accurately known, since it will change with season, time of the day, turbidity of the atmosphere, part of the sky used, etc. The intensity and structure will, in general, change from time to time. These facts can be more or less successfully modelled, determining different "standard" background spectral distributions to be entered into the program.

The same process as before is then used in order to obtain the system parameters. The process is lengthier because of the different N_λ's, and in this mode, according to the response curves obtained, drastic limitations on the use of the instrument (weather, time of day, etc.) may be imposed, if the allowable error in the measurement is to be kept under certain limits. By proper calibration of the instrument at the time of measurement, cL's above those that could be present in the zero offset can be measured.

This method of optimization and measurement can be very useful; there are further means of optimizing the response, sensitivity and discrimination by knowing how the interfering parameters are affecting these qualities and by knowing the proper combination of theoretical and experimental work.

7. THE DOUBLE-SIDED MEASUREMENT

In Section 4 the response curves for $(a_2 - a_1)$ (+) and (-) were obtained for a single slit, and in Section 5 we mentioned that although not as easily obtainable in an analytical form, the multislit or mask response follows the same basic patterns.

For a moment we will assume again that we have a single slit instrument. The slit is jumping with respect to the spectrum between two fixed positions; these two positions determine the $(a_2 - a_1)$ and $\phi(\xi)$ of the instrument's response curve. The types of curves that can be obtained were shown in Figures (4-1,2,3).

Consider one of the $(a_2 - a_1)$ (+) cases; if the value of $(a_2 - a_1)$ were to be changed from $(a_2 - a_1)$ (+) to $(a_2 - a_1)$ (-), the response for the same concentration would move from point A in the $(a_2 - a_1)$ (+) curve to point A' in the $(a_2 - a_1)$ (-) curve. If $\phi(\xi)$ and $|a_2 - a_1|$ remain unchanged from curve to curve, the distance AA' is the double-sided response of the system to the concentration cL, rather than the single-sided response $\overline{OA}$ under previous conditions (see Figure 7-1). $\overline{AA'}$ would depend exclusively on cL and more importantly, the variation of the response for a change of $\phi(\xi)$ would be less pronounced for the double-sided measurement than for the single sided. This can be demonstrated as follows:

Consider the one sided measurement $\overline{OA} = \alpha J \left\{ 1 - e^{-(a_2 - a_1)cL} \cdot \phi(\xi) \right\}$ (7-1)

and the double sided measurement:

$$\alpha J \left\{ 1 - e^{-|a_2 - a_1|cL \ \phi(\xi)} \right\} - \alpha J \left\{ 1 - e^{|a_2 - a_1|cL \phi(\xi)} \right\}$$

$$\overline{AA'} = 2 \alpha J \ \phi(\xi) \ \sinh \ (|a_2 - a_1|cL) \qquad (7\text{-}2)$$

Assume that $\phi(\xi)$ changes by a fraction r; thus

$$\phi(\xi) = (1+r) \ \phi(\xi) = \rho \ \phi(\xi)$$

$(\overline{OA})_1$ becomes $\alpha J \left\{ 1 - e^{-(a_2 - a_1)cL} \cdot \phi(\xi) \ \cdot \rho \right\}$ and

$(\overline{AA'})_1$ becomes $2\alpha J \rho \cdot \phi(\xi) \ \sinh (|a_2 - a_1|cL)$

The percentage errors between the new and the previous values, defined as

$$\frac{R_2 - R_1}{R_1} \cdot 100\% \text{ are:}$$

for the single-sided measurement:

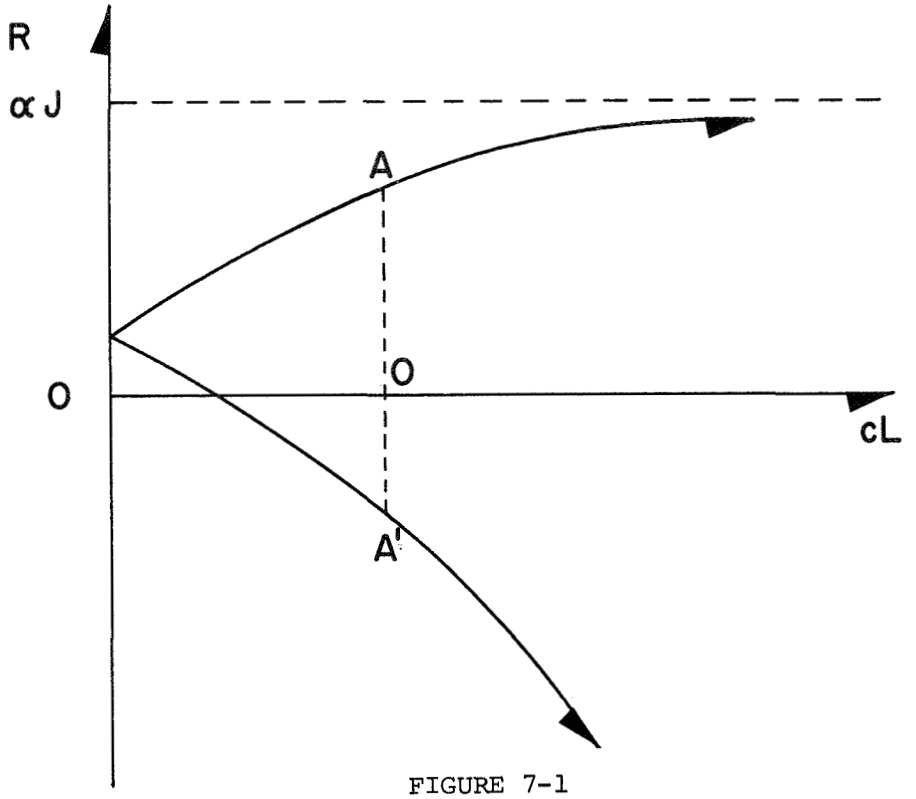

FIGURE 7-1

TWO SIDES OF THE RESPONSE CURVE,
OA FOR $(a_2 - a_1)$ (+)
and
OA' FOR $(a_2 - a_1)$ (-)

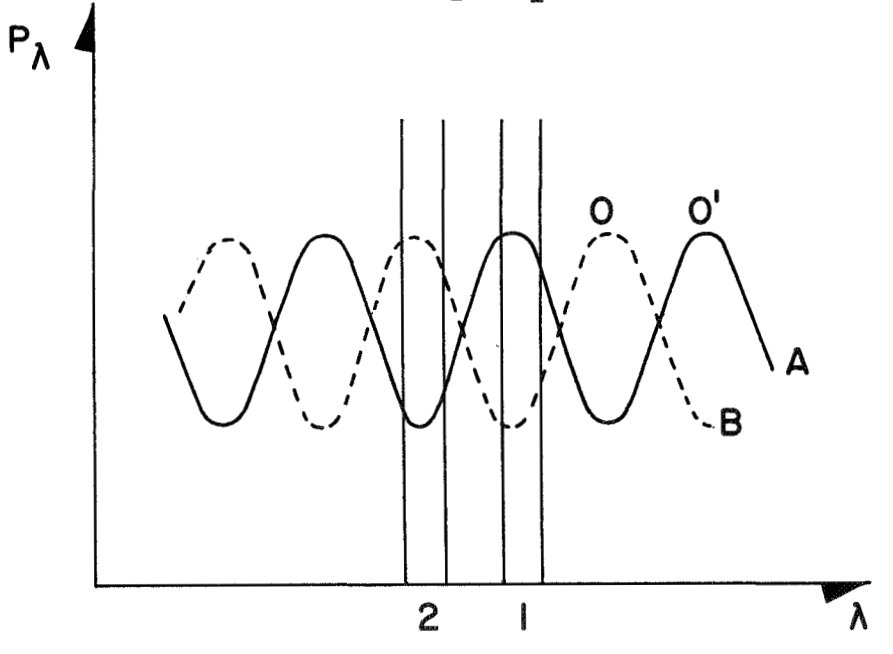

FIGURE 7-2

SHIFT OF THE POWER SPECTRUM $\overline{O\ O'}$,
PRODUCING A DOUBLE-SIDED RESPONSE

$$= \frac{1 - e^{-(a_2 - a_1)cL}.\phi(\xi).\rho - [1 - e^{-(a_2 - a_1)cL}\phi(\xi)]}{1 - e^{-(a_2 - a_1)\phi(\xi)}} \cdot 100$$

$$= \frac{r \cdot \phi(\xi) \cdot e^{-(a_2 - a_1)cL}}{\phi(\xi)\, e^{-(a_2 - a_1)cL} - 1} \cdot 100\% \qquad (7\text{-}3)$$

if $\phi(\xi) = 1$ the percentage error change in the measurement due to a percentage change of $\phi(\xi)$ is extreme for low values of cL.

if $\phi(\xi) > 1$ the same occurs at a value of $cL = \frac{\ln \phi(\xi)}{(a_2 - a_1)}$

if $\phi(\xi) < 1$ the percentage error change is also greater than (r) for low values of cL.

and for the double-sided measurement:

the percentage error is r, that is, the one imposed by the change in $\phi(\xi)$.

Thus, in the double-sided measurement the percentage error in the measurement would be that imposed by the variation of $\phi(\xi)$, regardless of the initial values of $(a_2 - a_1)$, cL or $\phi(\xi)$, while in the single-sided measurement, the ratio is a complicated function of these variables.

As a numerical example, let us consider that initially $\phi(\xi) = 1$ and $e^{(a_2 - a_1)cL} = 0.8$, for an increase in $\phi(\xi)$ of 10%, that is $\phi_1(\xi) = 1.1\ \phi(\xi)$.

The single-sided reading has changed

from $\frac{R}{\alpha J} = \{1 - 0.8\} = 0.2$ to $\frac{R_1}{\alpha J} = \{1 - 0.88\} = 0.12$, that is, a percentage change of (40%),

while the double-sided reading has changed by only 10%.

From observation of equation 7-3, it can be seen that high cL are desired for minimum error due to background effects in the single-sided measurement. Thus, single-sided measurements should be used only when measuring high values of cL. In the multiple slit, where $\psi(\xi)$ is much better behaved with regard to background and/or interference fluctuations, the effect is less pronounced, but the conclusion still applies. On the other hand, the double-sided measurement is the optimum when trying to measure low concentrations with the least background interference.

So far, we have not yet shown how to produce the double-sided measurement. The basis of its function is the following: Referring to Figure 7-2, let us first assume that the slit is sampling in positions (1) and (2), which correspond to the relative maximum and minimum transmission in the spectrum respectively. If the spectrum is displaced by an amount $\overline{0'0}$ by grating rotation to position B, the slit will sample between a relative maximum absorption in position (1) and a relative maximum of transmission in position (2). Because position (1) in the instrument controls the phototube voltage, from the slit point of reference a_2 and a_1 have interchanged values and $(a_2 - a_1)$ has changed sign. Therefore, as the spectrum passes through the jumping slit, the response to a fixed cL will lie on the corresponding curve of the $(a_2 - a_1)$ family, determined by the local $(a_2 - a_1)$ value for the slit. The double-sided measurement is the distance between the responses of any two of the curves of the family. When $|a_2 - a_1|$ is a maximum, the full deflection double-sided measurement is obtained. In particular cases, this full deflection is neither necessary nor wanted.

Considering the case cL = 0, the distance $\overline{AA'}$ would be zero if $\phi(\xi)$ remained constant through all the spectral scan. This usually does not occur, and we should generalize the previous definition of $\overline{AA'}$ to the distance between the responses of any two of the $\phi(\xi)$, $(a_2 - a_1)$ family curves determined by the local values of $\phi(\xi)$ and $(a_2 - a_1)$ for the position of the spectrum with respect to the jumping slit.

In this general case, when going from one curve to the other, $(a_2 - a_1)$ may not only have changed sign but also relative value, and $\phi(\xi)$ will have a changed value as well. This fact gives rise to three main possibilities, namely:

when $(a_2 - a_1)$ changes value and/or sign and

(a) $\phi(\xi)$ does not change.

(b) $\phi(\xi)$ increases from $(a_2 - a_1)$ (+) curve to $(a_2 - a_1)$ (-) curve; then separation takes place (see Figure 7-3a).

(c) $\phi(\xi)$ decreases from $(a_2 - a_1)$ (+) curve to $(a_2 - a_1)$ (-) curve; then cross over takes place (see Figure 7-3b).

Note: By definition, in the double-sided measurement it is not necessary that $(a_2 - a_1)$ change sign, but only that they change value. In Figure 7-3, any horizontal lines are $(a_2 - a_1) = 0$ curves with their corresponding value of $\phi(\xi)$, as ordinate.

If the transition between two predetermined end points, i.e., AA', is registered (as the spectrum slowly passes the jumping slit) by means of a recorder connected to the output of the instrument, cross-over on separation can take place between any two intermediate positions, aa' independent of the situation for the two end points.

In Figure 7-4a, a particular transmission function, $\beta(\lambda)$, is shown $[\beta_1(\lambda)\ ]$. The solid line in Figure 7-4b represents the unscanned function $N_\lambda \beta_1(\lambda)\ e^{-a(\lambda)cL}$ when cL = 604 ppm-m of SO_2. $\beta(\lambda)$ is the same as $\beta_1(\lambda)$, and N_λ is flat over the waveband of interest. Referring again to the case cL = 0, the graph of the recorder will represent the result of scanning $N_\lambda \beta(\lambda)$ (in the absence of other gases) past the "jumping" slit. The response would be $\alpha J\{1 - \phi(\xi)\}$, that is, the variation of the zero offset from one end of $N_\lambda \beta(\lambda)$ to the other. Figure 7-5a represents the single slit scan of $\beta_1(\lambda)$ [Δ= 6 Å, δ = 12Å]. The abscissa is the

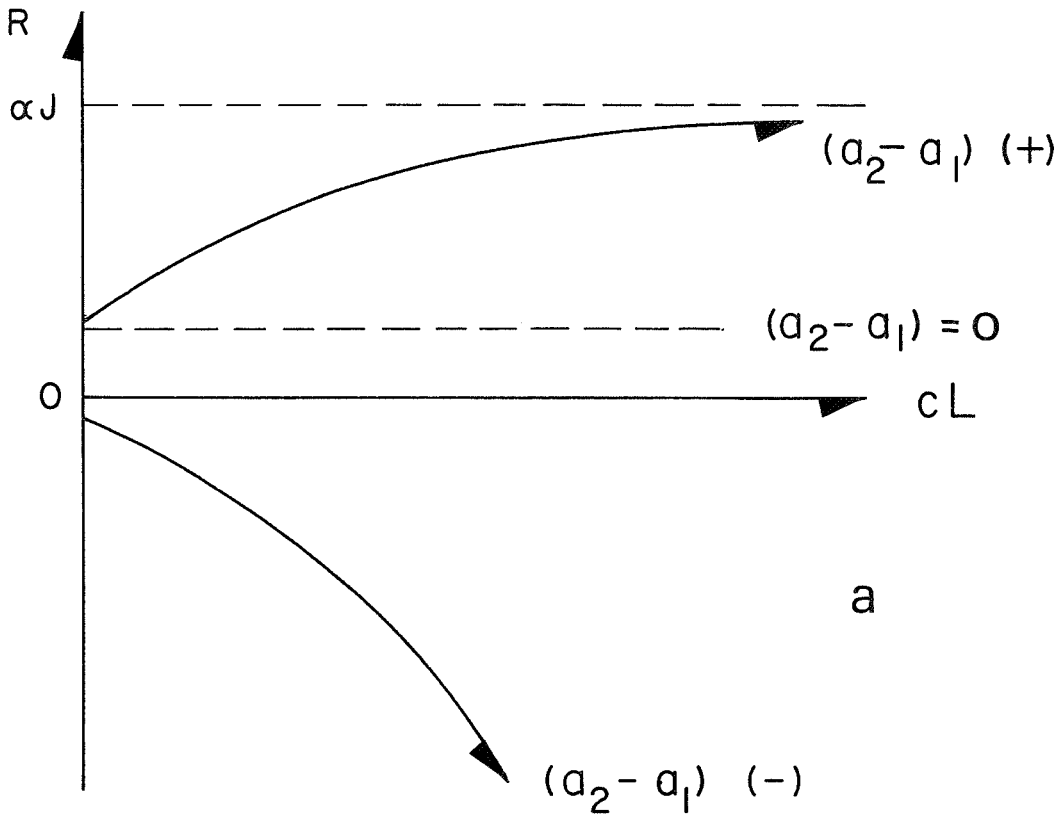

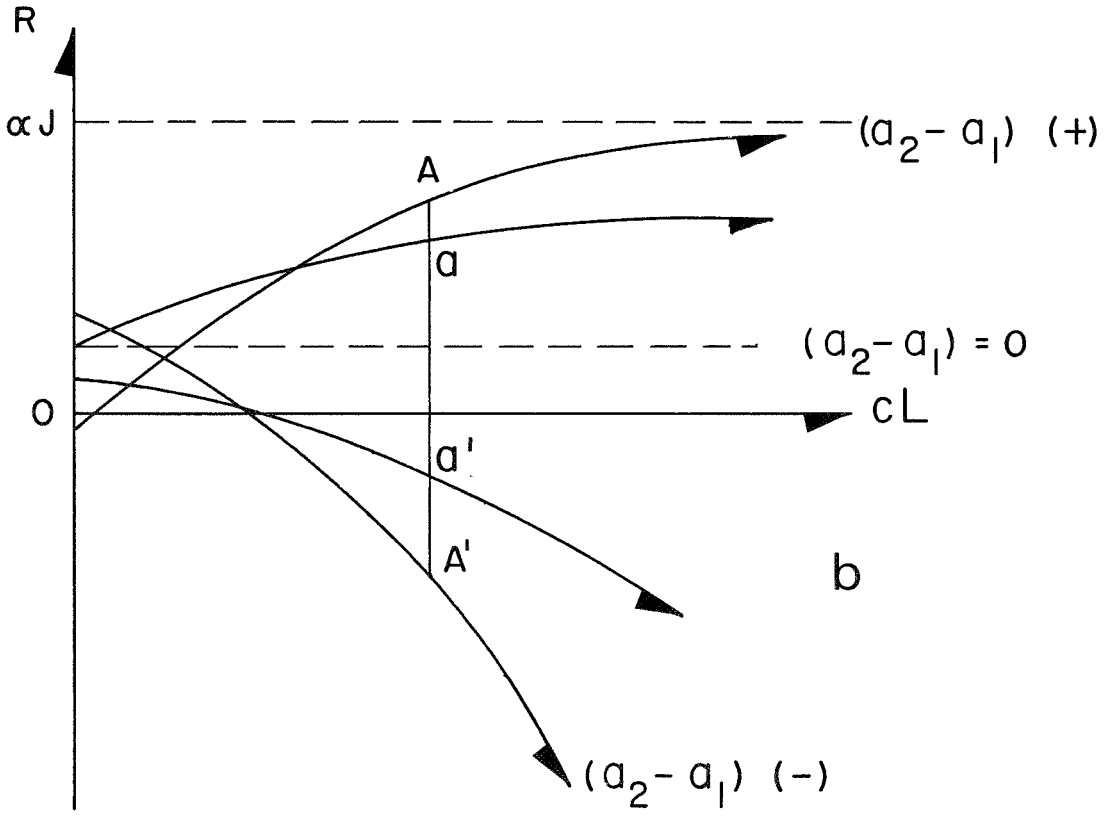

FIGURE 7-3
a) RESPONSE SEPARATION
b) RESPONSE CROSS OVER
SEPARATION IN THE LAST ONE ALSO
OCCURRED FOR A LIMITED SCAN a a'

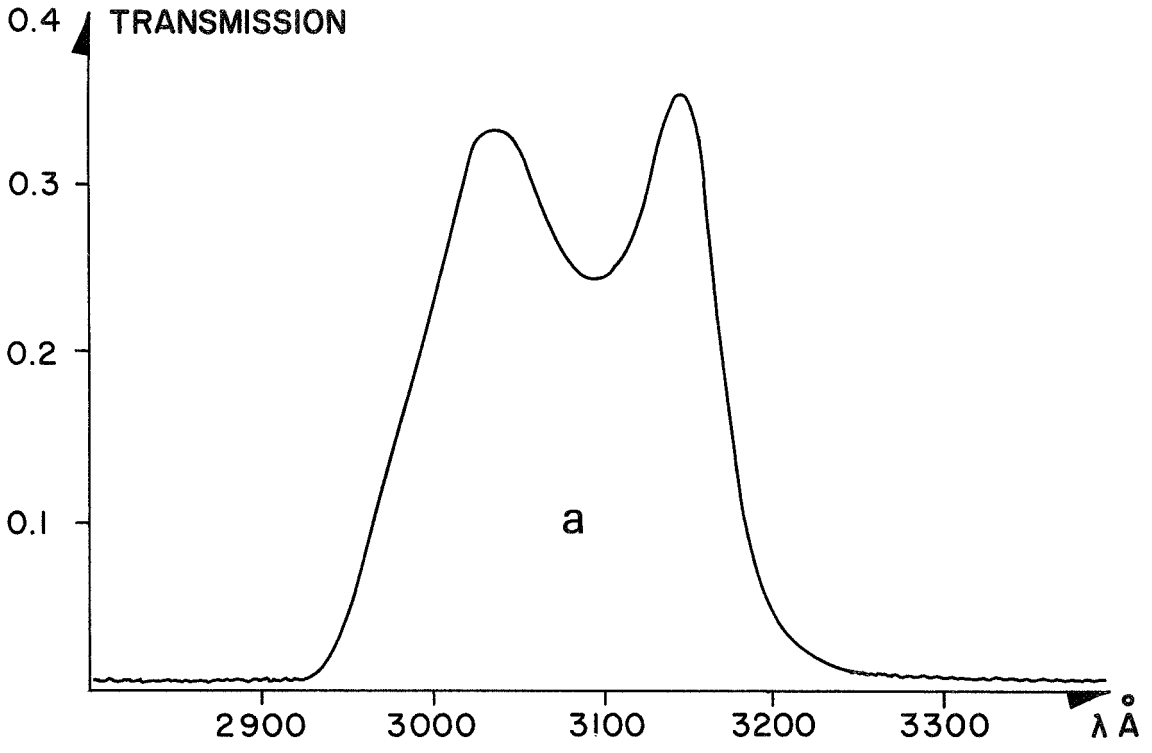

FIGURE 7-4
a) TRANSMISSION FUNCTION $\beta_1(\lambda)$ OF A TYPICAL FILTER USED IN THE ULTRAVIOLET REGION OF THE SPECTRUM

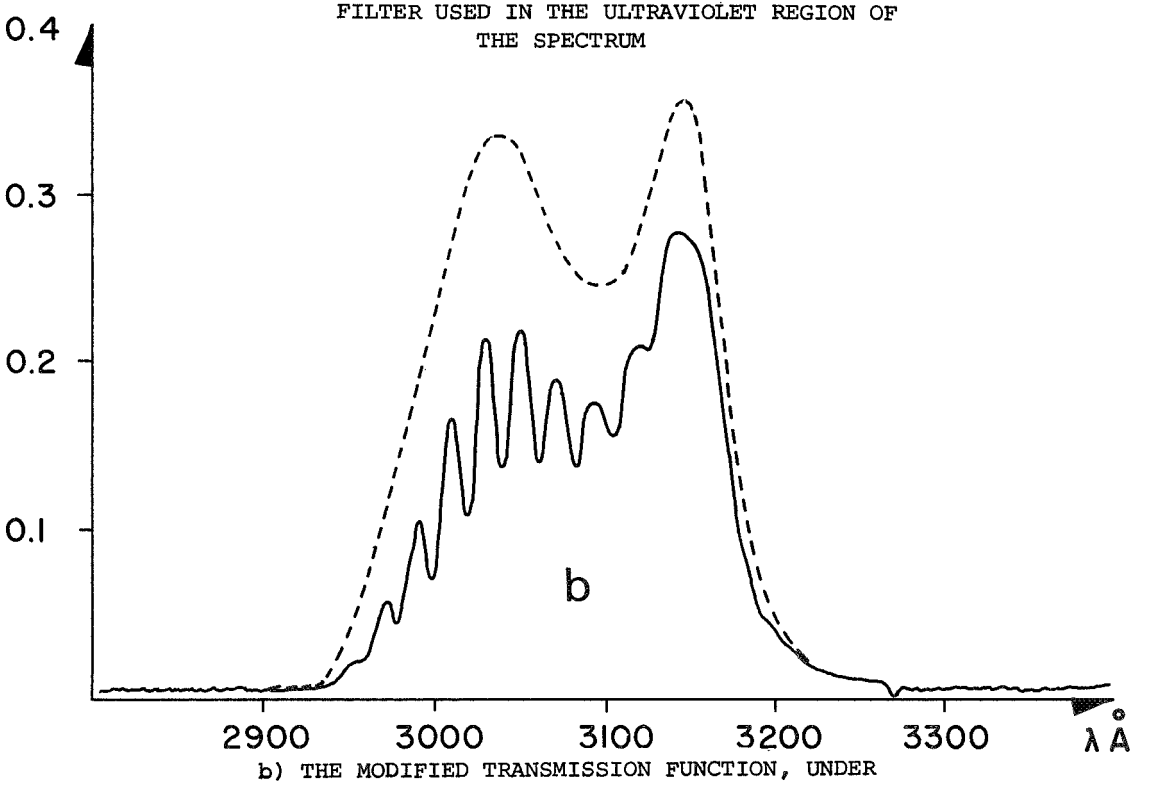

b) THE MODIFIED TRANSMISSION FUNCTION, UNDER THE PRESENCE OF AN AMOUNT OF SO_2 (604ppm-m). THE NEW FUNCTION BEING $\beta_1(\lambda)\ e^{-\bar{a}(\lambda)cL}$

FIGURE 7-5

SINGLE SLIT SCAN:

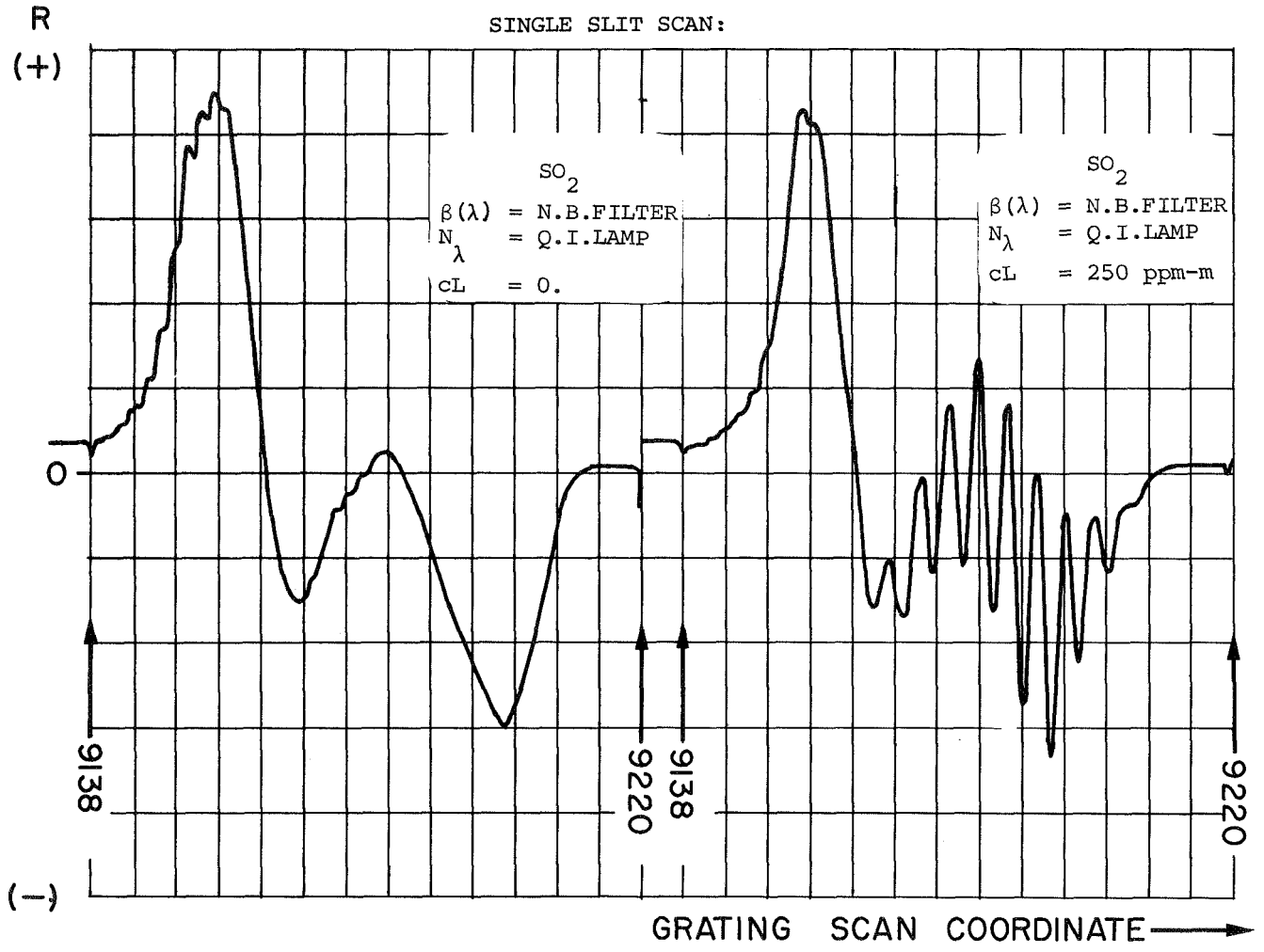

a) $N_\lambda \cdot \beta_1(\lambda)$, $\beta_1(\lambda)$ THE PREVIOUSLY SHOWN TRANSMISSION FUNCTION

b) MODIFIED TRANSMISSION FUNCTION IRRADIATED BY THE SAME LIGHT SOURCE

$N_\lambda \beta_1(\lambda)\ e^{-a(\lambda)cL}$

instrument's counter reading, recording the angular position of the grating as the scan takes place. In Figure 7-5b the same type of scan of the spectrum represented in Figure 7-4b is reproduced (except that it is for 250 ppm-m of SO_2). The successive oscillations of the response correspond to the effect of the successive values of $(a_2 - a_1)$ that the slit is encountering during the scan of the spectrum.

All the described phenomena, although less pronounced, apply to the multislit. When a similar scan is performed with a 6-slit mask [Figure 7-6], using the same light source and filter as for the scan in Figure 7-5a, two main features are apparent:

(1) The $\psi(\xi)$ function is better behaved than $\phi(\xi)$ in the sense of overall values, even for the steepest portion of the $\beta_1(\lambda)$ function, as compared with the single slit.

(2) By the proper selection of the number and width of the slits, and δ, their jump distance, the amplitudes of the maximum deflections due to the absorption bands have been conserved with respect to those of the single slit (compare Figure 7-6b with 7-5b).

If the amplitude of the scan over λ is limited mechanically to just slightly before the response corresponding to a $(a_2 - a_1)$ (+) curve [point B, Figure 7-7b] and slightly after the response corresponding to a $(a_2 - a_1)$ (-) curve (point B'), and repeated, the values A and A' will lie on two curves, as shown in Figure 7-7a. The repetitive scanning from B to B' is accomplished by grating rotation. The distance $\overline{OA}$ is different from $\overline{OA'}$ for any value of cL, and this effect is more pronounced for high values of cL. Figure 7-7a illustrates this fact. A cell was filled with 1000 ppm-m of SO_2 and allowed to empty itself while the grating scan was taking place. The zero offset line is shown as 0 - 0. The A and A' points are seen to follow the type of curves predicted by theory.

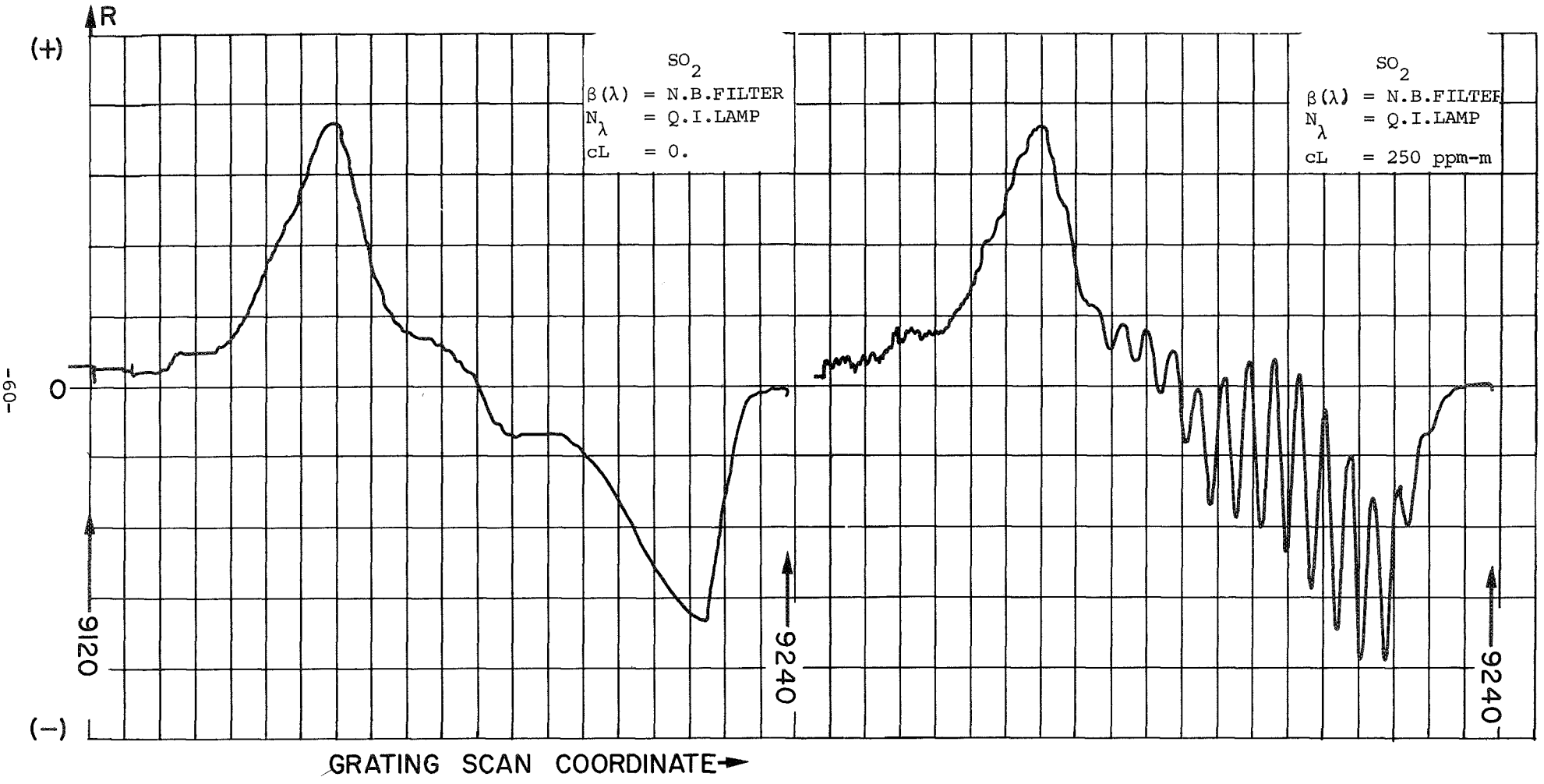

FIGURE 7-6
MULTIPLE SLIT SCAN OF THE SAME
a) $N_\lambda \beta_1(\lambda)$ FUNCTION AND
b) $N_\lambda \beta_1(\lambda)\, e^{-a(\lambda)cL}$ FUNCTION

FIGURE 7-7

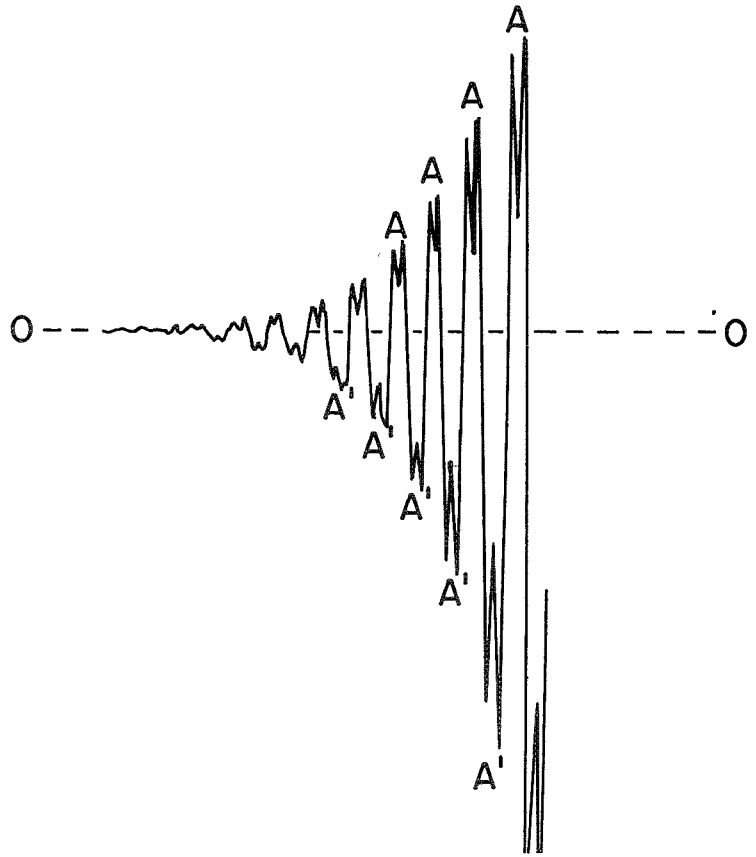

a) RECORDER TRACE OF THE REPETITIVE BB' SCAN, POINTS A CORRESPOND TO $a(a_2 - a_1)$ (+) BRANCH OF THE RESPONSE, AND POINTS A' TO $a(a_2 - a_1)$ (-) BRANCH

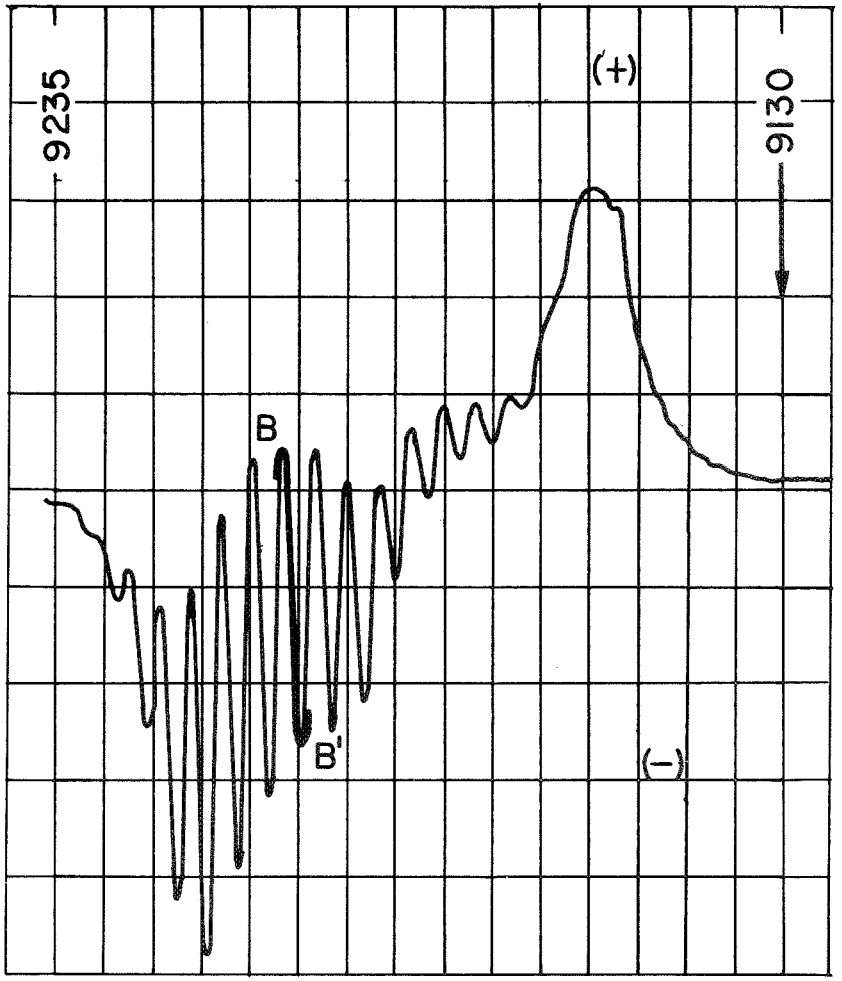

b) POINTS BB' SHOW THE AMPLITUDE OF THE PORTION OF THE FULL SCAN, USED FOR ACTUAL MEASUREMENT.

Response Simulation by Computer Study

A modified computer program was written with the same inputs as the previous one but with the following change: The optimum mask filter jump combination was found by means of the first program. From the integers defining the slits, the integer defining the initial wavelength of the first slit is subtracted. This is equivalent to translating the whole mask to the beginning of the chosen waveband. The response $R/\alpha J$ is obtained according to Equation 6-1, yielding the same outputs. Then the integers defining the slits are increased by one, and the process is repeated until the integer defining the last wavelength of the last slit plus the number of integers defining the "jump" δ equals the last integer of the waveband.

By this process the spectral scan expected with each optimized mask can be simulated. When the mask is in the position for which it was originally optimized, the $(a_2 - a_1)$ response will be the maximum obtainable, and this spike in the spectrum scan has been denoted the Q of the system for the specific mask-filter-jump combination.

By proper use of the two computer programs, (although the last one can actually perform both optimization and scan), a type of response close to the desired can be obtained and the system parameters that determine this response can be used for each specific application.

With the intended use of the instrument in mind, we have aimed for several types of response. The following areas are representative of different uses:

(a) Overall high $(a_2 - a_1)$ (+) to $(a_2 - a_1)$ (-) deflection, usually for low concentrations, is intended to be used with a controlled light source. Examples of this are given in Figure 7-8 obtained with 6 slits for SO_2 (Δ = 6 Å, δ = 12 Å), and in Figure 7-9 obtained with 8 slits for NO_2 (Δ = 6 Å, δ = 14 Å).

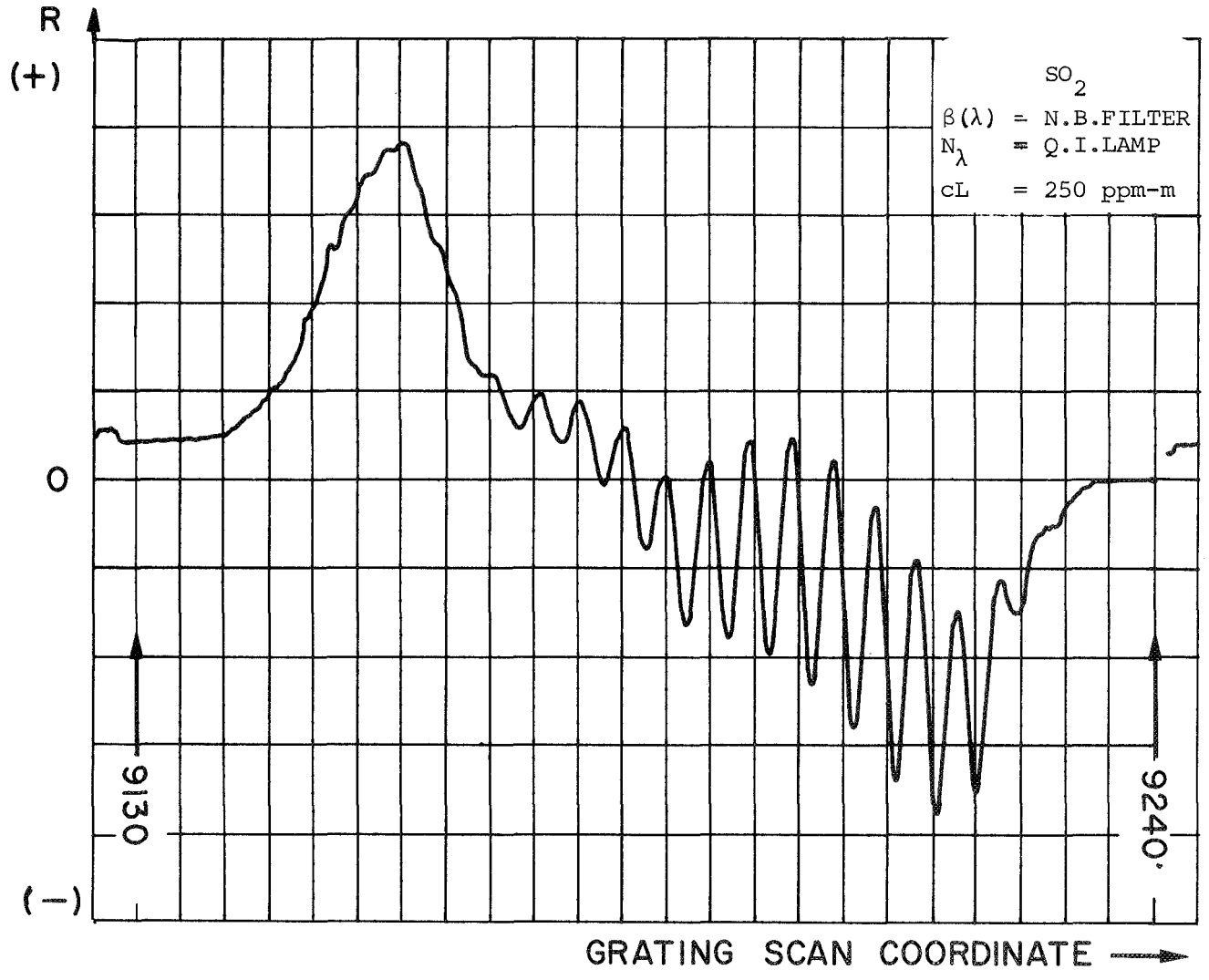

FIGURE 7-8
MULTIPLE-SLIT SCAN OVER $N_\lambda \beta(\lambda)\ e^{-a(\lambda)cL}$
PRODUCING SAMPLE PLOT OF RESPONSE VS.
GRATING POSITION (OR COUNTER READING)
USING A QUARTZ IODINE LIGHT SOURCE

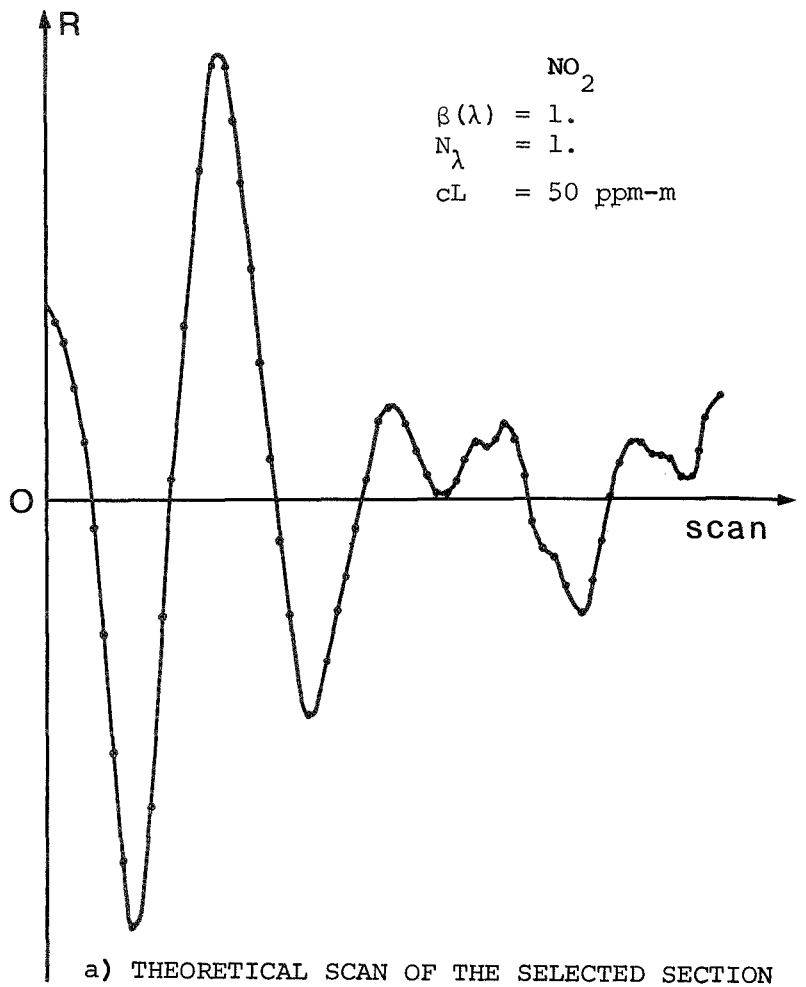

a) THEORETICAL SCAN OF THE SELECTED SECTION OF THE NO_2 ABSORPTION SPECTRUM WITH AN 8 SLIT MASK

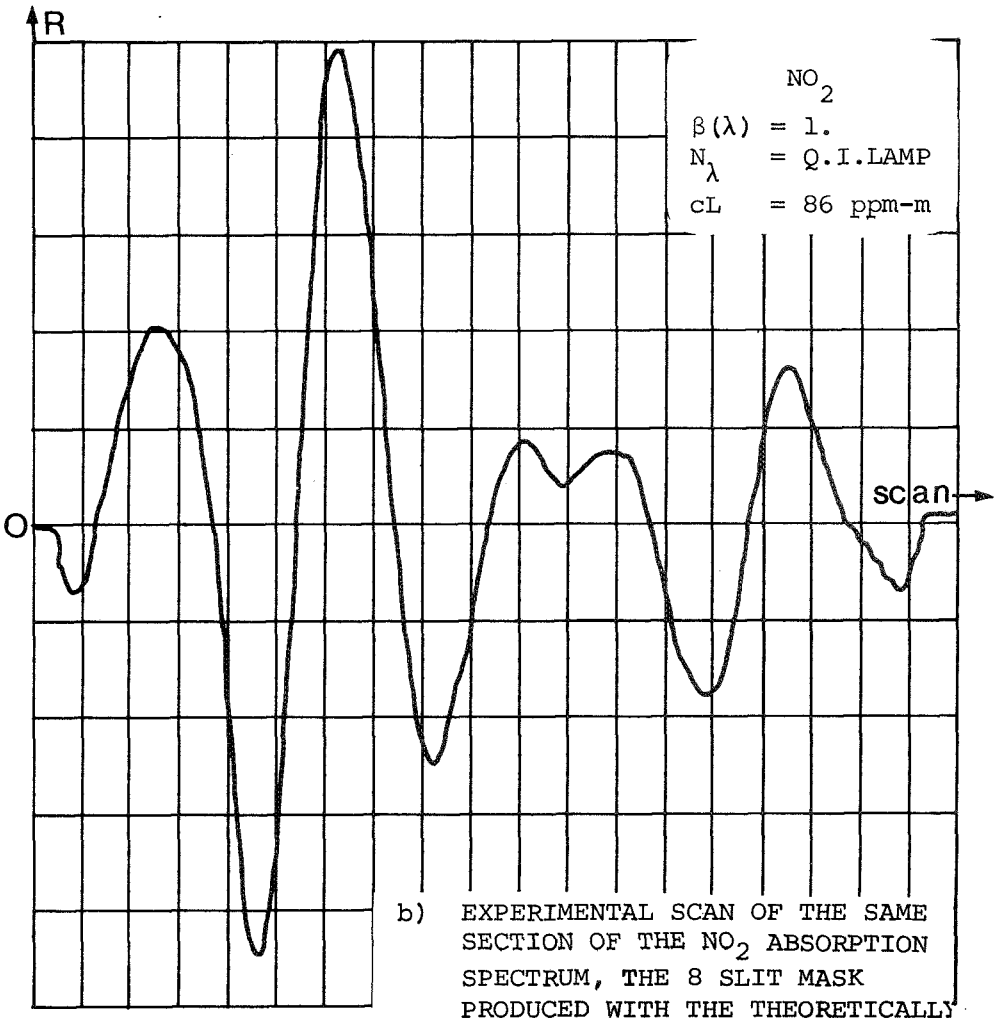

b) EXPERIMENTAL SCAN OF THE SAME SECTION OF THE NO_2 ABSORPTION SPECTRUM, THE 8 SLIT MASK PRODUCED WITH THE THEORETICALLY OBTAINED PARAMETERS

FIGURE 7-9

(b) Specific response intended to produce a highly recognizable pattern and have good sensitivity for use under the presence of structure and time change in the spectral distribution of the light source and/or interfering gases.

To calculate the optimum parameters in the last case requires a laborious theoretical-experimental approach, the more elaborate, the wider the use desired for the instrument. Corresponding to this type of approach is Figure 7-10 where a very specific NO_2 mask-jump was designed to show its NO_2 pattern in the 4200 Å - 4500 Å range, under the presence of numerous Fraunhoffer lines in the solar spectrum.

Figure 7-10a represents the theoretical computer-produced scan; 7-10b, the laboratory instrument scan; and 7-10c, the scan of the background spectral distribution (sky light) in the same waveband, showing the effect of the structure. Figure 7-10d represents the same scan when a few ppm-m of NO_2 have been inserted in the light path. Notice the NO_2 scan pattern in the spectral region as compared with that obtained in the laboratory under controlled conditions. The rest of the scan response is not highly affected, as can be expected from observations of Figure 7-10a and b. In this case, the question of whether there was any NO_2 absorption present in the sky light before the cell was inserted cannot be readily answered. Nevertheless, the following fact may be pointed out:

> The distance between point C and D in Figure 7-10b and that between D and E do not correspond to the respective distances in Figure 7-10c. Thus we can conclude that if NO_2 absorption were present in the incoming light, it was very small.

If the spectral scan is performed when certainty exists of no NO_2 absorption present, it will be the zero offset $\alpha J\ [1- \psi(\xi)]$ scan corresponding to the filter-mask-sky combination at that time. Because within reasonable limits imposed on the light source (like time of day, cloudiness etc.), the $\psi(\xi)$ function is expected to be well-behaved, (see Section 6), the form of this scan could be used

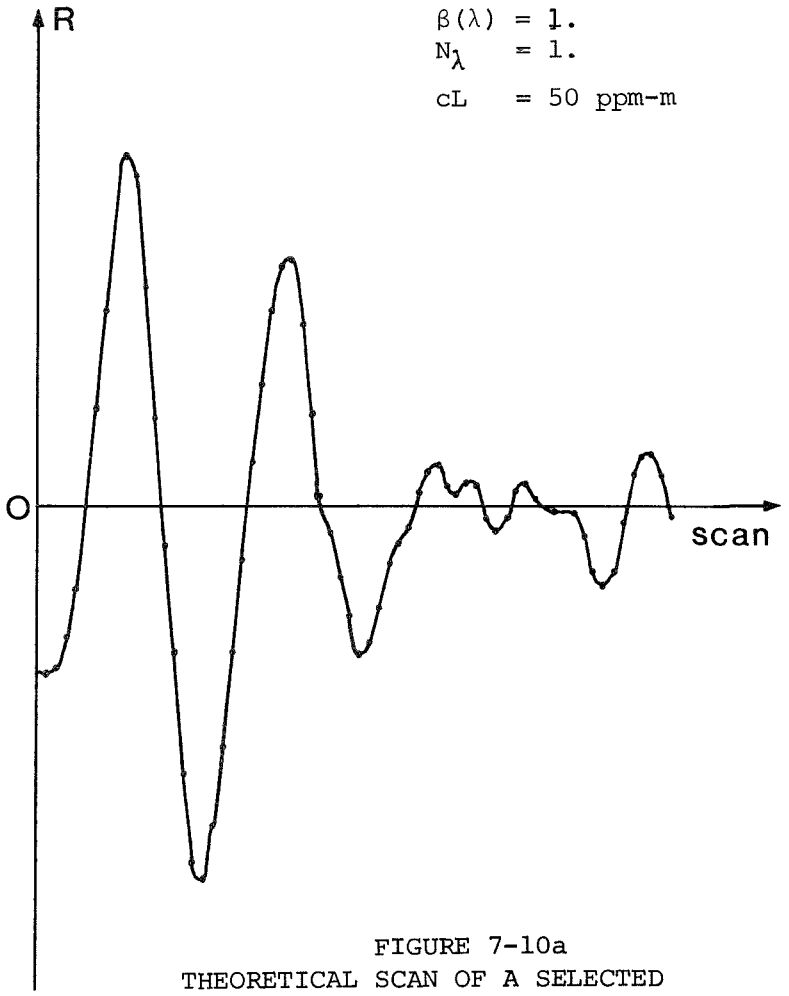

FIGURE 7-10a
THEORETICAL SCAN OF A SELECTED SECTION OF THE NO_2 ABSORPTION SPECTRUM WITH A 9 SLIT MASK

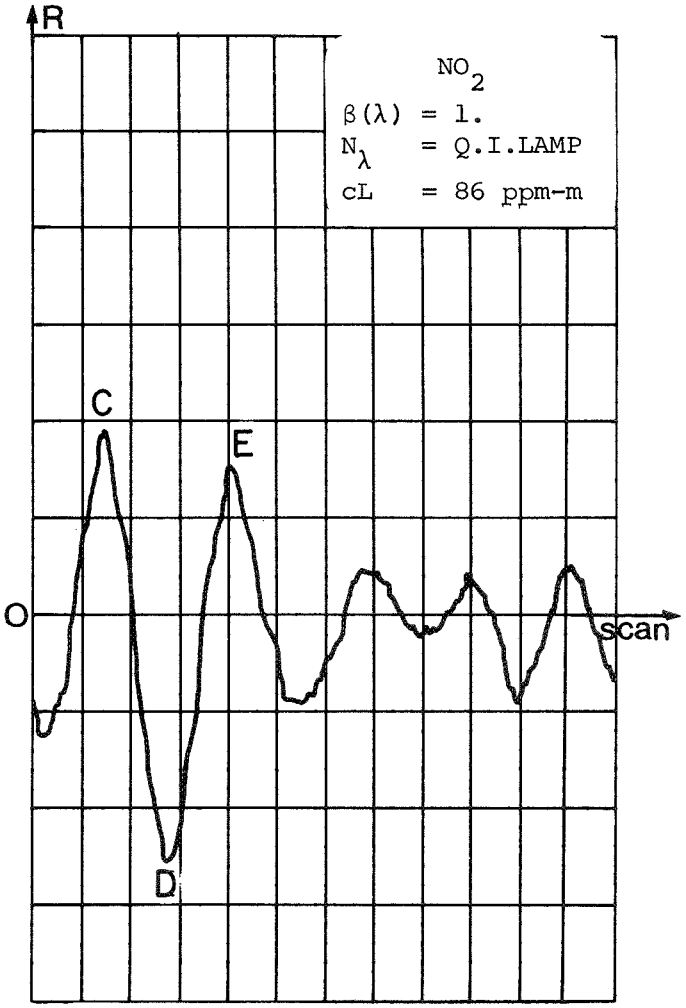

FIGURE 7-10b
EXPERIMENTAL SCAN OF THE SAME SECTION OF THE NO_2 SPECTRUM, THE 9 SLIT MASK PRODUCED WITH THE THEORETICALLY OBTAINED PARAMETERS

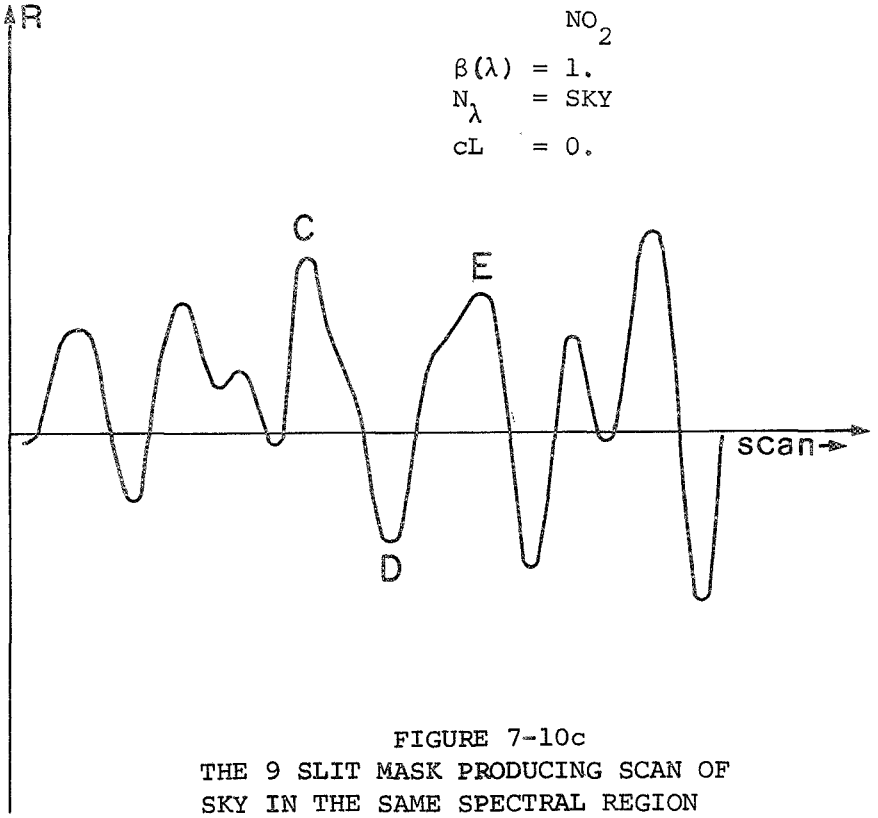

FIGURE 7-10c
THE 9 SLIT MASK PRODUCING SCAN OF
SKY IN THE SAME SPECTRAL REGION

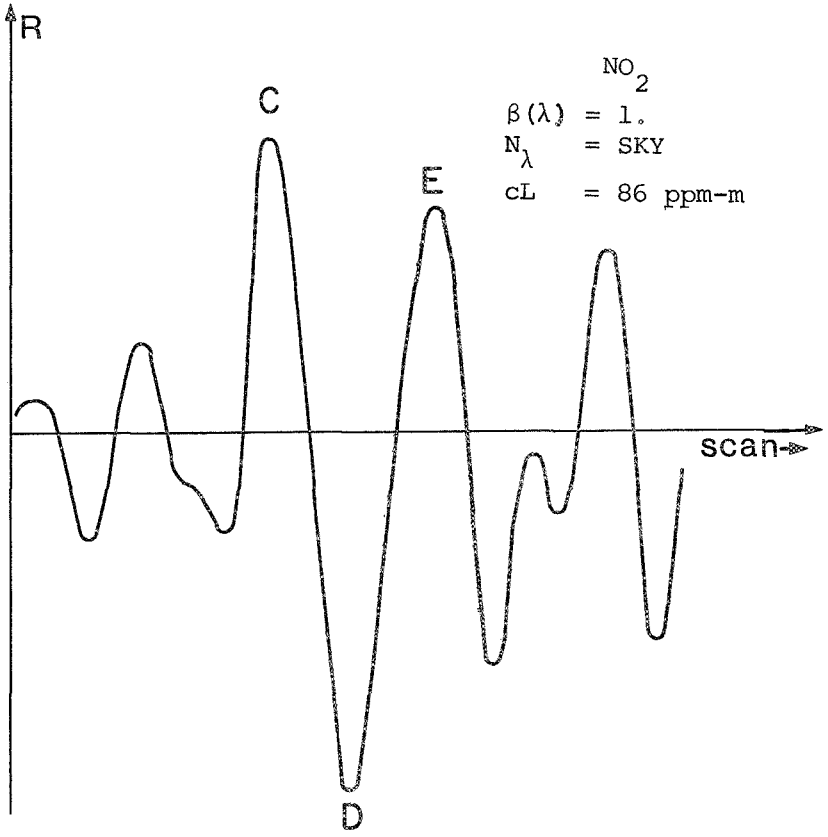

FIGURE 7-10d
THE 9 SLIT MASK PRODUCING SCAN OF
SKY UNDER THE PRESENCE OF NO_2

as the zero reference; any changes in the predetermined region of the scan leading to the expected response characteristics of NO_2 would then be due to the presence of NO_2 absorption. By proper calibration its concentration could be determined.

In the case of the SO_2 Figure:

7-11a - represents this specific type of response. (In the SO_2 absorption pattern of quasi-regularly spaced absorption bands, there are multiple Q's because the mask-jump-combination has more than one optimum point).*

7-11b - represents the spectral scan of the sky (instrument looking to the anti-solar position 40° from the zenith, sun zenith angle 35°); again the structure is due to the effect of the Fraunhoffer lines.

7-11c - represents the influence of 250 ppm-m of SO_2 in a cell on the response to the sky background structure shown in Figure 7-11b.

7-11d - This is the superposition of Figure 7-11c on Figure 7-11b to show the variation on the pattern, due to the presence of SO_2, corresponding to the SO_2 characteristics of Figure 7-11a. Notice the reference markers.

Figure 7-12 is similar to Figure 7-11 but corresponds to different slit spacings. By the proper theoretical study of the situation of the Fraunhoffer lines and their line strengths of some "standardized" sky spectral radiance distributions and of the proper computer handling, masks of the type b (sensitive and specific) can be produced, which achieve a semi-flat response to the sky N_λ where the SO_2 reports strongest, similar to the response of Figure 7-13 which represents an enlargement of Figure 7-12d in the region marked AA_1.

The same conclusions obtained for the NO_2 case apply here for SO_2, but with many more restrictions on the part of N_λ in this spectral region due to aerosol scattering and ozone absorption. Due to this scattering N_λ varies, and if a certain accuracy is desired and one must measure a certain range of concentration, restrictions have to be imposed on the variables affecting N_λ.

* Only one of them is the absolute maximum, but under the presence of the filter function $\beta(\lambda)$ that modifies $\psi(\xi)$, care has to be exercised to select the correct one, since artificial enhancement or decrease of the response occurs linearly with changes of $\psi(\xi)$, (see Equations 7-2 and 5-3).

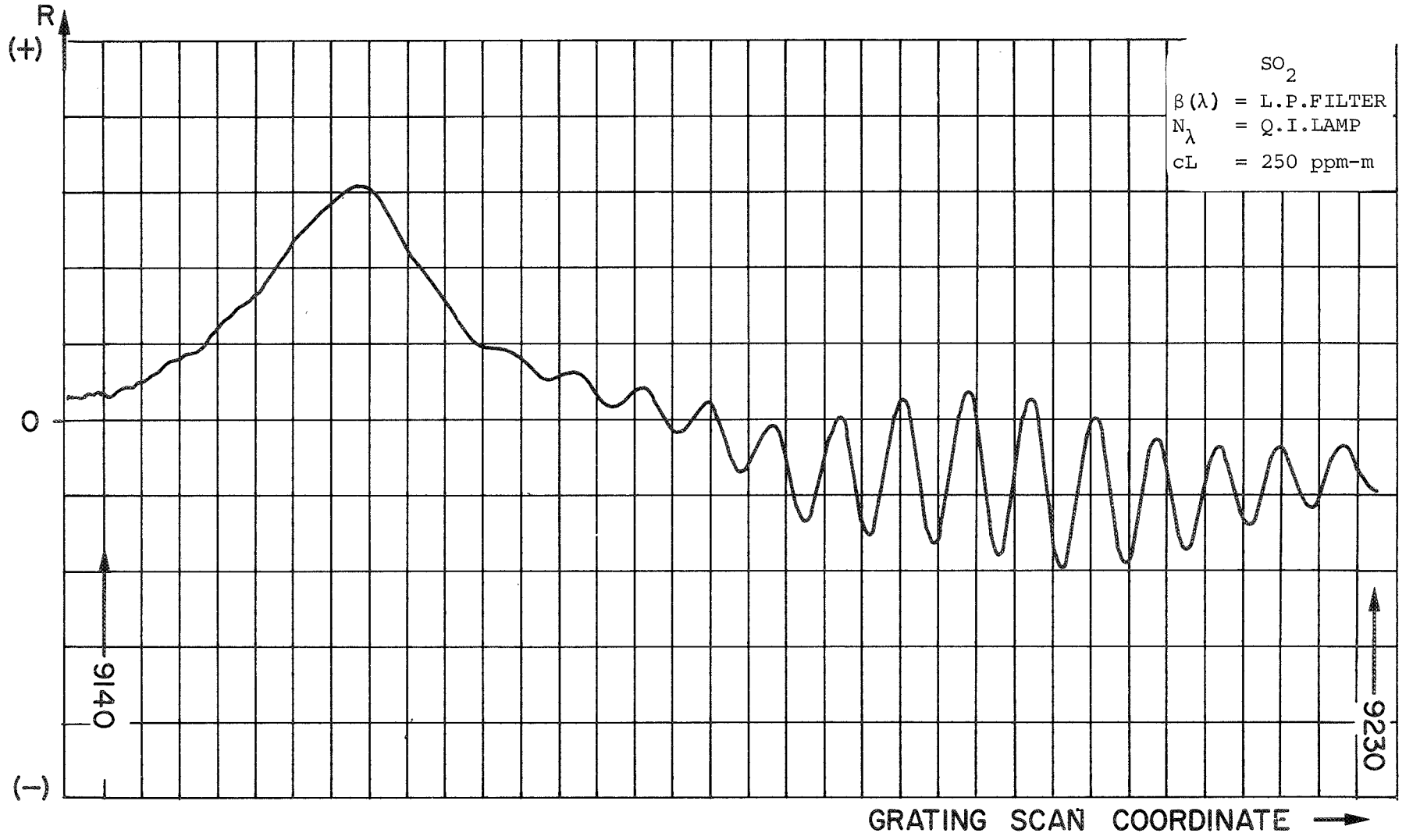

FIGURE 7-11a
SCANNING RESPONSE OF INSTRUMENT USING AN
SO_2 MASK OVER SPECTRUM

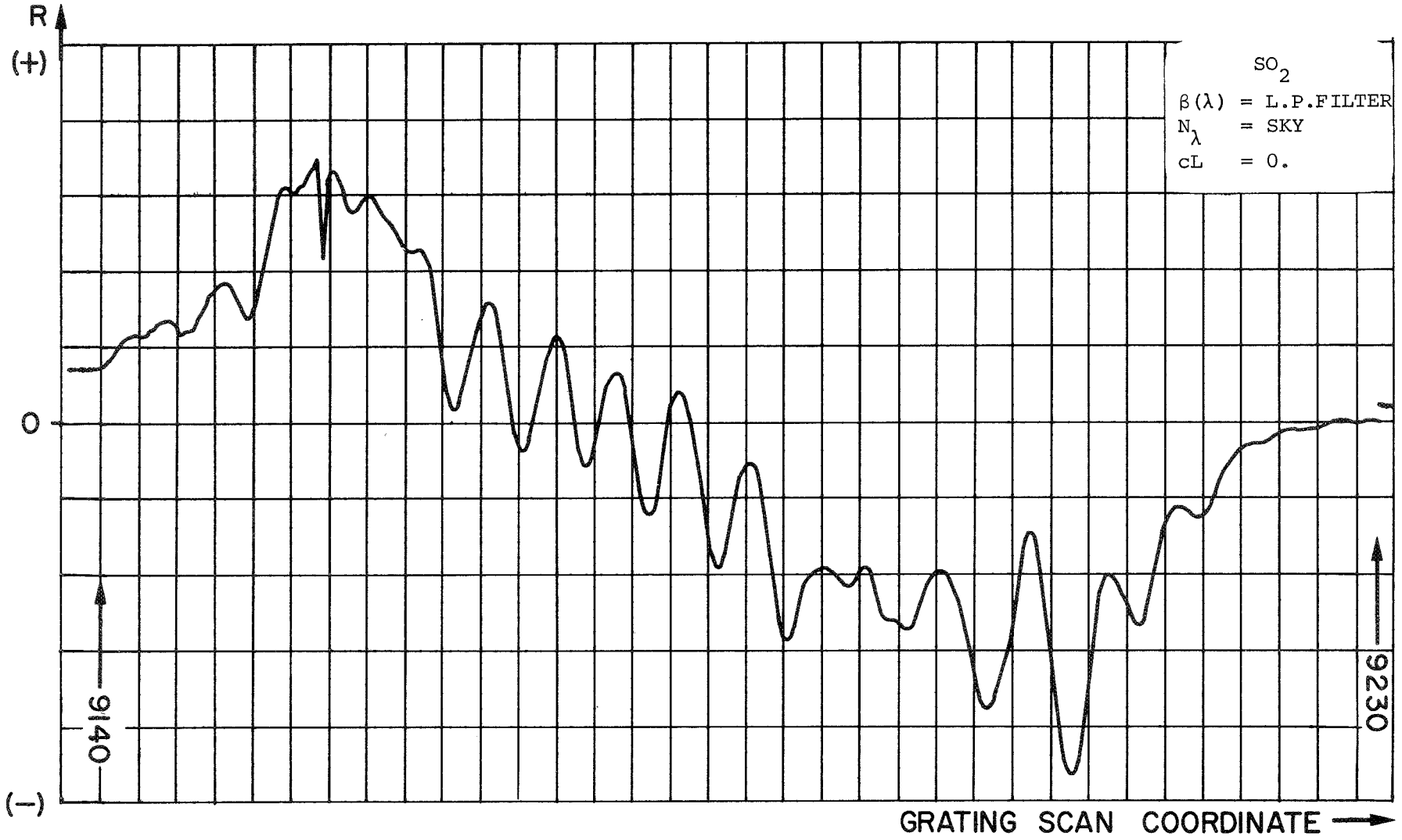

FIGURE 7-11b
SCANNING RESPONSE OF INSTRUMENT USING
AN SO_2 MASK OVER SPECTRUM

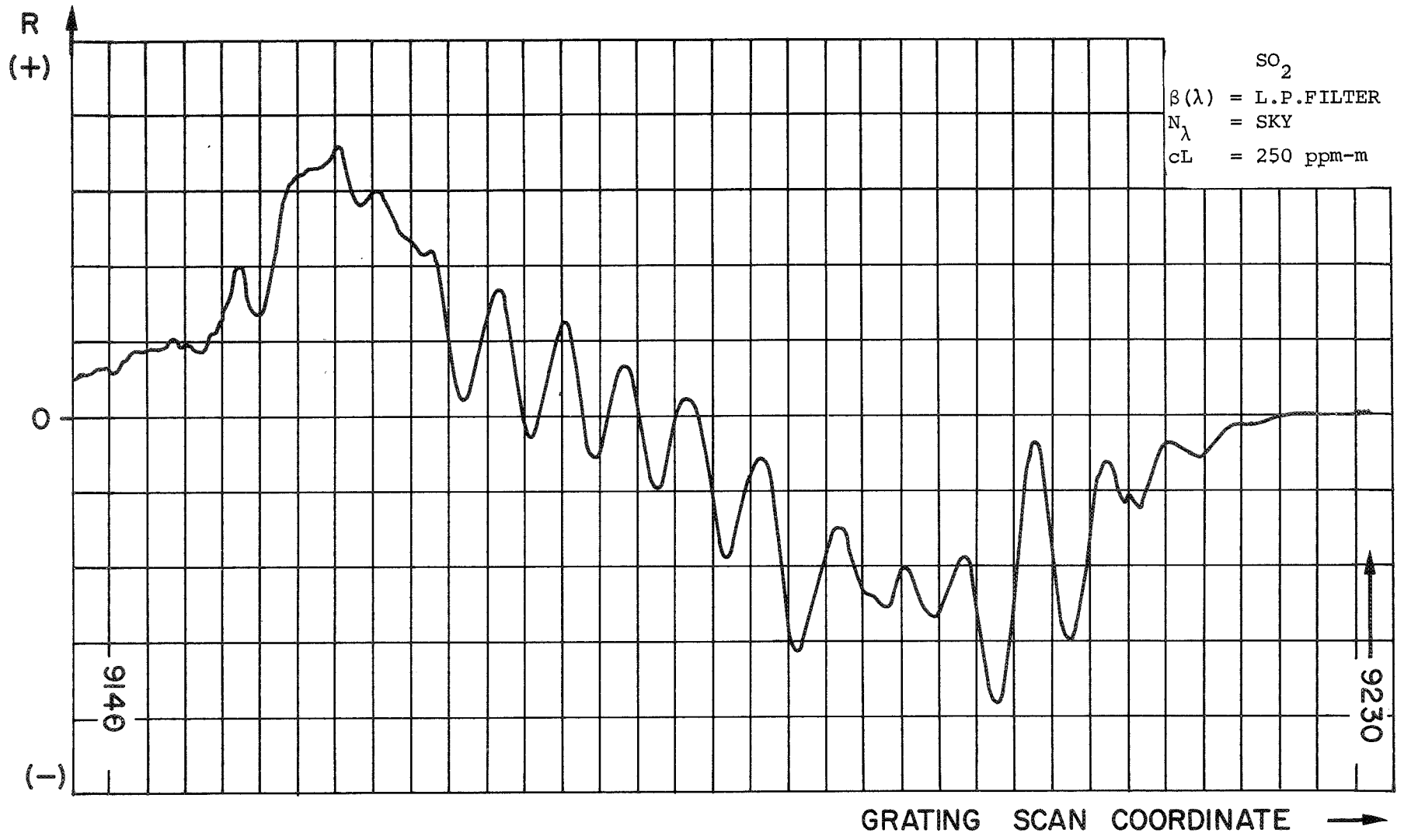

FIGURE 7-11c

SCANNING RESPONSE OF INSTRUMENT USING AN SO_2 MASK OVER SPECTRUM

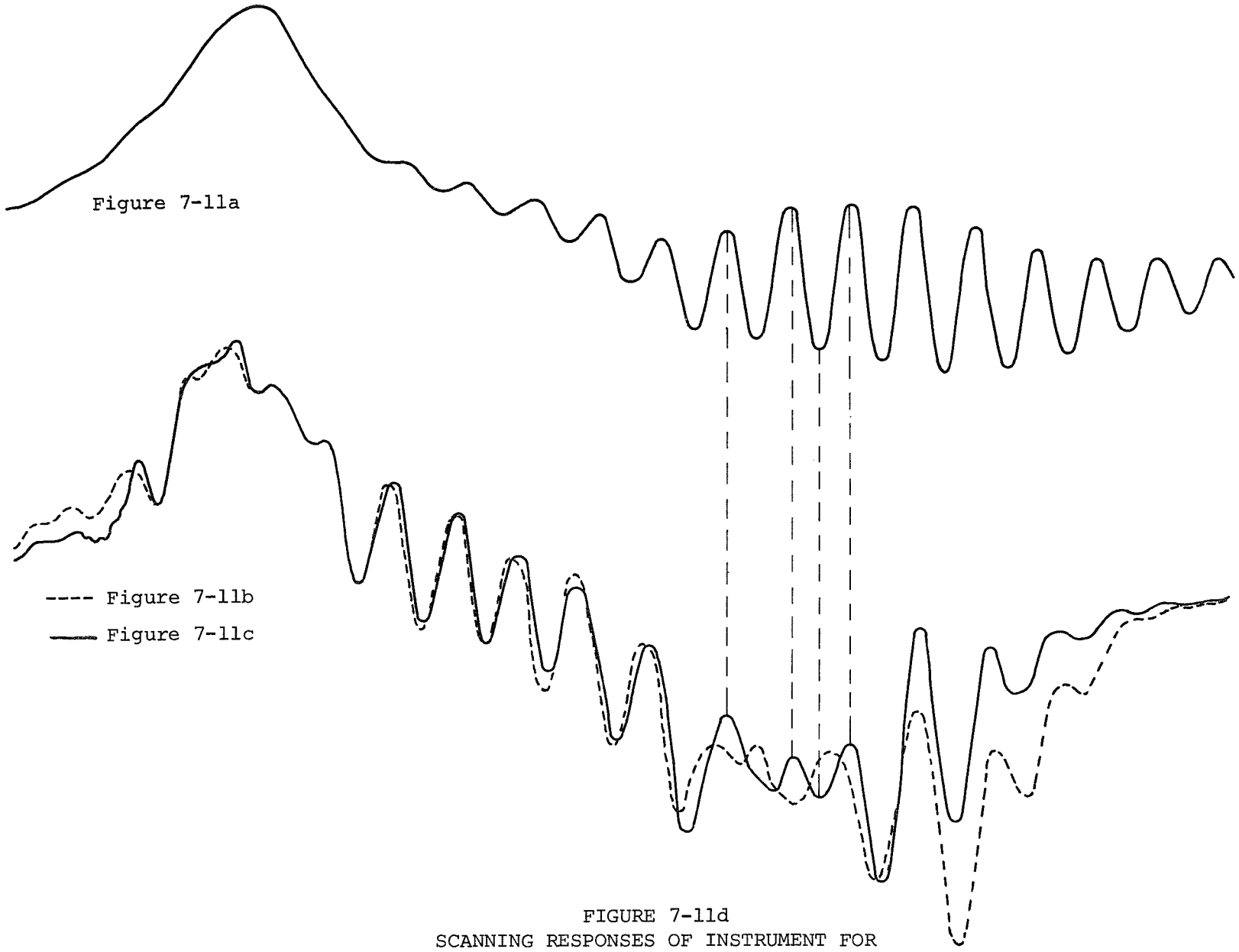

FIGURE 7-11d
SCANNING RESPONSES OF INSTRUMENT FOR
VARIOUS CONDITIONS

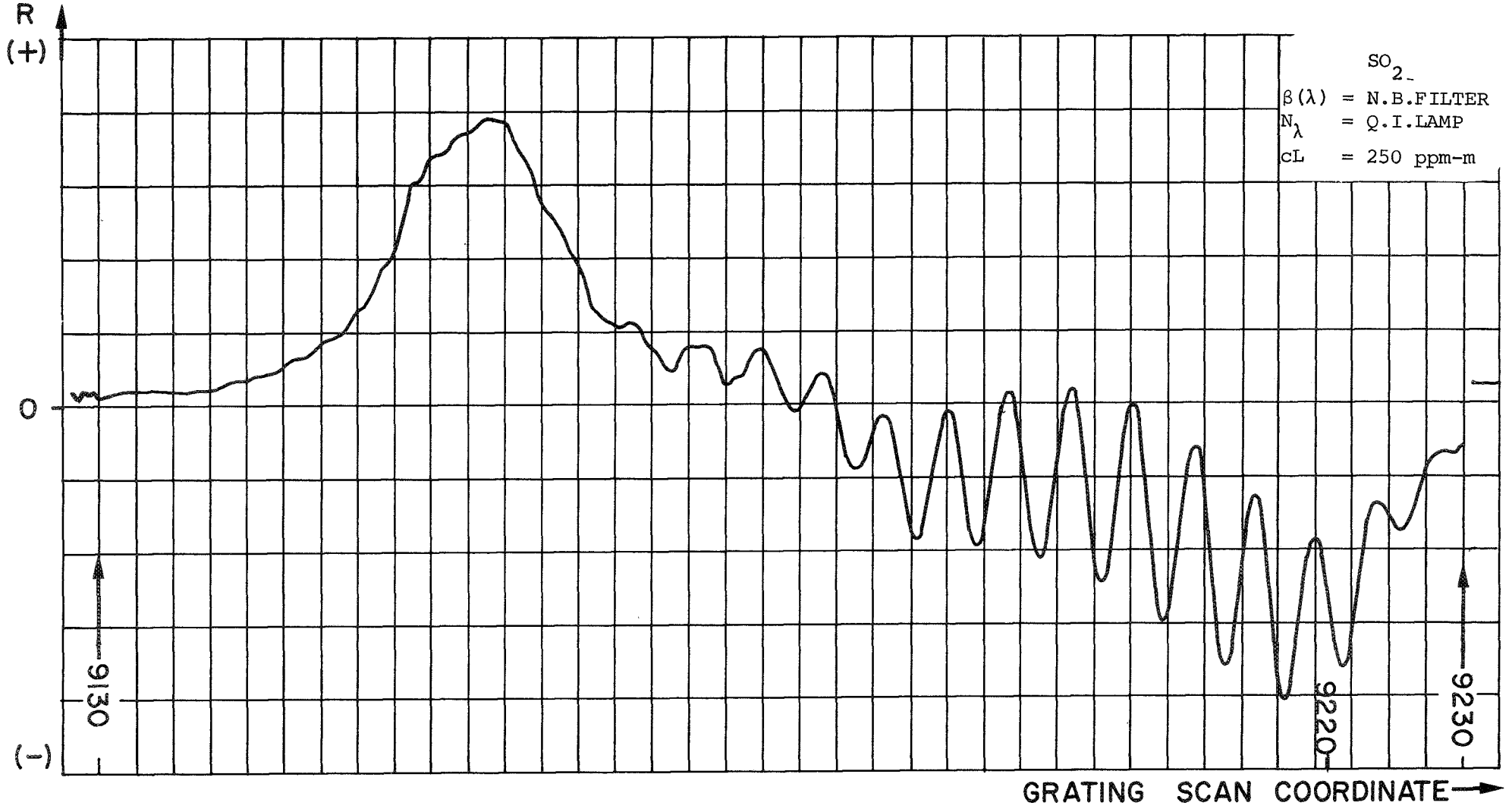

FIGURE 7-12a
SCANNING RESPONSE OF INSTRUMENT USING
AN SO_2 MASK OVER SPECTRUM

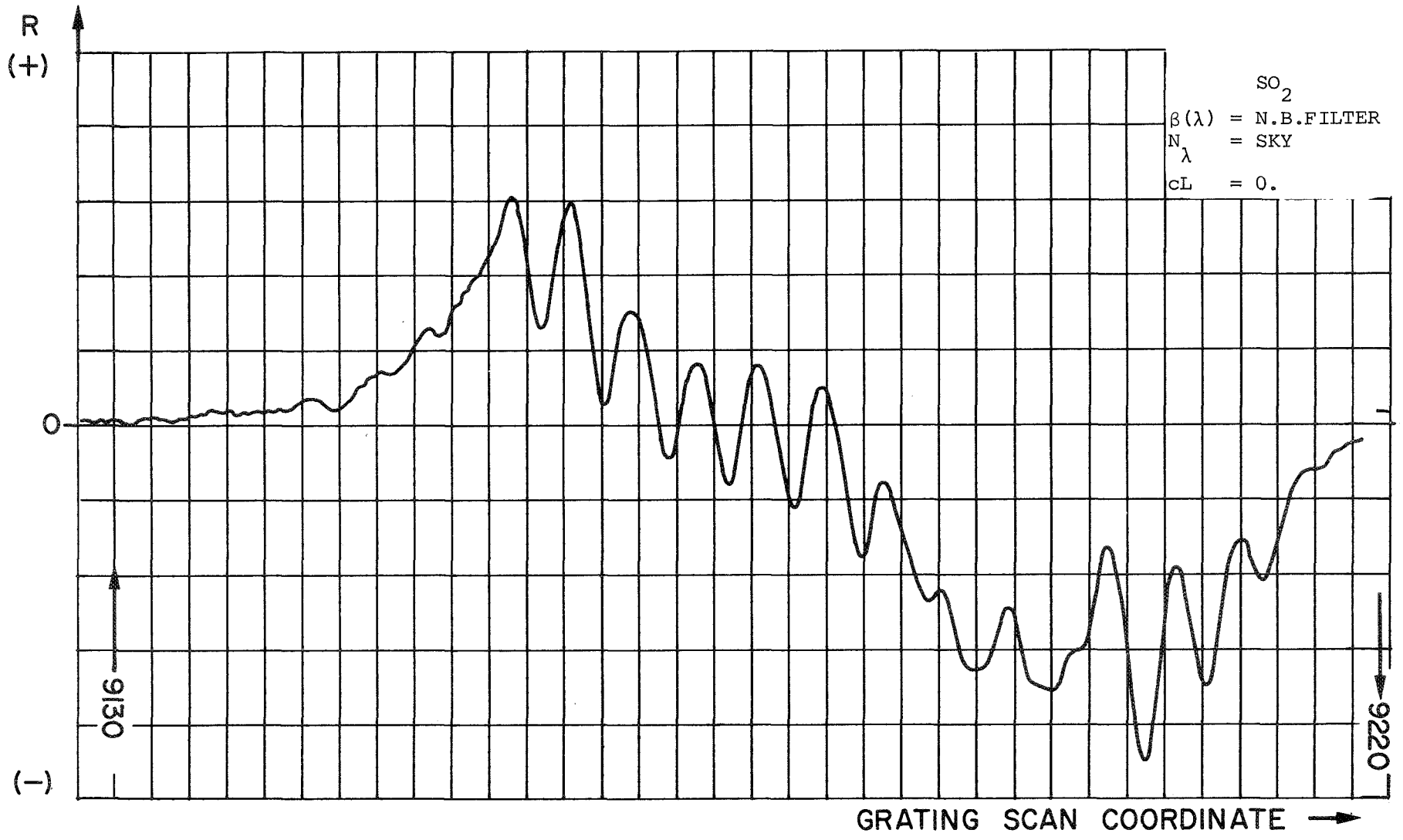

FIGURE 7-12b
SCANNING RESPONSE OF INSTRUMENT USING
AN SO_2 MASK OVER SPECTRUM

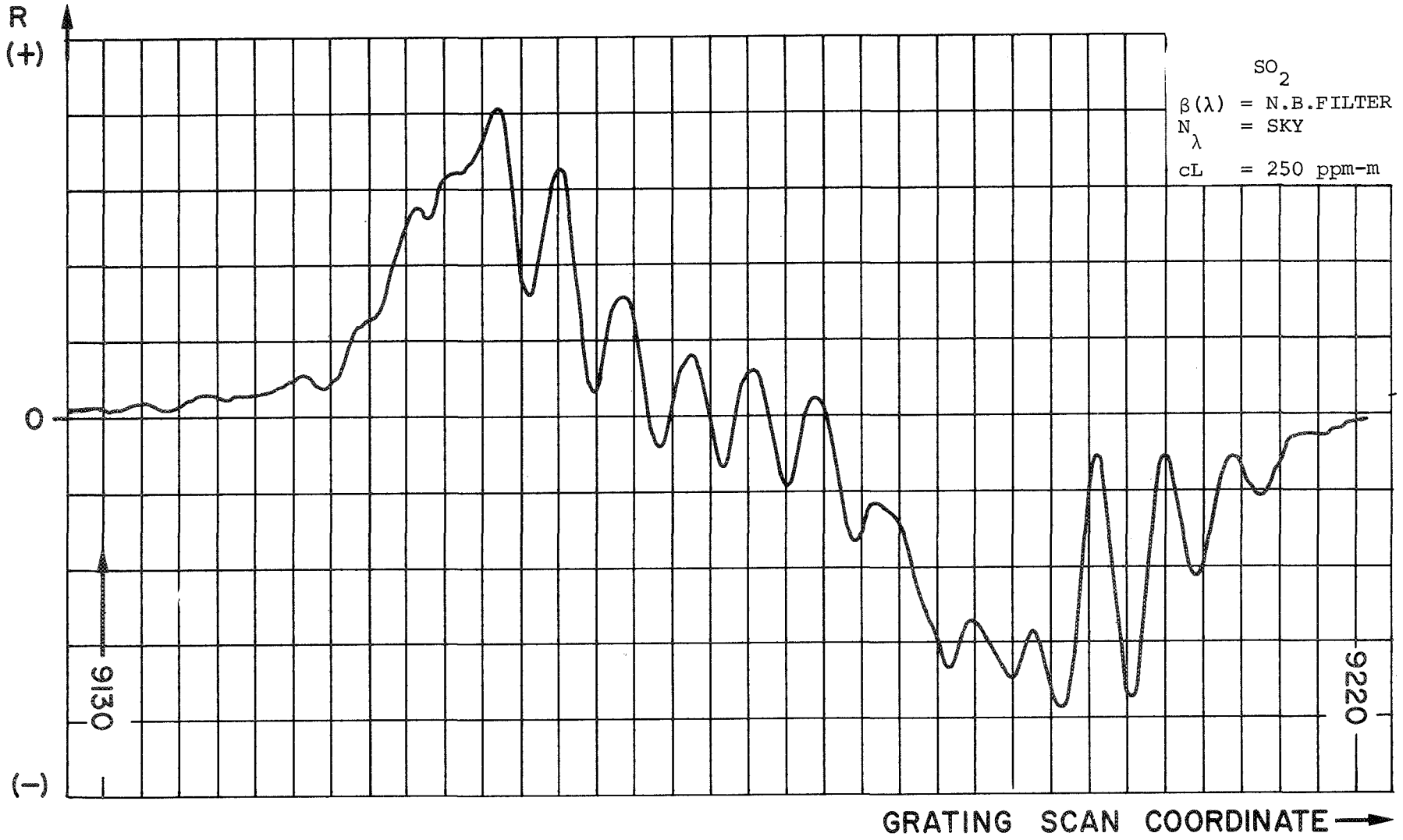

FIGURE 7-12c
SCANNING RESPONSE OF INSTRUMENT USING
AN SO_2 MASK OVER SPECTRUM

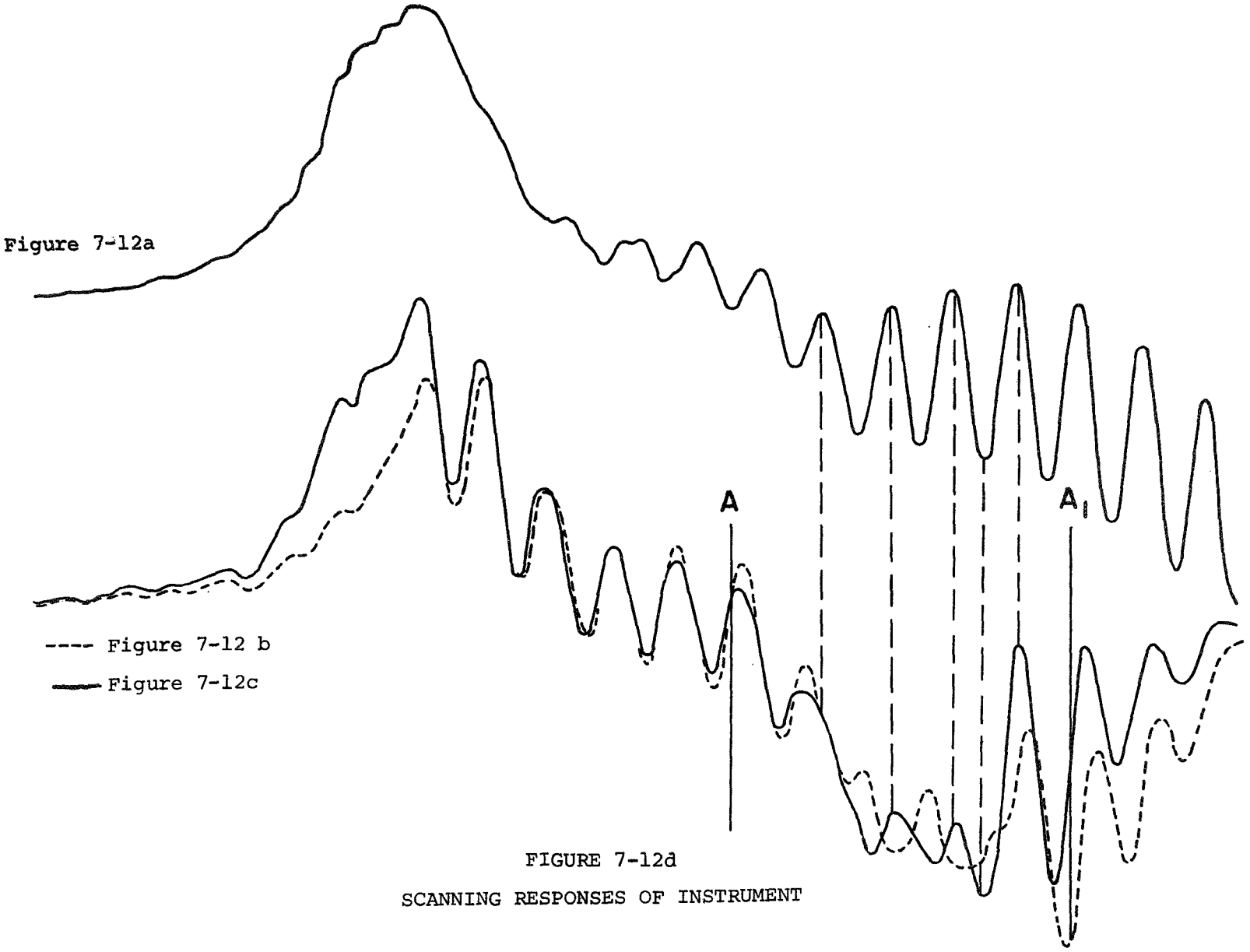

FIGURE 7-12d

SCANNING RESPONSES OF INSTRUMENT

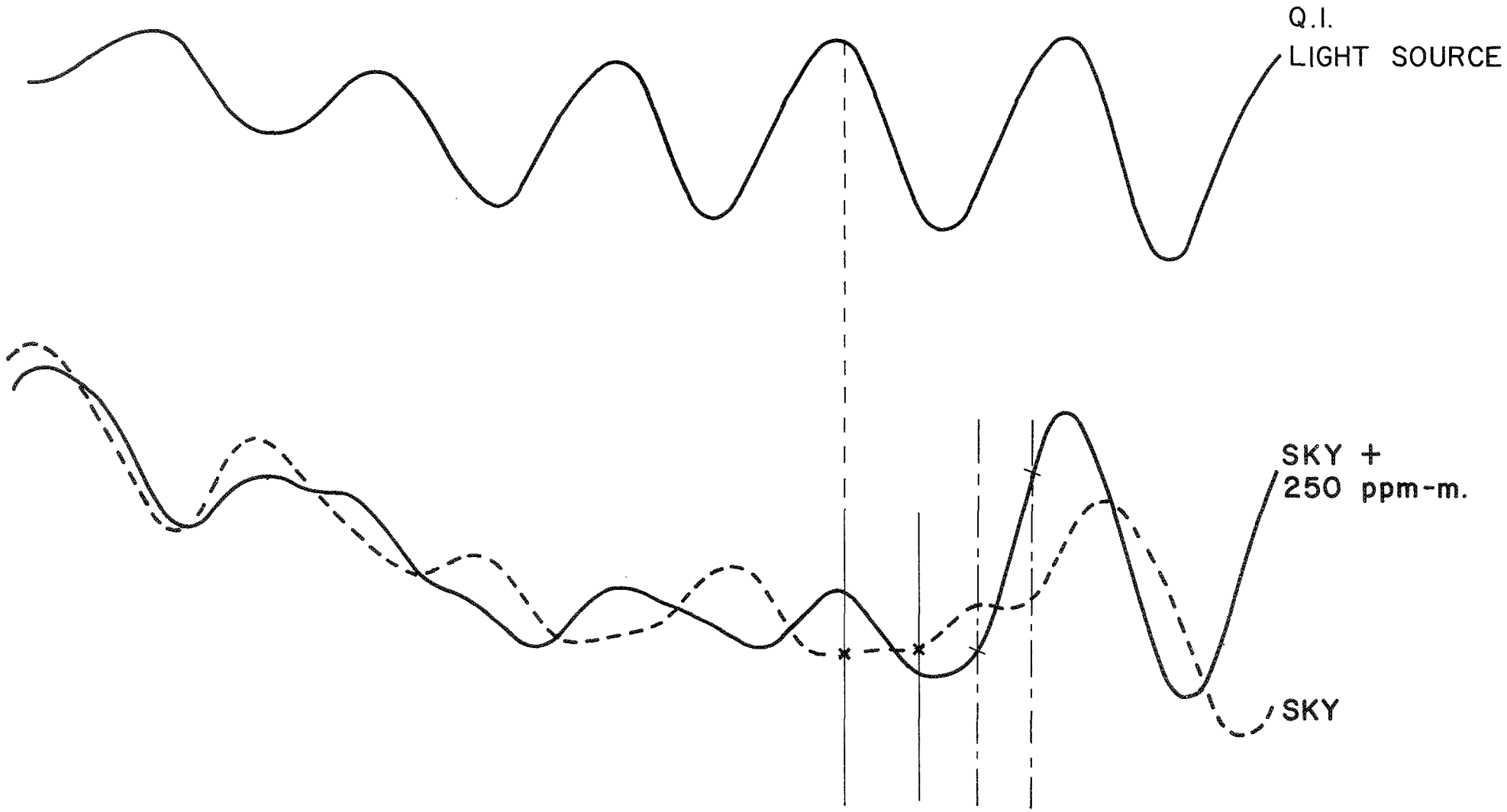

FIGURE 7-13
ENLARGEMENT OF THE AA_1 REGION
OF FIGURE 7-12d

These could include the time of day, the time of year, the degree of cloud cover, the degree of atmospheric haze and turbidity, etc.

The conclusions of the section are the following: By having knowledge of the uncontrollable parameters affecting the behaviour of the instrument under known conditions and knowledge of its response to the power-affecting parameters, any sensitivity and specificity desired, within limits, can be achieved.

8. REMOTE SENSING OF PLUMES

Of the numerous possible applications of the system, described in detail in more specialized reports, the remote sensing of plumes has been chosen as a representative application for analysis here.

The problem may be stated as follows:

How can quantitative measurements be made of stack effluents and under what circumstances? The principal condition applicable for a quantitative measurement is: The instrument's field-of-view at the stack top should be smaller than any representative dimension of the plume in such a way that cL can be assumed constant along the line of view.

The kind of situation encountered when attempting this type of measurement is shown in Figure 8-1.

$N_\lambda(r)$ is the spectral radiance of the patch of the sky behind the plume, in the line of sight of the instrument.

$N'_\lambda(r)$ is the spectral distribution of light coming into the field-of-view of the instrument and being diverted into the acceptance angle of the instrument, due to scattering of sun and sky light between the plume and the instrument.

$\sigma(r)$ is an extinction coefficient to account for energy being diverted from the acceptance angle of the instrument due to scattering between the plume and the instrument.

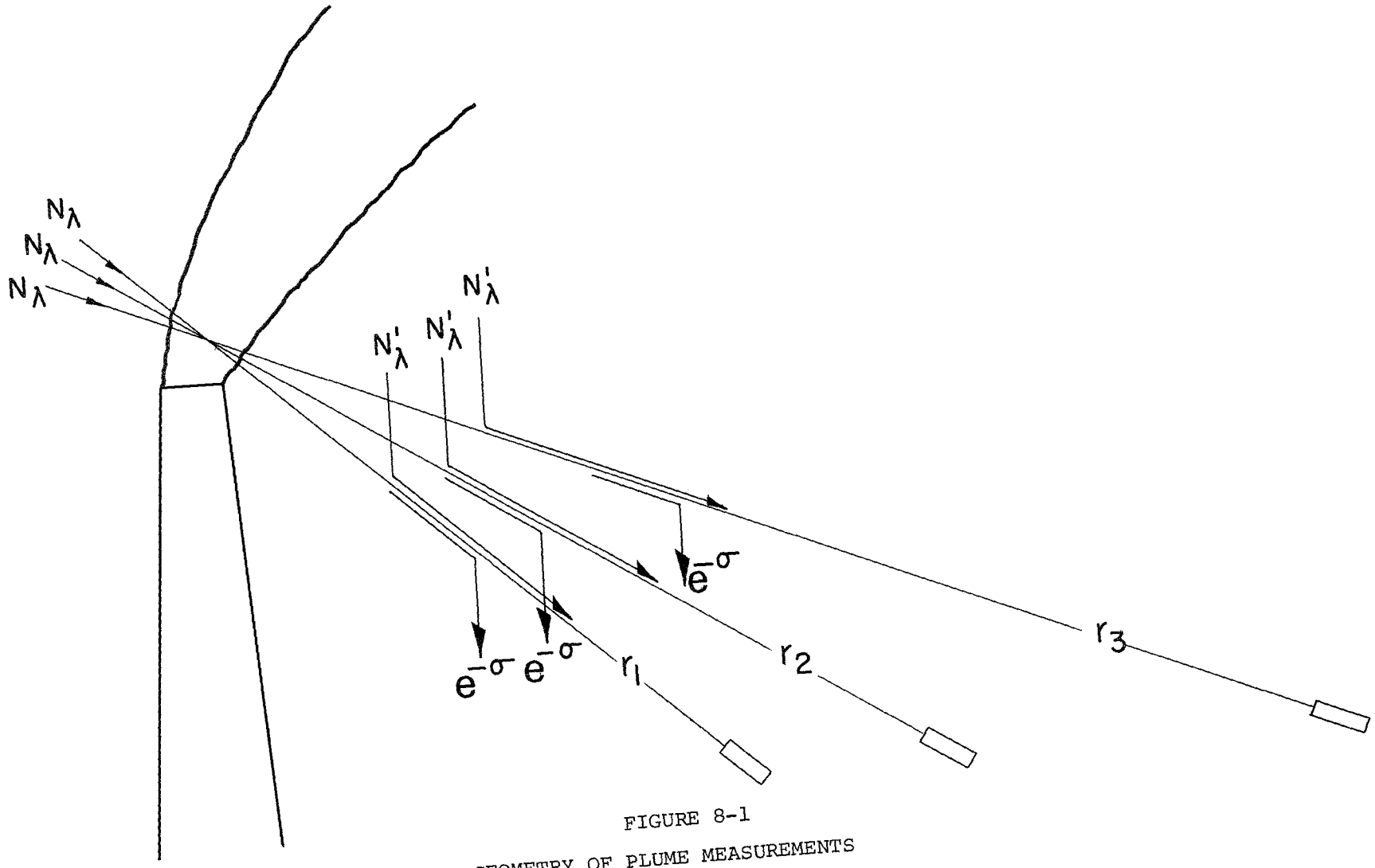

FIGURE 8-1

GEOMETRY OF PLUME MEASUREMENTS

N_λ, N'_λ and σ are functions of several parameters, although we are interested mainly in their dependence on the instrument's distance from the plume (r), and we assume that they are bounded continuous functions at least over a range of distances.

When the instrument is set as shown in Figure 8-1, the reading is:

$$R = \alpha J \left\{ 1 - \frac{\sum_{i=1}^{n} \int_{\lambda_{2i}}^{\lambda'_{2i}} [N_\lambda(r)\, e^{-a(\lambda)cL} . e^{-\sigma(r)} + N'_\lambda(r)]\beta(\lambda)d\lambda}{\sum_{i=1}^{n} \int_{\lambda_{1i}}^{\lambda'_{1i}} [N_\lambda(r)\, e^{-a(\lambda)cL} . e^{-\sigma(r)} + N'_\lambda(r\, \beta(\lambda)d\lambda} \right\} \quad (8\text{-}1)$$

where it can be seen that the effect of both $\sigma(r)$ and $N'_\lambda(r)$ is to decrease the influence of $a(\lambda)cL$, thus diminishing the response to the chosen gas. Under these circumstances, with only one reading and with neither N_λ, σ or N'_λ known, the measurement of cL cannot be made. However, by taking advantage of the reasonably well behaved response of the multislit system, the difficulty can be overcome. The basis for overcoming the difficulty lies in the N_λ, N'_λ and σ dependence on (r).

Assume:

(a) The scattering within the plume is neglected, or else included in the overall response that we want to measure.

(b) At different distances (r), the same section of the plume is observed.

(c) The cL of this section remains constant during the time of the measurements.

Then, when looking at the plume at range r_1 the response follows expression 8-1. After the reading is taken, the instrument is pointed slightly away from the side of the plume and two calibration cells are inserted into the light path. These calibration readings each follow the expression:

$$R_c = \alpha J \left\{ 1 - \frac{\sum_{i=1}^{n} \int_{\lambda_{2i}}^{\lambda'_{2i}} [N_\lambda(r)\ e^{-\sigma(r)} + N'_\lambda(r)]\ .\ e^{-a(\lambda)[cL]}\ \beta(\lambda)\,d\lambda}{\sum_{i=1}^{n} \int_{\lambda_{1i}}^{\lambda'_{1i}} [N_\lambda(r)\ e^{-\sigma(r)} + N'_\lambda(r)]\ .\ e^{-a(\lambda)[cL]}\ \beta(\lambda)\,d\lambda} \right\} \qquad (8\text{-}2)$$

When comparing both equations 8-1 and 8-2, the following characteristics of both are known:

(a) If the scattering is zero, the curve given by Expression 8-1, when representing R versus range, is a horizontal line whose ordinate is the response produced by the cL of the section of the plume through which we are looking. At the most, it departs little from a straight line due to the $N_\lambda(r)$ dependence on the distance (there is then a condition imposed on N_λ, thus introducing restraints on time, cloudiness, etc.)

(b) For very severe scattering (heavy haze or fog) at a relatively short distance, the plume will not be seen at the waveband chosen (i.e. in the ultraviolet the visibility is much smaller than in the visible), and the instrument's response will be

$$R = \alpha J \left\{ 1 - \frac{\sum_{i=1}^{n} \int_{\lambda_{2i}}^{\lambda'_{2i}} N'_\lambda(r)\ \beta(\lambda)\,d\lambda}{\sum_{i=1}^{n} \int_{\lambda_{1i}}^{\lambda'_{1i}} N'_\lambda(r)\ \beta(\lambda)\,d\lambda} \right\} \qquad (8\text{-}3)$$

a constant determined by the local value of $N'_\lambda(r)$ [far enough from the plume, N'_λ becomes independent of (r)]. For the calibration response curve in this circumstance, Expression 8-3 is nothing more than its local zero offset. This is also the zero offset curve defined by $O_o\ O_1\ O_2$ in Figures 8-2 and 8-3 when, at various values of distance r, the instrument is pointed slightly off the

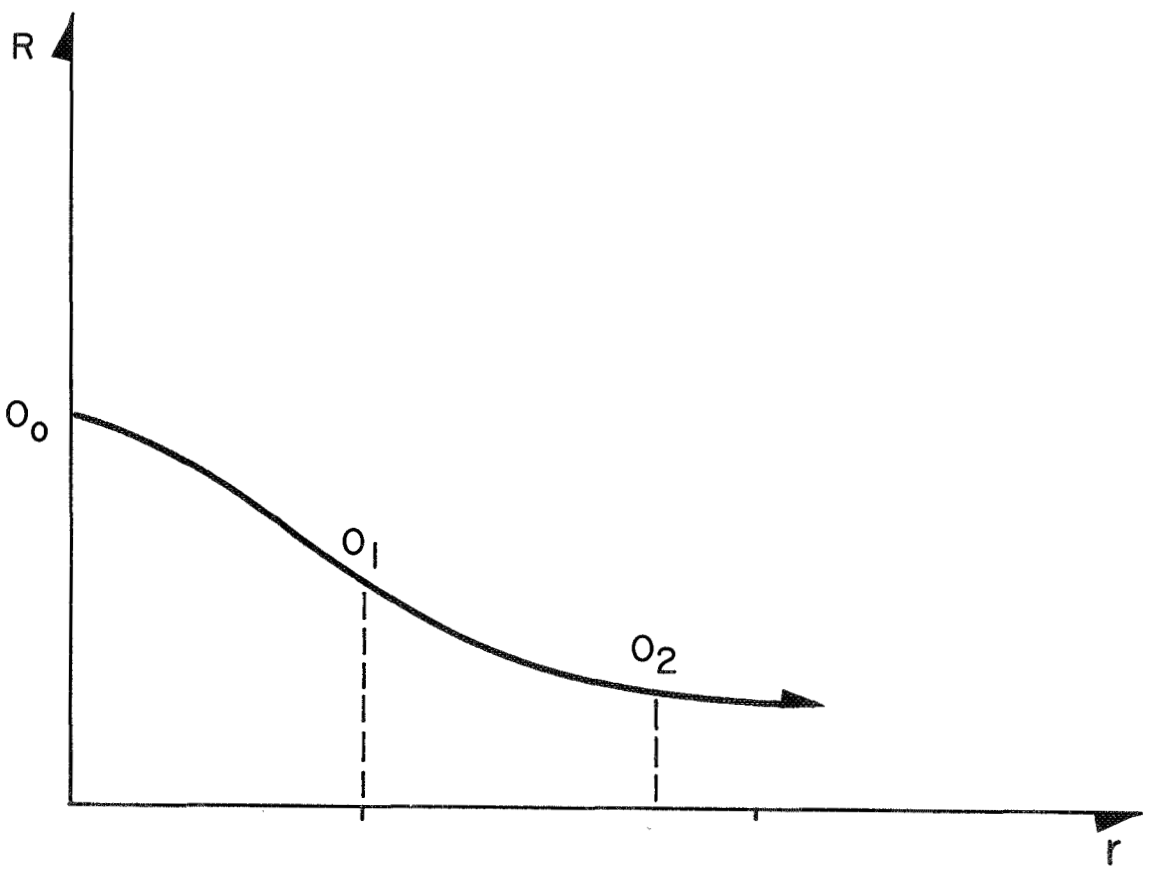

FIGURE 8-2
ZERO OFFSET RESPONSE VS. RANGE FOR
SEVERE SCATTERING

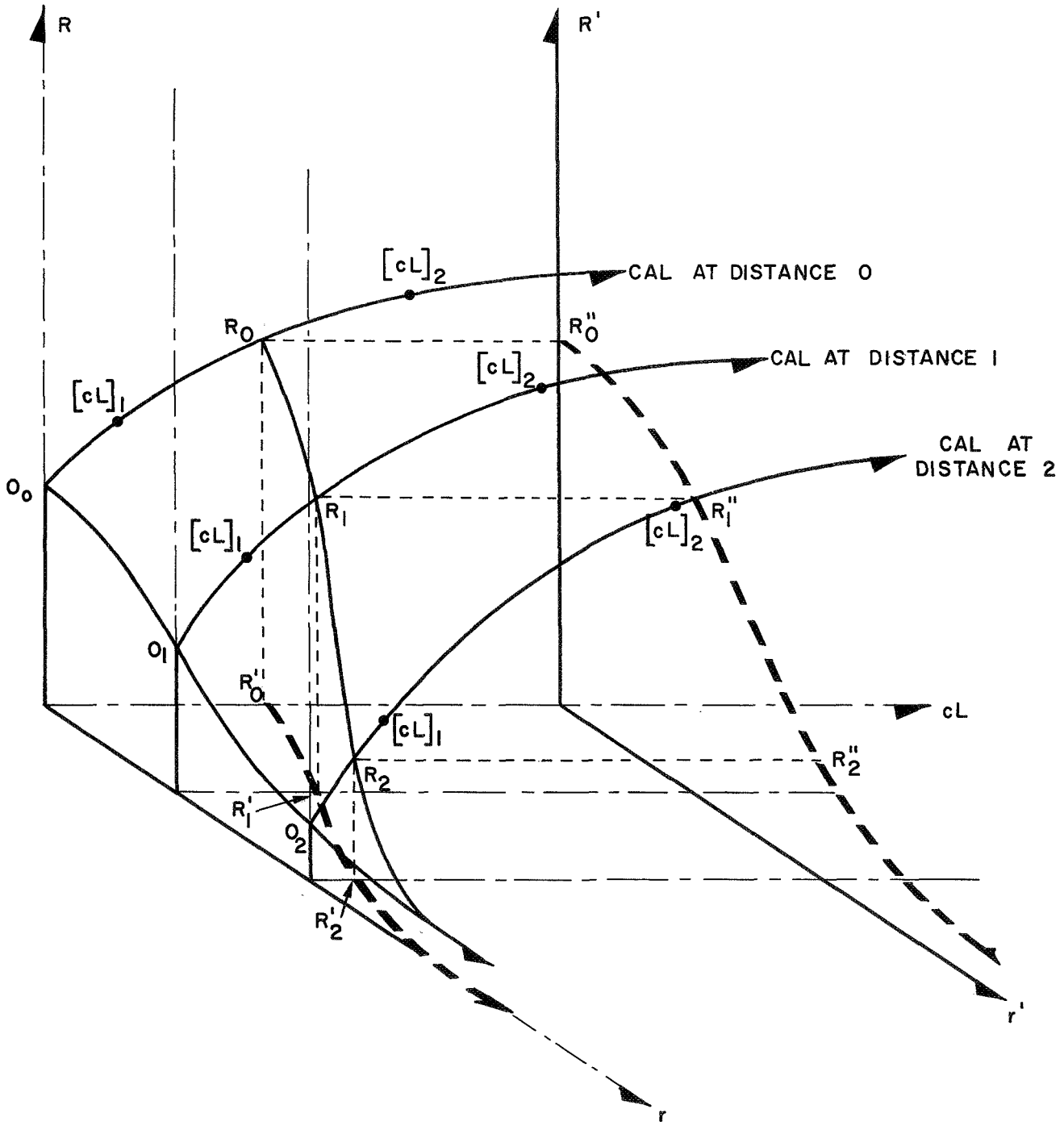

FIGURE 8-3
VARIATION OF RESPONSE, AND APPARENT
CONCENTRATION X PATHLENGTH VS. RANGE

plume and the response measured with no test cell inserted.

The reading taken at a given distance r when looking directly through the plume is placed onto the calibration curve determined by expression 8-2 and expression 8-3 when $[cL]_1$ and $[cL]_2$ are inserted. The apparent cL determined is obviously lower than the true value of cL. Thus, the apparent calibration curve response coincides with the real response for r = 0 and becomes a zero offset at a distance (r) dependent on the visibility from the observation point to the plume.

Assume now that we are trying to measure high values of cL and are thus using a one-sided response. Remembering that when aerosol scattering is present, a redistribution of radiant energy takes place towards the shorter wavelengths (making N'_λ increasingly flat, with increased scatter), for a situation similar to the one shown in Figure 8-1, the zero offset of the calibration curves varies with distance from the plume as shown in Figure 8-2.

If we represent in a three-dimensional diagram the variation of the calibration curves with distance (r) we obtain Figure 8-3.

The dotted curve in the cL - r plane represents the apparent calibration readings. The dotted curve in the plane R', r' shows the instrument reading versus distance. Either one of the two curves can be extrapolated to zero distance in order to obtain the cL of the plume.

In Figures 8-4, 8-5, 8-6, and 8-7, four curves of the type cL - r have been plotted from actual field measurements. Notice the expected shape of the curve.

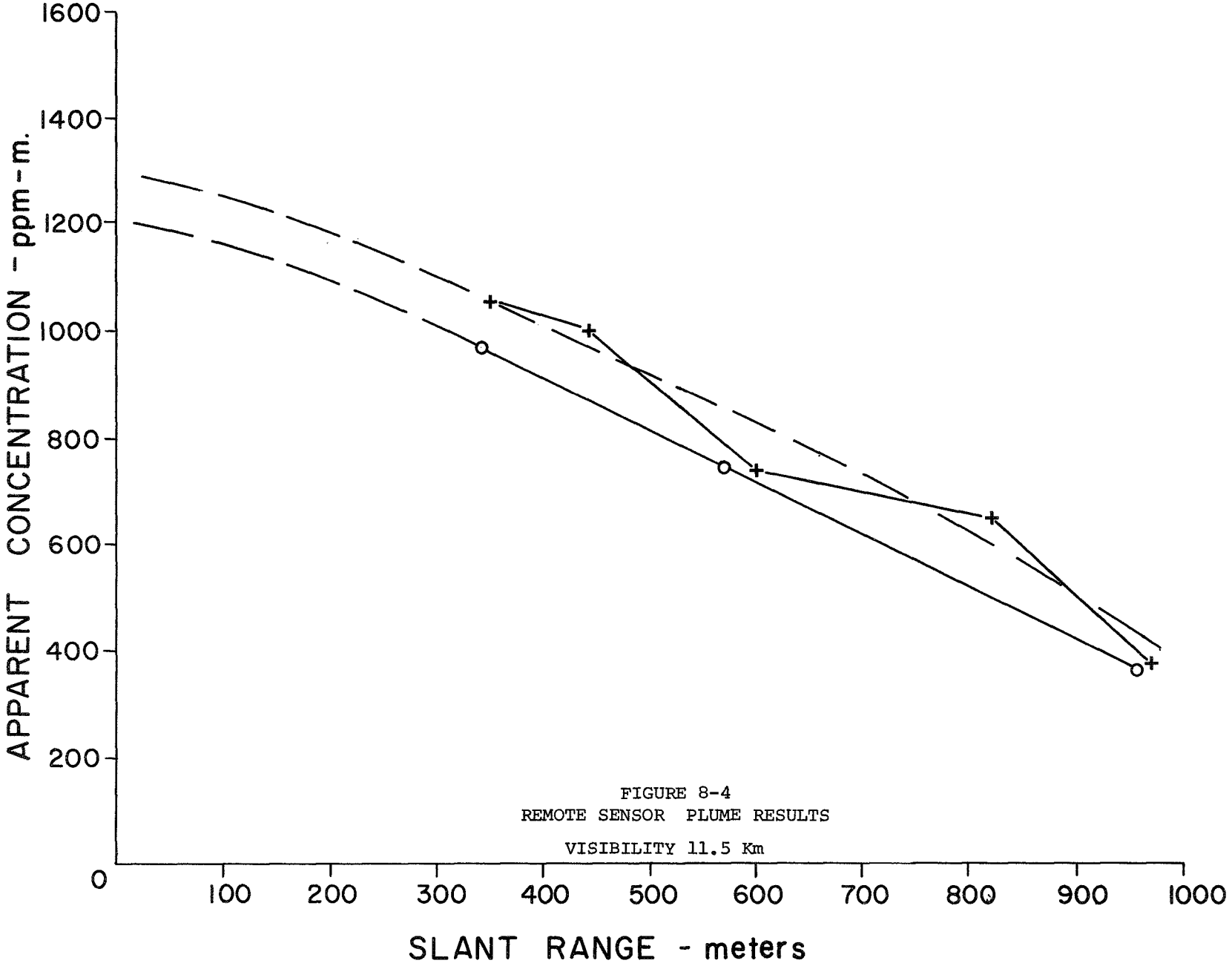

FIGURE 8-4
REMOTE SENSOR PLUME RESULTS

VISIBILITY 11.5 Km

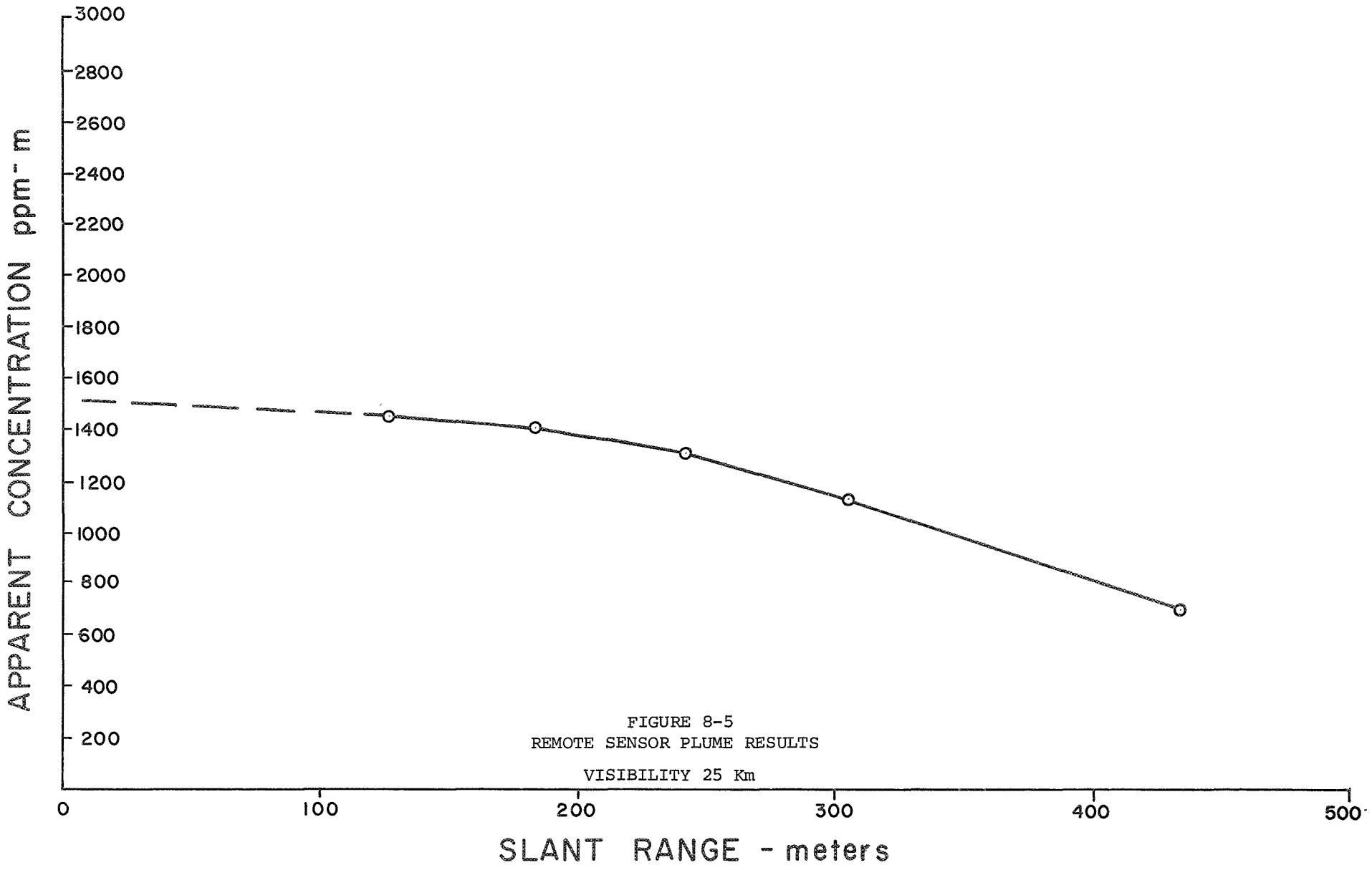

FIGURE 8-5
REMOTE SENSOR PLUME RESULTS

VISIBILITY 25 Km

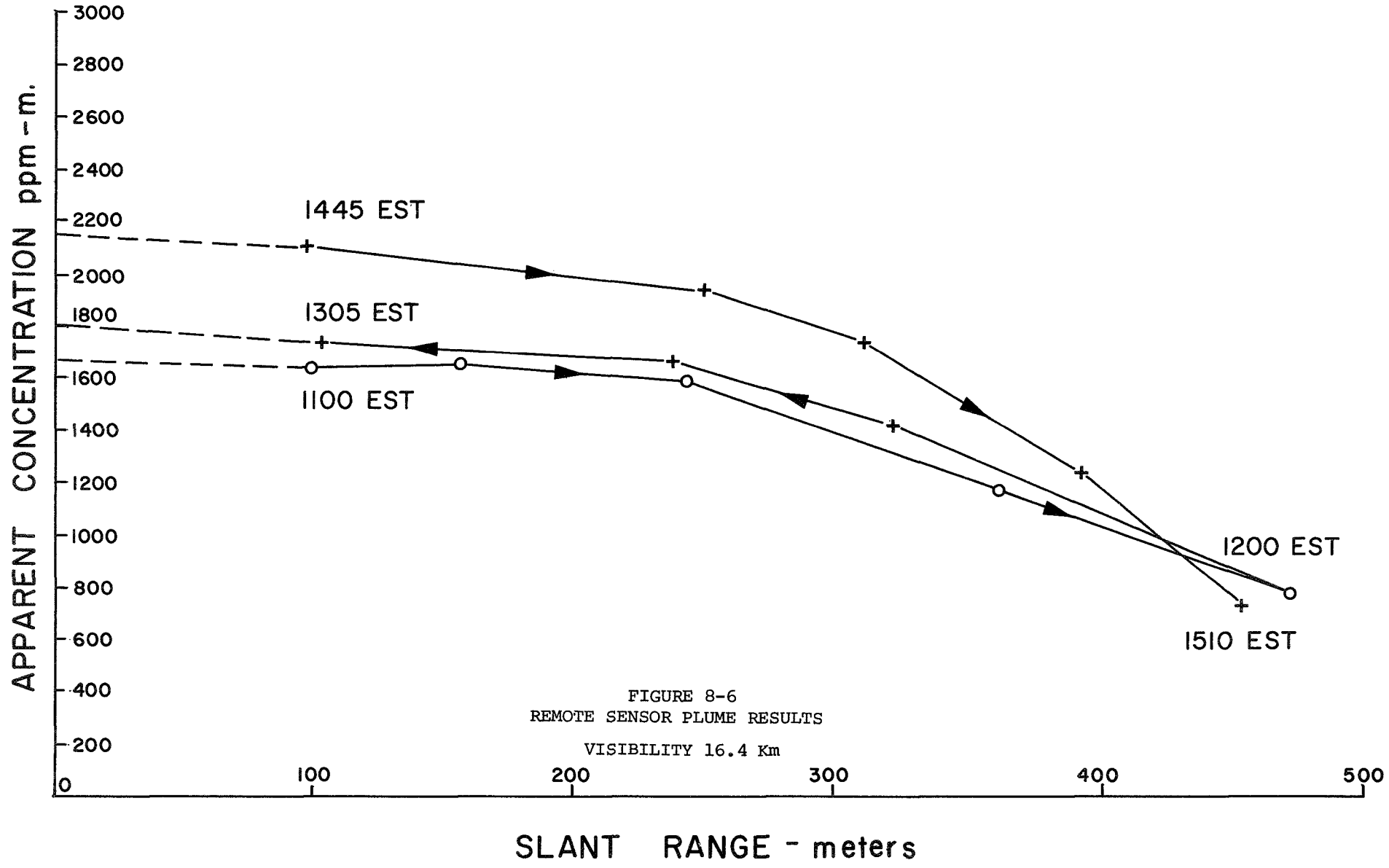

FIGURE 8-6
REMOTE SENSOR PLUME RESULTS

VISIBILITY 16.4 Km

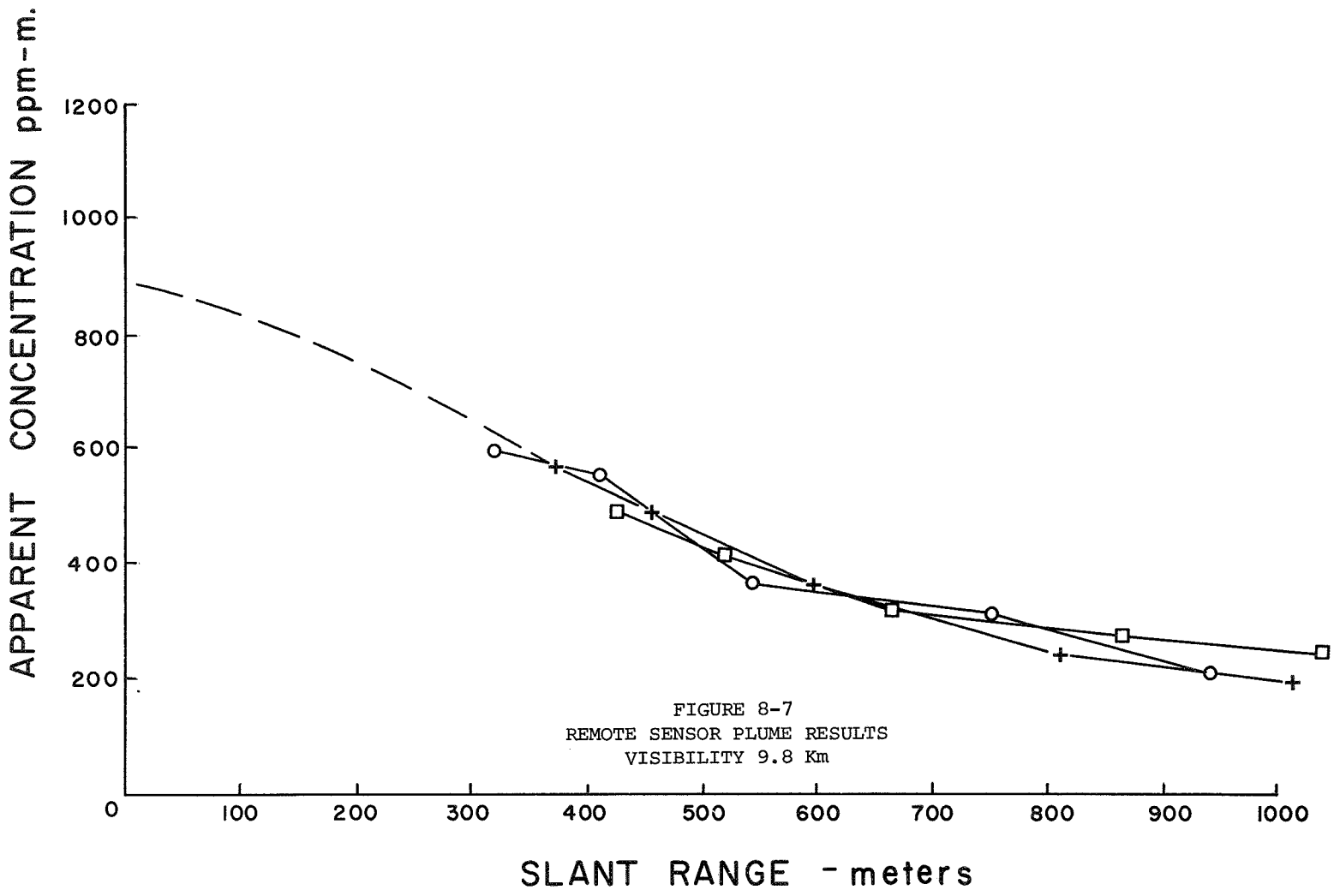

FIGURE 8-7
REMOTE SENSOR PLUME RESULTS
VISIBILITY 9.8 Km

9. REMOTE SENSING FROM A BALLOON-SUPPORTED PLATFORM

On September 3, 1969 an experiment was carried out by Barringer Research Limited under contract to NASA in order to determine the feasibility of flying the correlation spectrometer on a satellite platform and detecting and measuring pollutants in the atmospheric column below the spacecraft.

A scientific package containing two correlation spectrometers, one for SO_2 and NO_2, and a radiometer were carried on board a high altitude balloon flown over Chicago at an altitude of 35 km. The target size is extensive and the heavily industrialized area is a strong source of gaseous pollutants, particularly SO_2 and NO_2, making the megalopolis an ideal choice for such a test. The balloon was launched by the National Center for Atmospheric Research (NCAR) and Winzen Research, Inc. from Dowagiac, Michigan at 8:30 a.m. and was borne in a counter-clockwise pattern over the Chicago area as shown in Fig. 9-1. The flight path was calculated to place the instrument package over Central Chicago at noon in order to achieve maximum solar illumination from above.

Coincident with the balloon sensors looking down, a mobile unit moving along the balloon's ground track was aimed vertically upward, scanning over the same spectral range as the airborne units. Comparison of results from the airborne and ground-mounted sensors would tend to indicate the extent of the dilution of the airborne reading from Rayleigh- and Mie- backscattered radiation between the balloon and the gas-bearing layer below, Fig. 9-2.

The data are still being reduced and will be presented in a separate publication.

10. CONCLUSION

A detailed analysis of the Barringer Refractor-Plate Correlation Spectrometer has been carried out. The interactions between the characteristics of the light source irradiating the gas, the transmission spectrum of the instrument, the transmission spectrum of the correlation mask, and the electronic circuitry have been discussed. An analysis is presented of how to create and use correlation masks in order to optimize both the response sensitivity and the discrimination to a chosen gas.

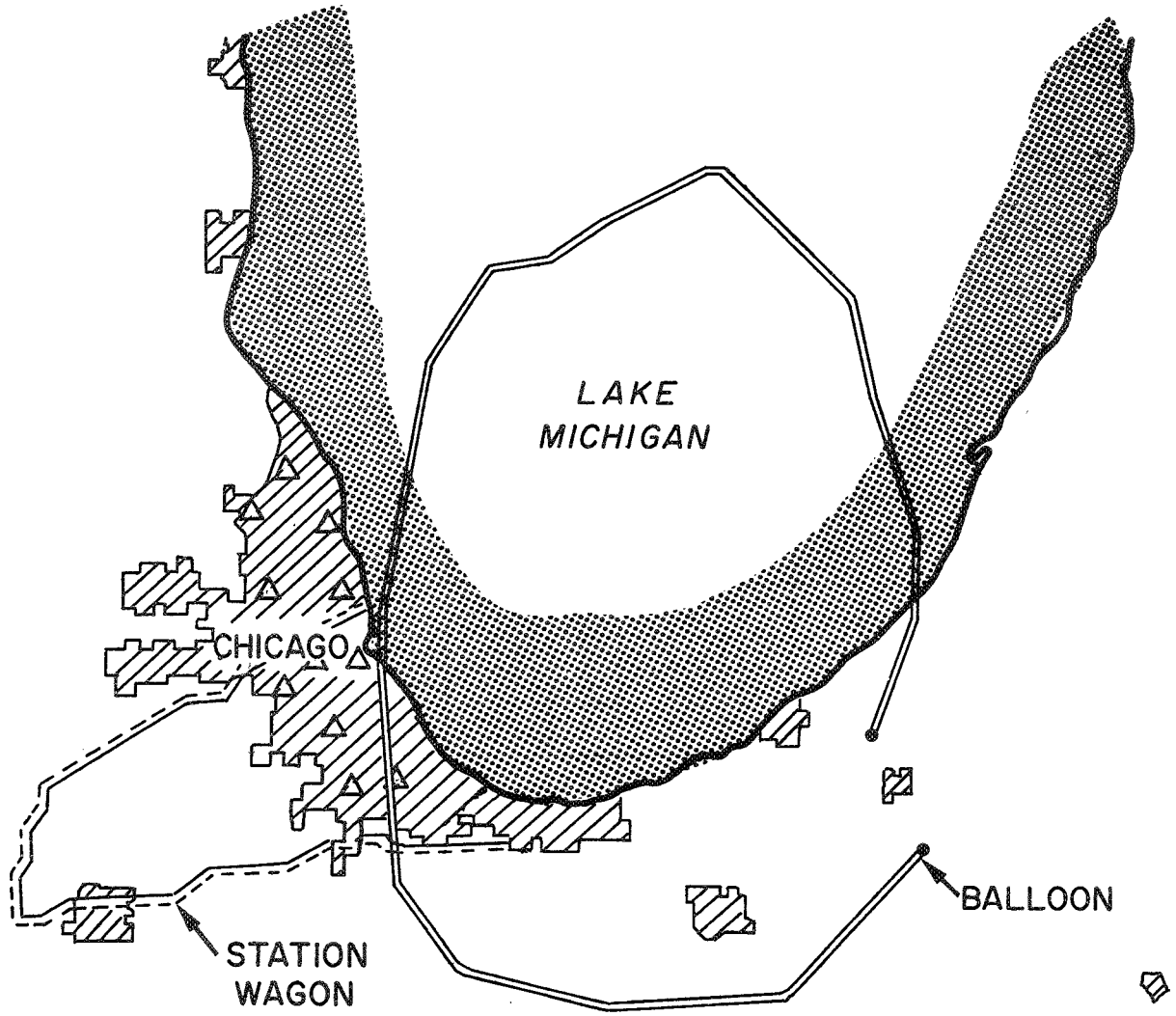

FIGURE 9-1
BALLOON FLIGHT PATH OVER CHICAGO
ALTITUDE 35 Km

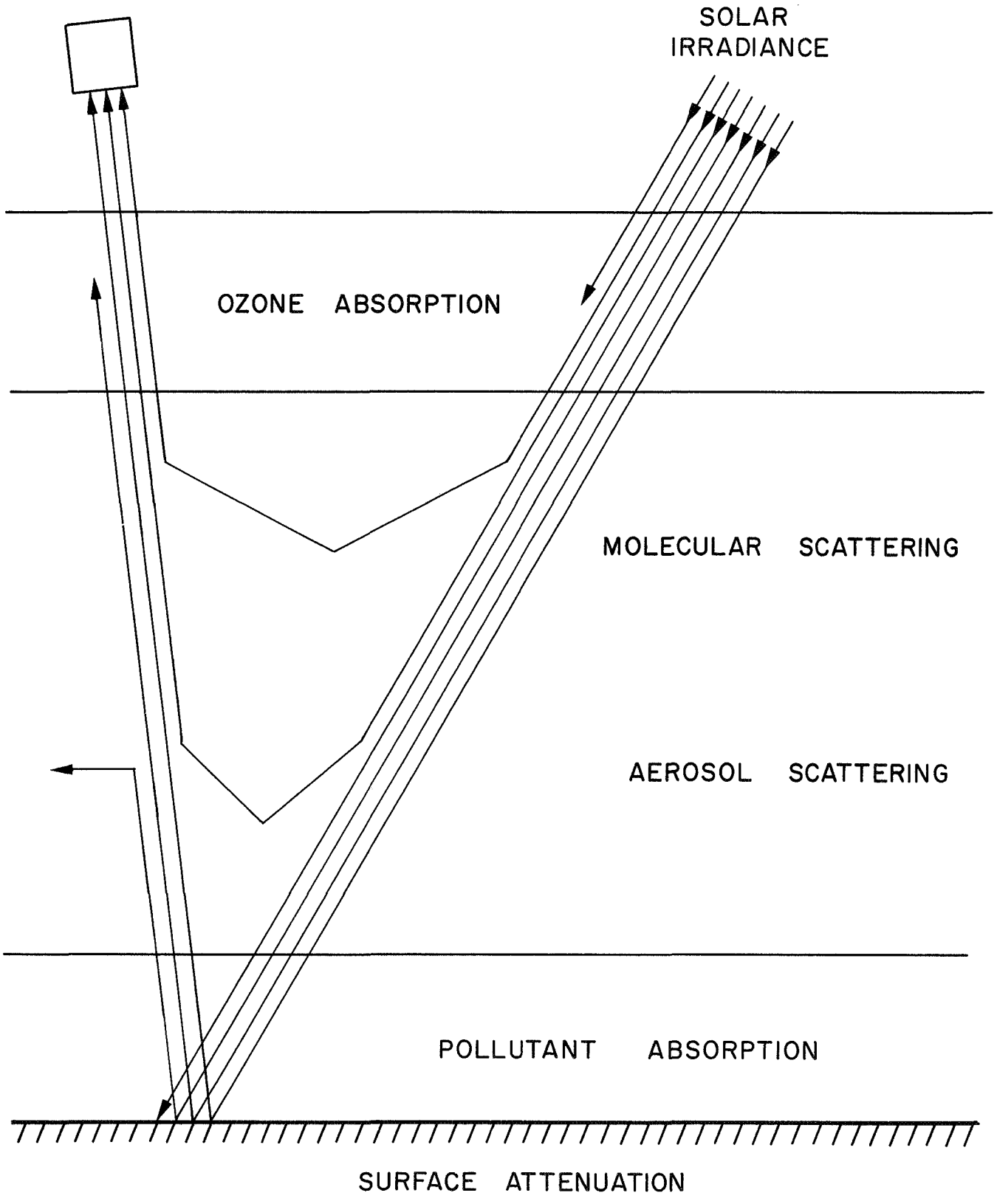

FIGURE 9-2
SCHEMATIC PATH OF ENERGY ARRIVING AT THE
BALLOON LOCATED SENSOR